CHALMERS
UNIVERSITY OF TECHNOLOGY

Thermal Runaway Propagation and Fire Safety Modeling of Large-Scale Marine Battery Rooms

Master's thesis in Innovative Sustainable Energy Engineering (Heat and Power)

ASAD MEHMOOD

DEPARTMENT OF INDUSTRIAL AND MATERIALS SCIENCE
CHALMERS UNIVERISTY OF TECHNOLOGY, Gothenburg, Sweden, 2025

CHALMERS UNIVERSITY OF TECHNOLOGY
Gothenburg, Sweden 2025
www.chalmers.se

Author Asad Mehmood

Title of thesis Thermal Runaway Propagation and Fire Safety Modeling of Large-Scale Marine Battery Rooms

Programme Innovative and sustainable energy engineering (Nordic Master)

Major Heat and power engineering

Thesis supervisor Prof. Jani Romanoff

Thesis advisor(s) Prof. Annukka Santasalo-Aarnio, (Aalto) and Prof. Jinhua Sun, (Chalmers)

Date 29.09.2025 **Number of pages** 114+18 **Language** English

Abstract

The transition to fully electric ships is an essential step toward reducing greenhouse gas emissions in the maritime industry. This change requires significant modifications to the operations and construction of ships. This thesis makes a contribution to the study of the thermal runaway (TR) behavior of lithium iron phosphate ($LiFePO_2$ or LFP) battery systems. The objective is to gain an understanding of how fire, heat, and gas spread throughout a marine battery room during a TR event.

To investigate the process by which a fire spreads from a single cell to an entire battery room, a thermal runaway simulation model was developed in Spreadsheet. The model is based on experimental heat release rate (HRR) and total heat release (THR) data from recent fire tests. It employs a hierarchical structure that extends from the cell to the module to the rack to the room. In addition, it incorporates flame propagation that is based on the direction of the flame, variable state-of-charge levels ranging from 0% to 100%, and battery room sizes. For each scenario, the tool computes the peak HRR, the total energy release, combustion duration, and the structural heat load on the steel in the room.

The analysis show that state of charge (SOC) is the strongest lever for safety: 100% SOC gives the fastest roof failure, 50% SOC extends survival by about 30-50%, and at 0% SOC many layouts do not reach roof melting at all. Rack spacing controls room density and creates a practical trade-off more spacing lowers heat concentration and increases melt time, but also increases steel mass and ship space. A moderate spacing band (≈0.5-0.9 m) offers the best balance for design, especially for 15-25 MWh rooms. The seawater flooding analysis further showed that early flooding can completely prevent roof failure, while late flooding has limited effect and may even increase explosion risks. The tool therefore gives designers a simple, validated way to compare layouts, operating modes and to set safe design limits for marine battery rooms. In doing so, it directly supports compliance with DNV's 5 MWh threshold rule for single spaces, while offering quantified methods to justify larger 10-25 MWh installations where compensatory measures are required.

Keywords Thermal runaway (TR), Lithium iron phosphate (LFP), Marine battery safety, Energy storage systems (ESS), Early-stage ship design, Battery room design

Table of Contents

List of Figures

List of Tables

Preface and acknowledgements

First and foremost, I'd like to express my gratitude to Aalto University for providing me with the opportunity to study and grow during this incredible journey. I am especially grateful to my supervisor, Prof. Jani Romanoff and advisor Prof. Annukka Santasalo-Aarnio from Aalto University and my advisor at Chalmers University, Professor Jinhua Sun, for their ongoing support and guidance. Their advice, encouragement, and feedback helped me stay on track and improve my work throughout the process.

I'd also like to thank my family, particularly my mother and father, for their unwavering love, support, and sacrifice. They've always been my main source of strength and motivation. This thesis reflects not only months of research and writing, but also the encouragement and kindness of many people around me. And finally, thank you to curiosity itself for always reminding me to keep asking questions and never stop learning.

Aalto University, 29 September 2025
Asad Mehmood.

Symbols and abbreviations

Symbols

Q	Heat release rate (HRR)
t	Time (s)
m	Mass (kg)
$\dot{m}$	Mass loss rate (kg/s)
T	Temperature (°C / K)
T_ign	Ignition temperature (°C)
T_melt	Steel melting temperature (°C)
H_c	Heat of combustion (MJ/kg)
E	Energy (MJ / kWh)
V	Volume (m^3) / Voltage (V)
A	Area (m^2)
q"	Heat flux (kW/m^2)
h	Height / flame length (m)
c_p	Specific heat capacity (J/kgK)
L_f	Latent heat of fusion (kJ/kg)
r	Distance (m)
χ_r	Radiative fraction (–)
σ	Stefan–Boltzmann constant (W/m^2K^4)
Q_d(t)	Total HRR at time t
t_ign,n	Ignition time of nth module
Δt	Propagation delay (s)
ΔH_c	Heat of combustion
ρ	Density (kg/m^3)
P	Power (W / kW)
Q_conv	Convective heat release rate
Q_rad	Radiative heat release rate

Abbreviations

TR	Thermal runaway
HRR	Heat release rate
THR	Total heat release
SOC	State of charge
BU	Bottom-up propagation
TD	Top-down propagation
MO	Middle-out propagation
LFP	Lithium iron phosphate

NMC	Nickel manganese cobalt oxide
LIB	Lithium-ion battery
ESS	Energy storage system
BESS	Battery energy storage system
EMBC	Electric marine battery cabinet
BMS	Battery management system
PDM	Pack disconnect module
RoPax	Roll-on/Roll-off passenger
eCSOV	electric commissioning service operation vessel
IMO	International Maritime Organization
SOLAS	Safety of Life at Sea Convention
DNV	Det Norske Veritas
EMSA	European Maritime Safety Agency
NMA	Norwegian Maritime Authority
RINA	Registro Italiano Navale
ABS	American Bureau of Shipping
LR	Lloyd's Register
CFD	Computational fluid dynamics
FEA	Finite element analysis
FM Global	Factory Mutual Global
MPS	Multi-point source (radiation model)
CO_2	Carbon dioxide
H_2	Hydrogen
SSW	Synthetic seawater
DI	Deionized water
LFL	Lower flammability limit
ACH	Air changes per hour
AC/DC	Alternating current / direct current
VDC	Volts direct current
EV	Electric vehicle

1 Introduction

Maritime transport is quickly moving toward electrification, with increasing number of ships adopting battery electric and hybrid propulsion to reduce emissions.[13] Global environmental initiatives, like the IMO's plan to cut greenhouse gas emissions, have led to more investment in battery-powered ships as a way to reach zero operational emissions. Besides being good for the environment, electrification can make operations more efficient by lowering fuel costs, maintenance needs, and noise and vibration on board.[14] The Alternative Fuels Insight database says that there are now more than 800 ships with battery systems in use. This is more than three times the number that were in use five years ago. These include roll-on/roll-off ferries, passenger ships, harbor tugs, offshore service vessels, and more, mostly on short routes where current battery technology can meet energy needs.[15] Only about 13% of ships with batteries are fully electric; the rest are hybrids or plug-in hybrids. This shows how battery range limits longer trips. Nevertheless, battery systems have become a viable solution for an increasing range of ship types and sizes as technology improves and the industry seeks to decarbonize. [15]

In addition to this progress, safety issues related to big lithium-ion battery installations have become more important. Lithium-ion batteries hold a lot of energy and create new risks that aren't there with regular marine fuels. The primary safety risks are well known to be fire and explosion resulting from battery thermal runaway events and the release of flammable gases.[15] Thermal runaway can happen when a cell fails inside, overheats, is overcharged, or is damaged from the outside. This can cause the battery cells to heat up on their own and possibly explode. Battery compartments, on the other hand, store electrical energy and combustible electrolyte in a small space, which makes people worry about putting out fires and letting gas escape. [16] Fire detection, ventilation, and extinguishing systems should be specifically designed for battery hazards, and crews require training to effectively manage these incidents. The maritime sector has tackled these challenges by creating new safety standards, yet recent incidents show that the risk is very much real.

In summary, fully electric vessels represent a promising path to greener shipping, but they demand close attention to safety due to the hazards of lithium-ion batteries. The use of high-energy batteries on ferries, tugs, and other ships has resulted in tangible benefits in terms of emissions reduction and efficiency. At the same time, real-world incidents have shown that lithium-ion battery failures can quickly escalate and even endanger a vessel if proper safety measures are not taken. The maritime industry is thus combining its push for electrification with a strong emphasis on risk management and regulation, from selecting safer battery chemistries (such as LFP over NMC) to improving design standards, emergency procedures, and crew training. Ongoing research, experience, and regulatory initiatives

(by organizations such as DNV, EMSA, and national authorities) are constantly improving the safety framework for marine battery systems.[15]

1.1 Battery Systems: Ship Scale vs. Boat Scale

The design and size of marine battery systems are very different for big ships and small boats. One important difference is how much energy storage is needed. A small electric ferry or workboat might only need a few hundred kilowatt-hours (kWh), while a large ship (like a cruise ferry or Ro-Pax ship) might need many megawatt-hours (MWh) of batteries. For instance, New Zealand's 19-meter electric ferry has enough batteries to run for about an hour, which is about 550 kWh.[17] A common saying is that "a ship can carry a boat, but a boat can't carry a ship." In practice, this means that ships are built to carry a lot of cargo or hundreds of people, while boats are built to carry much smaller loads. As an example, the ferry can accommodate more than 2,000 people on long ocean routes whereas small boat, might only hold a few people.[18]

The Ika Rere is a fully battery-electric ferry made of carbon fiber that is 19 m long and can carry 132 people at speeds of up to 20 knots (Fig 1). It has two battery banks with 72 liquid cooled XALT XMP76P battery packs that deliver 550 kWh of power. These battery packs power two 325 kW electric motors, giving it speed and backup power in a small package. [17, 19]

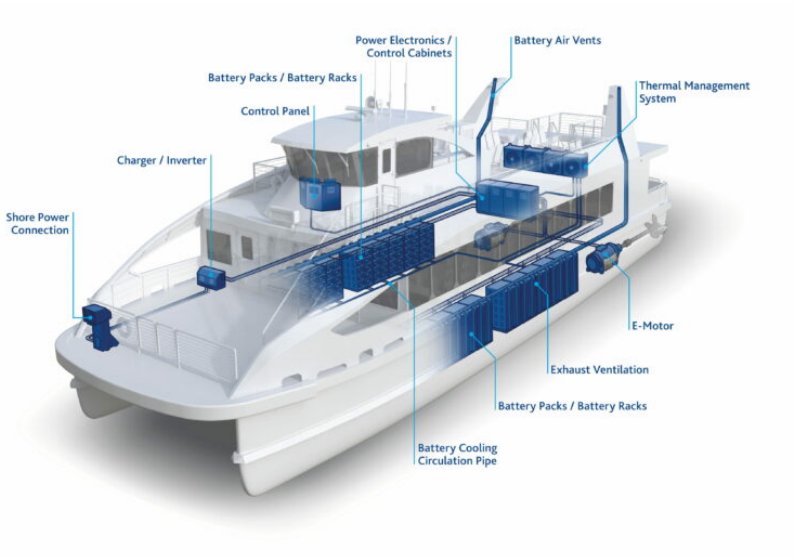

Figure 1 XALT Modular Battery Packs Distributed Across Two Rooms. [6]

A ship, on the other hand, is usually a bigger, ocean-going vessel made for long trips and carrying more people. P&O Ferries' hybrid battery electric ship for the Dover–Calais route is a good example. Each of these strong ships has

about 1,200 XALT lithium-ion battery packs, which add up to 8,816 kWh. They are installed in four separate battery rooms using modular XALT XRS 2 rack systems to meet strict maritime safety and performance standards. [20]

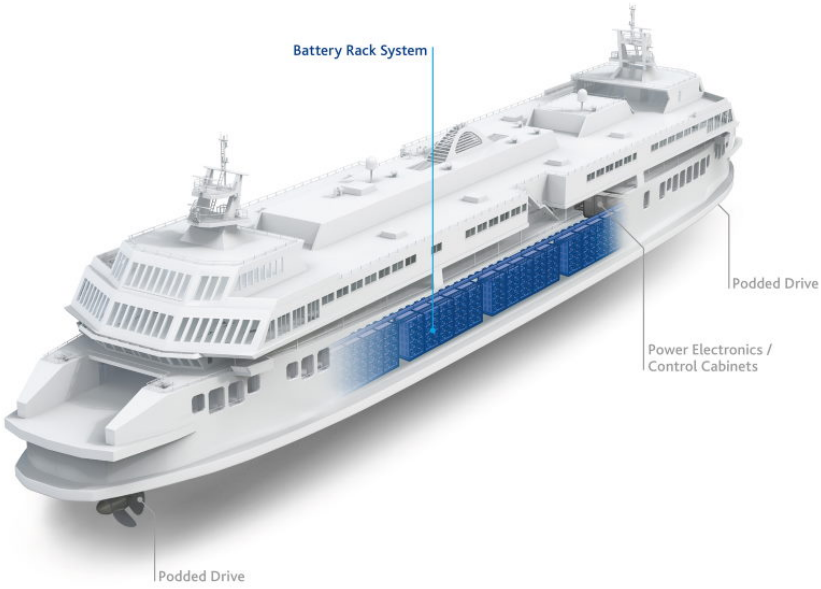

Figure 2 Battery Racks in Dedicated Rooms on Larger Vessel [9]

1.2 Marine Battery Room Solutions

Marine battery room solutions are used by modern ships to safely store large energy storage systems (ESS) on board. These battery rooms can be either separate container modules or built-in compartments that are only for batteries. They are engineered with careful consideration for layout, battery type, safety features (thermal management, fire protection), and integration with ship systems to meet maritime standards (SOLAS, class rules) for fire safety (e.g. A60 fire-rated enclosures). Below is a summary of important solutions from major providers, with examples from different types of vessels (cruise ships, ferries, tugs, and workboats).

The corvus energy provided 248 kWh of battery storage for the Geir, a 61.7-meter Norwegian longliner fishing in the Barents Sea north of Murmansk, Russia, in 2020. The battery bank, which is installed below deck for safety and cooled by forced air, helps the ship use power more efficiently. Sveinung Odegard of Corvus Energy says that batteries on these kinds of ships have three main jobs: they help engines run smoothly by absorbing load spikes, they collect energy from deck equipment like winches and cranes, and they balance loads in hybrid systems to make the best use of fuel. Batteries and

hydrogen fuel cells are sometimes used together to protect system parts and handle load changes.[21]

Figure 3 Below-Deck Corvus Battery Bank on Longliner Geir with Forced-Air Cooling. [10]

Hurtigruten AS has also led the way in hybrid-powered expedition cruising with the MS Roald Amundsen, which was the first of its kind to operate in polar regions. The ship has two big battery packs that allows the engines run more efficiently and, for short periods of time, only on battery power. This setup cuts emissions by about 20%, making it possible to travel to Antarctica, and the Arctic. The battery system also helps keep backup engines from starting, which saves fuel and cuts down on greenhouse gas emissions. [22]

Figure 4 MS Roald Amundsen, a hybrid powered expedition cruise ship. [22]

Havila Voyages, a Norwegian cruise line that debuted in 2022, operates hybrid ships equipped with the largest passenger-ship batteries at sea. These vessels can operate emission-free for up to four hours, allowing for quiet navigation in Norway's UNESC O-protected fjords. Batteries are recharged in port using clean hydropower, and they can power the ship while docked. While currently paired with LNG propulsion, the vessels are designed to be converted to hydrogen fuel, supporting the company's goal of emissions-free operation. [23, 24]

Figure 5 Havila Hybrid Ship Capable of Four Hours Battery-Only Operation [12, 13]

Corvus Energy has installed more than 300 MWh of ESS capacity around the world, including 24 MWh in North America. There are also more than 20 vessels flying U.S. and Canadian flags that are either already in service or being built. The company's range of products meets the needs of different types of vessels:[25]

1. Orca ESS is based on Li-NMC and can be scaled from 80 to 10,000 kWh. It is very flexible and charges and discharges quickly.

2. Dolphin ESS has the highest energy density in the industry and is made for applications where weight is important, like high-speed ferries.

Figure 6 Corvus Dolphin ESS for High-Speed and Weight-Sensitive Vessels.

3. Blue Whale ESS: $LiFePO_4$-based and made for very large ships, it has the highest volumetric energy density for battery room installations.

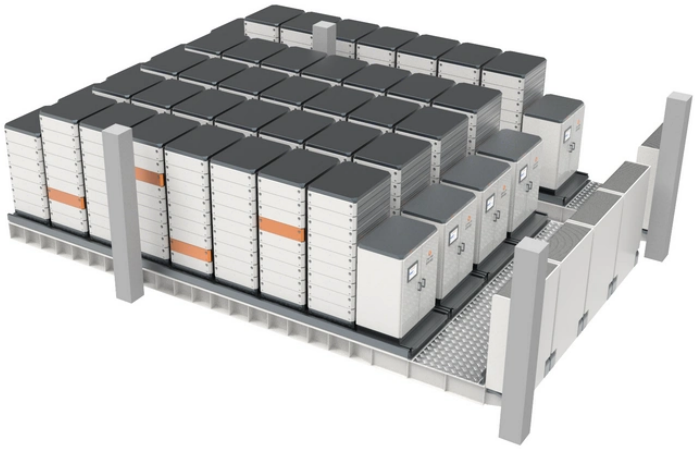

Figure 7 Corvus Blue Whale, a compact ESS to optimize battery rooms in large-scale.

1.2.1 Performance of Different Battery Chemistries

There are a number of different chemistries that could be used in marine settings. Lithium-ion batteries are the most common type used in current projects, mostly in LFP or NMC. However, lithium-titanate, sodium-ion, and lithium-sulfur batteries are also important to think about for the future. Table 1 shows how these battery chemistries compare in terms of important performance metrics.

Parameter	LFP ($LiFePO_4$)	NMC ($LiNiMnCoO_2$)	LTO ($Li_4Ti_5O_{12}$)	Na-ion	Li–S
Energy Density	~90–160 Wh/kg [2]	~150–250 Wh/kg; [5]	~50–80 Wh/kg [2]	~75–200 Wh/kg [6]	~450 Wh/kg[7]
Cycle Life	2,500–9,000+ cycles[8]	1,000–2,000 cycles [2]	3,000–7,000 cycles [2]	>2,000; current ~2–3k [6]	Often < 300 cycles (historically); up to ~1,000+ in recent lab demos[7]
Nominal Cell Voltage	~3.2 V [8]	~3.6–3.7 V[2]	~2.4 V[2]	~3.0–3.1 V [6]	~2.1 V (discharges 2.5→1.7 V) [7]
Thermal Stability TR onset	Thermal runaway occurs at approximately 270 °C, which is significantly higher than cobalt-based chemistries. [2]	Moderate thermal runaway can start around 160–210 °C [9]	Very stable, with no significant exotherm up to high temperatures, making it one of the safest Li-ion chemistries.[2]	A lot of Na-ion cells have safer cathodes, and some have electrolytes that don't catch fire[6].	Low to moderate: If Li–S gets too hot, it can go into thermal runaway. Even solid-state designs can fail at high temperatures due to the cross-reaction of Li and S[10]
Fire Risk & Behaviour Severity, propagation	Less severe fires: LFP cells are harder to set off Onset needs more heat (about 230 °C instead of 160 °C for NMC) [9]	More severe fires: NMC cells catch fire more easily and burn hotter. TR creates flaming jets and ejected debris. Up to 40–50% of the cell mass can be explosively vented as burning gas, molten aluminum, e.t.c. [9].	LTO cells are safe by design, and there have been no reports of thermal runaway spreading when they are abused in normal ways. They don't break down as easily as graphite anodes do, and they don't easily release oxygen from the cathode [2].	Na-ion cells are not likely to catch fire or blow up [11]. Thermal runaway propagation is not frequently observed; however, standard precautions (ventilation, monitoring) remain necessary due to the utilization of organic electrolytes in the majority of Na-ion cells.	The presence of lithium metal means that any internal short or overheating can result in a fire. If thermal runaway occurs, the reaction can be violent; the flammable electrolyte and polysulfide gases may ignite, and molten lithium can spread fire.[12]

Table 1 Comparison of Battery Chemistries for Marine Energy Storage[1]

1.3 Maritime Incidents Involving Lithium-ion Battery Fires

This section reviews documented incidents involving lithium-ion battery fires in marine vessels. These incidents show the real-world problems and safety gaps that come with thermal runaway, bad suppression systems, exposure to seawater, bad ventilation, and not enough detection systems.

1.3.1 MF Ytterøyningen Fire Incident (2019, Norway)

The Norwegian hybrid ferry MF Ytterøyningen underwent a maritime battery fire incident in October 2019, which is considered to be one of the earliest and most serious incidents in the maritime industry. A Corvus Orca Energy lithium-ion battery system with a capacity of 1.9 MWh had been recently installed on the vessel. This system was comprised of 16 packs and 352 liquid-cooled modules, each of which utilized lithium iron phosphate ($LiFePO_2$) chemistry. The battery had a state of charge (SOC) of approximately 50% at the time of the incident, and the system was disconnected from the ship's AC/DC grid because it was undergoing continued maintenance. The official root cause analysis discovered that a twisted gasket allowed coolant, which was a mixture of 30/70 ethylene glycol and water, to leak onto high-voltage electrical components within the Pack Disconnect Module (PDM). This resulted in electrolysis, arcing, and ultimately the ignition of a fire at approximately 1000 VDC. Since the battery management system (BMS) was not functioning, the monitoring system of the ship did not receive any alarms, which allowed the fire to develop without being discovered. The external fire generated sufficient heat to set off thermal runaway (TR) in a number of battery cells located above the voltage distribution module (PDM).

Subsequently, the utilization of seawater from the emergency sprinkler system, in conjunction with the absence of ingress protection guards, made it possible for water to enter the racks. This resulted in multiple ground faults, additional short circuits, and the spread of the fire. The following day, the sealed battery and switchboard rooms were filled with a flammable atmosphere due to the accumulation of gases from damaged cells. These gases included hydrogen, ethylene, and carbon monoxide. An explosion occurred as a result of a spark that ignited this gas mixture, which led to the exposure of twelve firefighters to gas.[26]

Figure 8 Battery Room Fire on Norwegian Ferry Contained by Firefighters

1.3.2 MS Brim Explorer Fire (2021, Norway)

The hybrid-electric vessel MS Brim Explorer was sailing through the outer Oslofjord on March 11, 2021. The vessel was powered by a lithium-ion battery system that had a capacity of 792 kWh and was constructed using Corvus Dolphin Energy modules that were stacked in a total of twelve stacks. Every stack was made up of six battery modules and a stack controller within it. The fire started in Module 1 of Stack 6 after seawater entered through the ventilation outlet of the tunnel, traveled through a fan that was not sealed, and then splashed directly onto live high-voltage components. Smoke detectors indicated that there was a fire in both the engine room and the battery room; however, the crew misidentified the source of the fire because smoke spread through a bulkhead that was not smoke-tight. As a result of this, the Novec 1230 fire suppression system was initially delivered to the engine room, and only after a delay of seven minutes was it delivered to the battery room. At that point, the fire had already advanced, and the Novec fire agent was only able to provide temporary benefits in terms of cooling. The National Safety Institute (NSI) highlighted the importance of rapid and automatic fire suppression for lithium-ion battery fires and identified a wider safety gap in both the design of the system and the oversight of regulatory agencies.[27]

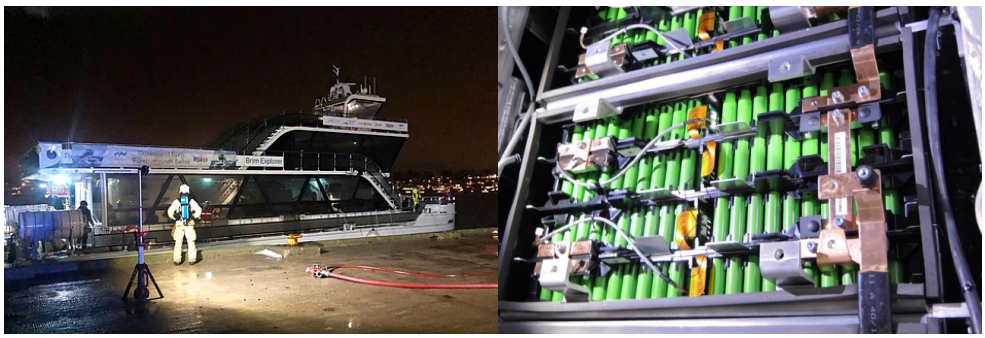

Figure 9 Battery Fire Incident on Electric Ferry and Exposed Battery Modules.[27]

Figure 10 Damage to the battery room, seen from the left to right: battery stacks.[27]

These battery room incidents on ships have highlighted the importance of strong safety measures. These incidents have raised awareness that, while battery propulsion eliminates traditional engine-room fires, it introduces new failure modes that can be catastrophic, if not managed properly. They also show that emergency response procedures for battery incidents (from gas detection to cell isolation and cooling) are constantly evolving. Since then, the ferry and offshore industries have actively shared "lessons learned" from these incidents, emphasizing transparency and collaboration to improve safety.[28]

1.4 Project Details

This project aims to create a simple simulation tool that assists engineers and ship designers in estimating the potential ignition and propagation of fires within a ship's battery room. The tool also calculates how much heat is released, how long the fire lasts, and whether the heat could damage the room's walls, floor, or ceiling. The study utilizes available experimental data, literature on fire testing, and relevant maritime battery specifications, including standard modular rack-based systems constructed using prismatic cells. The methodology is intended to be applicable across a variety of battery manufacturers, vessel types and battery room layouts.

In the early stages of ship design, designers need quick, defensible estimates to make sure the project is possible before they spend time and money on detailed tools. The design spiral is iterative by nature: you make an initial layout and key assumptions, test them, refine them, and loop until the design "closes." That is why tool is made for this loop. It's fast, easy to change, and focuses on the most important decisions early on.[29]

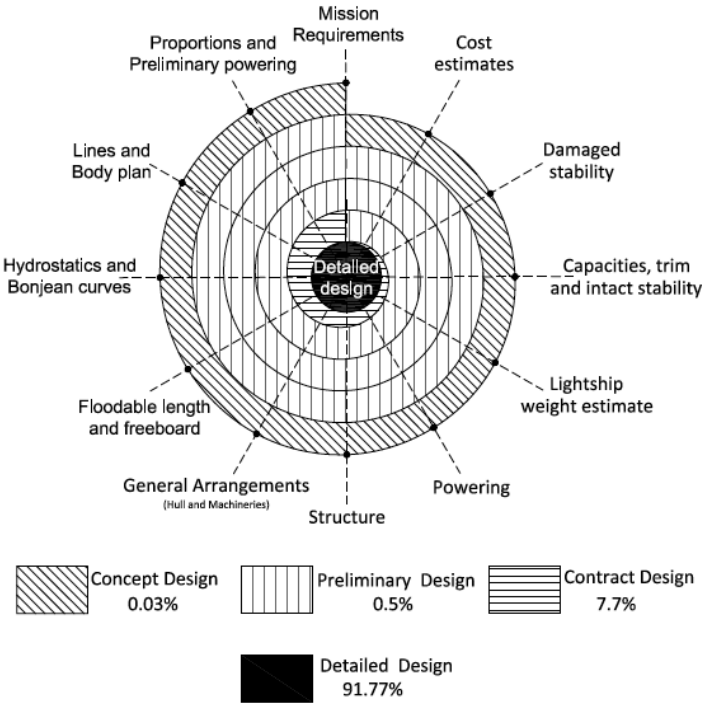

Figure 11 Typical design Spiral of a large merchant ship.[29]

One major reason to perform this task is that there aren't any tools or data. Big battery systems are still rather new in the maritime sector, and we don't know exactly what happens when these big batteries fail and start fires. There are simply generic safety requirements right now, and there isn't any real fire testing data for massive marine batteries yet. This makes it hard for designers to plan protection systems like ventilation, fire barriers, and cooling.

DNV's class rules DNV-CG-0660 put limitations on the level of energy that can be accommodated in a single battery room. To reduce the risk of thermal runaway event, capacity in a single space is limited to 5 MWh unless extra safety features are installed. If a vessel would need between 5 MWh and 25 MWh in a single space, extra barriers must be installed. They consist of singe-cell thermal runaway isolation design, special off-gas ventilation provision, and at least one other protective measure such as thermal barriers between modules, spacing increase, use of safer chemistries such as LFP, LTO or internal fire-extinguishing and cooling systems. [30]

The model is built in spreadsheet and allows users to choose how many modules or racks are affected, what direction the fire spreads, and how long each module burns. It also looks at cooling strategies, like using seawater, and estimates the thickness of steel needed to avoid failure during a battery fire. Although this thesis does not simulate how thermal runaway starts, in our analysis, we assume that thermal runaway has already occurred and evaluate its impact on heat release, propagation across modules and racks, and the

structural response of the battery room, especially in terms of steel wall exposure and required safety measures. Designer can later do detailed analyses (like CFD, FEA, or Multiphysics thermal-runaway models) in later spiral turns.

1.5 Limitations

The modeling work that is included in this thesis is based on a combination of engineering estimations, experimental fire data, and assumptions that are derived from the literature. The absence of large-scale experimental thermal runaway data for full-scale battery rooms that make use of LFP prismatic cells is one of the most important limitations. Most of the available data comes from small scale single cell, module, or rack-level fire tests, and this introduces uncertainty when scaling to larger battery rooms. Even though the model incorporates flame propagation logic from cell to room, it is difficult to validate the precise timing and intensity of fire spread between racks without conducting full-scale trials.

The simplification of the fire dynamics and thermal behavior is another significant limitation that must be considered. The simulation tool assumes uniform propagation within racks, simplified flame shapes, and TR durations per module that are constant depending on combustion temperature. The simulation excludes dynamic feedback between gas generation, pressure rise, and suppression system performance. Furthermore, it does not account for the effects of different ventilation configurations, gas leakage, or the use of fire suppression systems like water mist or nitrogen flooding.

The steel structure is modeled based on a passive exposure assumption, meaning that the estimated heat flux and structural load on the room assumes no active cooling or insulation. In reality, cooling systems and materials that are resistant to fire may be able to lower the peak temperature of exposed area.

In addition, the modeling tool does not take into account localized effects such as flame impingement on particular steel surfaces, structural deformations that occur during heating, or buckling that occurs as a result of temperature gradients. These effects are more complicated and would call for more advanced finite element analysis. In addition, the resolution of the simulation is restricted, and it is not possible to fully capture the thermal expansion or transient heat transfer in three dimensions.

Lastly, the accuracy of the results is dependent on the assumed HRR curves and total heat release values. These values were obtained from published fire tests and then adjusted for the Corvus module by using simplified scaling. It

is possible that the results could be significantly impacted by variations in real-world installations, such as the type of thermal insulation or the arrangement of racks. Despite these limitations, the simulation approach provides a method that is both practical and transparent for estimating the effects of thermal runaway and heat in marine battery rooms.

1.6 Objective

This research aims to explore fire behavior, structural impact, and design safety in fully electric marine battery rooms by:

Modeling Thermal Runaway Initiation, Propagation, and Fire Behavior
Simulate how thermal runaway (TR) starts and spreads within modular marine battery systems.

a) Analyze the effect of TR starting at the top, middle, or bottom module within a rack on flame direction, heat release, and fire growth.
b) Model the progression of TR from cell → module → rack → battery room, including how rack spacing affects fire spread.
c) Assess the influence of battery State of Charge (SOC) (0%, 25%, 50%, 75%, 100%) on: Heat release rate (HRR), Total heat released (THR), Combustion duration and flame behaviour.

Evaluating Battery Room Size, Layout, and Structural Fire Risk
Estimate how fire affects the structure of the battery room based on different room sizes and rack configurations.

a) Simulate heat flux to structural steel and determine when the fire's energy output exceeds the melting thresholds of the: Roof only, Roof + walls, Entire battery room enclosure.
b) Estimate the minimum required steel for battery room to avoid failure under thermal stress during worst-case fire events.

Investigating the Role of Seawater Submersion in Delaying Structural Failure
Assess the effect of partial and full seawater flooding of the battery room on fire suppression.

a) Model how flooding at different time steps after TR affects combustion and steel melting timelines.
b) Evaluate whether seawater slows down or stops TR propagation, especially in rooms with higher capacities and compact layouts.
c) Analyze how room shape and space distribution influence the effectiveness of submersion in limiting structural damage.

2 Literature review

2.1 Installation of Lithium-ion Battery Systems on Ships

A lithium-ion battery system installed on a ship consists of several layers. At the smallest level, individual cells are grouped together into modules. Several modules form a sub-pack, and multiple sub-packs make up a complete battery pack. As shown in Fig 12, each level includes sensors and is managed by control systems such as the Battery Management System (BMS) and sub-BMS. These systems monitor temperature, voltage, and current to ensure the battery operates within safe limits. The battery room includes not only the battery packs but also systems for ventilation, fire suppression, thermal management, and emergency disconnection.[31]

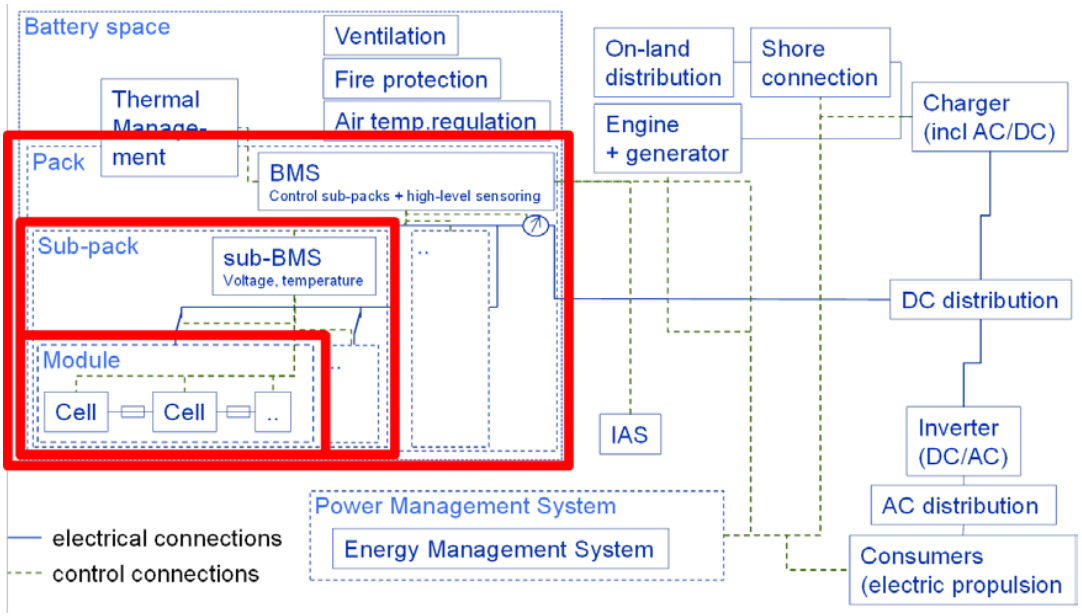

Figure 12 Battery System and related sub-systems.

2.2 Hierarchical Structure of Battery Units

At the cell level, failures may be caused by internal short circuits, often triggered by mechanical deformation, particle contamination, or dendrite growth. External heating, overcharging, or physical penetration can also cause the cell temperature to rise, as shown in the figure 6. This can lead to exothermic reactions inside the cell, resulting in venting of gases, fire, or even explosion. At the module and sub-pack level, problems such as sensor failure, control errors, loss of cooling, or insulation faults can occur.[32]

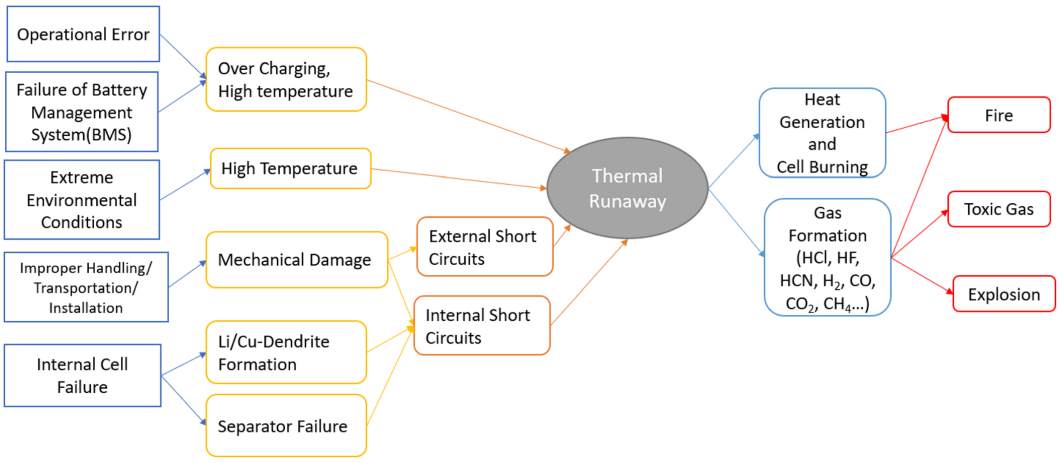

Figure 13 Li-ion battery thermal runaway schematic.[33]

The TR process gives off heat and flame at the cell level, which can quickly affect cells nearby in a battery module. The jet flame and hot gases from a burning cell can heat up cells nearby, which could set off their TR in a cascading way. This cell-to-cell spread can cover an entire module if it isn't stopped. Also, a module that is on fire can set off other modules in the same rack or pack, because the heat and fire can spread to nearby modules and shut down the whole system. Each level in the hierarchy increases the risk and gives you chances to do something about it. [33]

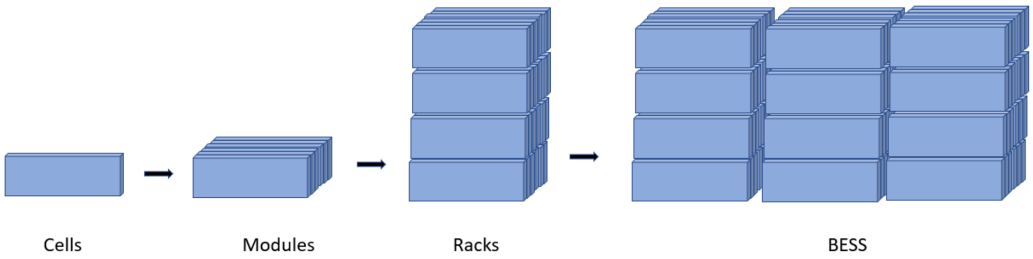

Figure 14 General BESS arrangement

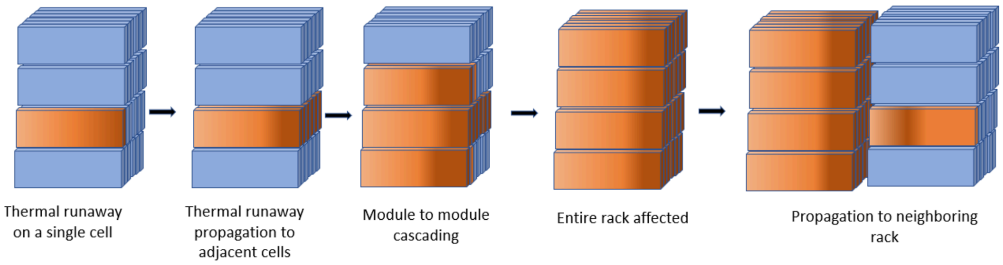

Figure 15 Thermal runaway propagation phenomenon in a BESS

2.3 Regulatory Requirements (A0 and A60 Standards)

DNV classifies these risks into different categories and requires a systematic approach to managing them. Ventilation systems must be able to perform at least 6 air changes per hour (ACH) and be designed to prevent the build-up of flammable gases. The most common gases released during thermal runaway include hydrogen, carbon monoxide, carbon dioxide, and various hydrocarbon vapors. These gases are toxic, corrosive, and potentially explosive. Therefore, gas sensors must be installed in the battery room, and certain automatic responses are mandatory. At 30% of the lower flammability limit (LFL), the battery system must automatically disconnect. At 60% of LFL, emergency ventilation must be activated. In the case of an explosion, pressure relief panels must open to limit the pressure to 0.05 barg or less [barg = pressure above atmospheric; 0.05 barg = ~5 kPa]. Without proper venting, explosion pressure can exceed 6-8 barg in enclosed rooms, posing a severe threat to the structural integrity of the battery space.[32]

DNV also mandates that the battery space must meet fire resistance standards of at least A-0, and A-60. To further protect adjacent spaces, battery rooms are typically built with A-class fire divisions: A-0 prevents flame spread but gives no insulation time, while A-60 can withstand fire for 60 minutes with limited heat transfer (≤180 °C on the unexposed side). Battery systems must be designed so that thermal runaway can be contained either at the module level or at least within the battery room. If containment cannot be guaranteed, additional physical barriers or passive cooling strategies must be used. Furthermore, DNV recognizes the possibility of flooding and requires an assessment of seawater submersion risks. Saltwater intrusion can lead to short circuits and dangerous gas formation, particularly hydrogen, and may trigger arc faults if not properly isolated.[32]

2.4 Thermal Runaway Phenomenon

Recent research has shown that a thermal runaway (TR) event that begins in an intermediate layer can spread vertically to the layers that are adjacent to it in stacked battery solutions. TR was triggered in the middle layer (Layer 2), it would then ignite both the upper layer (Layer 1) and the lower layer (Layer 3). The upward propagation was more aggressive, characterized by higher heat release and faster energy transfer, whereas the downward spread was delayed and less intense. The study found that propagation delays might be as long as 226 seconds within the same layer, and they could be as long as 596 seconds between adjacent layers.

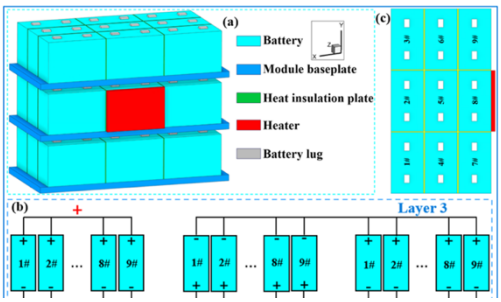

Figure 16 Overall structure and electrical connection of the EMBC. (a) Overall structure of the EMBC; (b) Electrical connection of the EMBC; (c) Battery arrangement diagram of the same layer. [3]

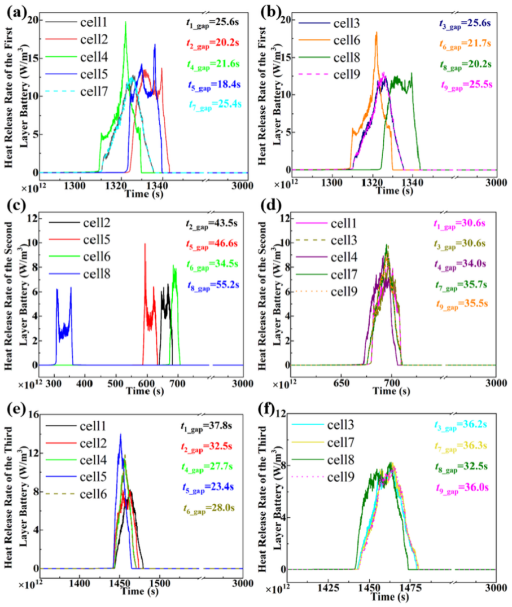

Figure 17 HR rate of the battery. t1_gap is the battery No. 1 HR duration. (a) and (b), HR rate of Layer 1 battery; (c) and (d), HR rate of Layer 2 battery; (e) and (f), HR rate of Layer 3 battery.

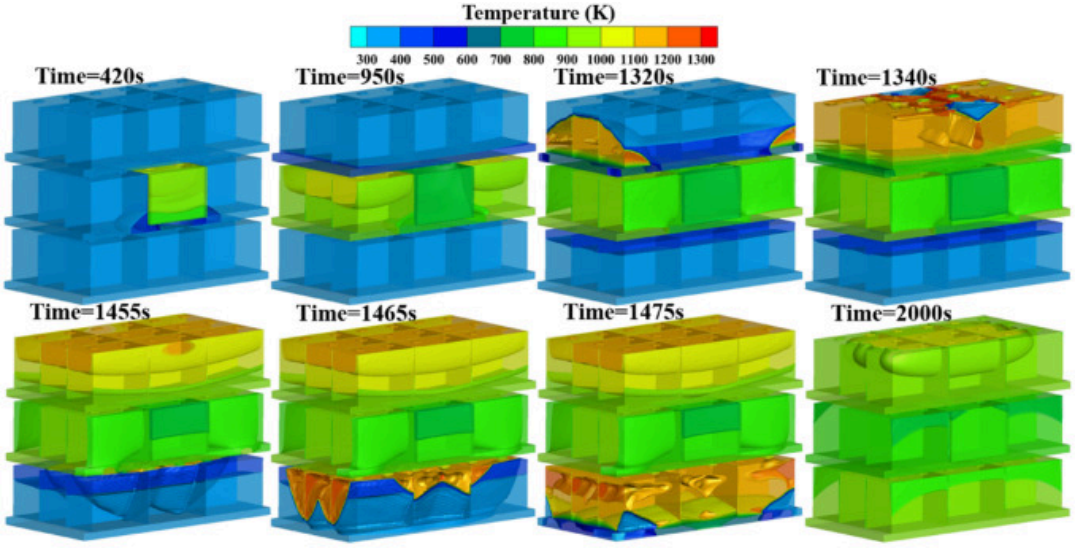

Figure 18 Transient temperature of EMBC TR.

As shown in Figure 19, the triangular plot of maximum temperature, total heat output, and time of combustion provides a clear illustration of this phenomenon. When TR began in Layer 2, the adjoining top layer, which was Layer 1, had the highest peak temperature (1568 K) and the longest heat release duration (up to 860 s). This was mostly caused by the vertical convective heat increase and the preheating of the material. In contrast, the lower

layer, which was Layer 3, had much lower peak temperatures (including temperatures as low as 1160 K) and shorter durations of combustion, which reflected delayed and attenuated downward propagation. A variation in the overall heat release was also seen, with the top layer gathering the greatest amount of energy. Heat rises upward and amplifies the thermal impact in upper levels, which is why bottom-initiated TR situations are the most dangerous in vertical cabinet arrangements. It is clear from these data that layer-level thermal barriers, top-down venting, and the strategic positioning of high-risk components in lower sections of marine battery systems are all necessary. [3]

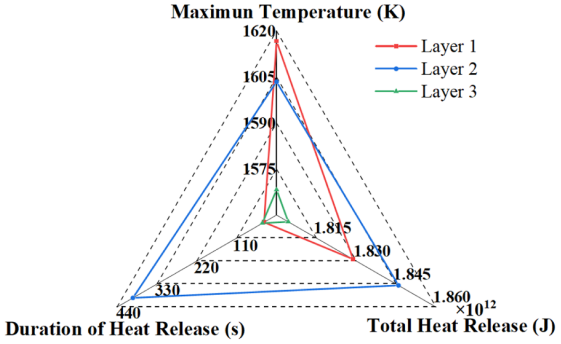

Figure 19 Thermal runaway parameters across layers.[3]

FM Global [4] conducted comprehensive fire tests on lithium iron phosphate (LFP) battery energy storage modules to characterize their fire behavior and hazards. In these experiments, a single LFP battery module 5,1 kWh was heated with external radiant heaters (flat 900 W heating elements mounted under the module) at a controlled rate to induce thermal runaway. In order to evaluate the amount of heat released and effluent gasses, the tests were carried out inside of a full-scale calorimetry hood. When the interior cells of the module reached a temperature of approximately 126 degrees Celsius, they started to release combustible gases, which were visible as white smoke. Following the occurrence of ignition, the burning LFP module went through a series of distinct stages of combustion. These stages included an initial jet of flame as the first cells went into runaway, a period of steady flaming combustion, and one or more secondary flare-ups as additional cells erupted. Finally, the fire died down gradually and extinguished itself. For a single 120Ah (LFP) module, the peak heat release rate (HRR) reached roughly 0.4 megawatts (MW), with around 0.21 megawatts of the HRR being convected into the environment. The total amount of heat that was released by a single module was approximately 140–150 MJ, which is roughly equivalent to half of the energy that was stored in the module.

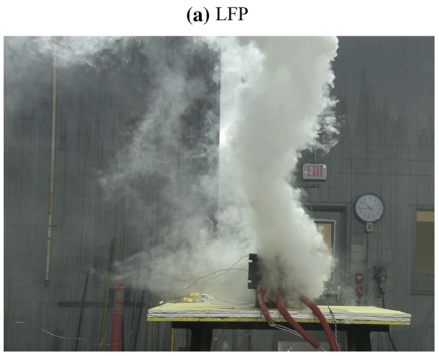

Figure 20 LFP batteries vented a thick white smoke.[4]

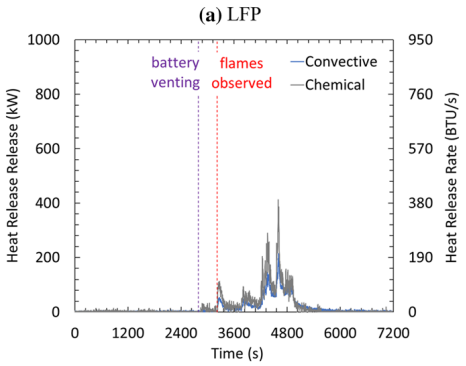

Figure 21 Single-module 5,3kWh heat release rate; LFP[4]

A representative heat release rate (HRR) profile Fig. 22 for a full-scale 16-module LFP battery rack fire test, showing both the convective HRR and the total chemical HRR as a function of time to illustrate the relationship between the two. The LFP rack displays a multi-peak fire development. Following an initial delay, the HRR increases as thermal runaway spreads from the lit module to the entire rack, reaching a peak of approximately 2.5 MW. Subsequently, the HRR steadily decreases as modules burn out. The large-scale fire test involved exposing a full LFP battery rack, which consisted of sixteen modules stacked in a metal cabinet with an open front, to the same overheating ignition approach at the bottom module.

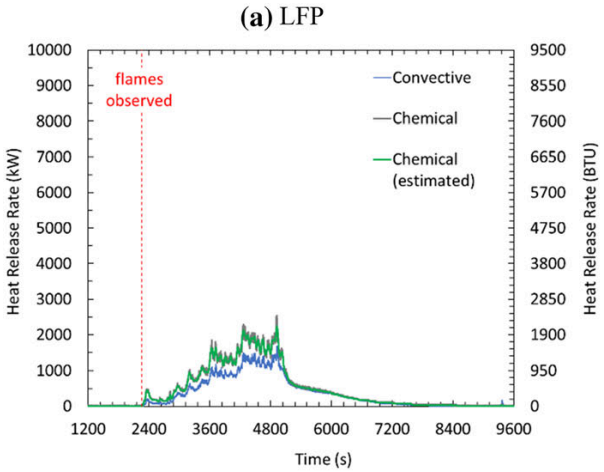

Figure 22 Large-scale (16 module) heat release rate for LFP[4]

The subsequent fire served as evidence that a failure of a single module may, in fact, result in the collapse of all of the modules contained within the rack. After around 37 minutes of heating, flames began to form at the face of the bottom LFP module. By approximately 1 hour 11 minutes into the test, the fire had passed through the stack and ignited every module in the stack. Flames were observed to reach roughly three meters above the rack at the height of the fire, and flame jets were venting out from the front entrance and even through holes in the top and rear of the rack, which indicated that the

rack was subjected to severe thermal exposure on all sides. After about 1.6 hours, only the top half of the modules were still on fire. After about 2.3 hours, the LFP rack fire put out itself without any help, leaving the metal structure of the rack badly damaged and warped from the heat. The heat release characteristics of the 16-module LFP rack followed a pattern that was comparable to that of the single module, but on a much greater scale. The LFP rack's highest HRR was about 2.54 MW (chemical), and its highest convective HRR was about 1.68 MW. During its whole length, the LFP rack fire produced about 3,810 MJ of energy, which is about 85% of the rack's theoretical chemical energy content. This means that the fire burned through almost all of the materials that could have caught fire. The heat flux sensors that were mounted all over the test enclosure recorded moderate quantities of thermal radiation that was caused by the LFP rack fire. For instance, at a few meters distance, the peak incident heat flux was on the order of 4–7 kW/m². This magnitude of heat flux is sufficient to cause heating and charring of nearby surfaces, and it has the potential to ignite adjacent combustibles if left exposed for a sufficient amount of time. However, it is lower than that of more energetic lithium chemistries, and as a result, it presents a somewhat reduced radiative fire spread hazard at a distance.

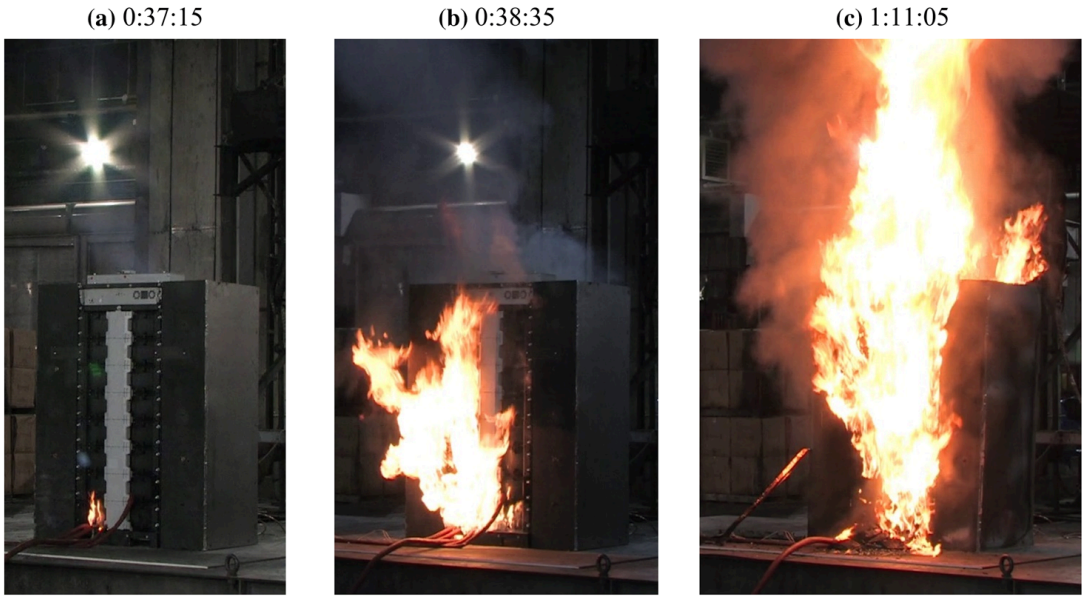

Figure 23 LFP fire development during large-scale (16 Modules) 83kWh free burn test: near time of ignition (a), near time of predicted sprinkler[4]

2.5 Control of Thermal Runaway

Meelapchotipong et al. (2024) looked into how well submerging cylindrical lithium-ion batteries in seawater stopped thermal runaway (TR) in 18650 NMC cells that were fully charged. The study used external heat abuse testing to mimic overheating, followed by submersion in either deionized (DI) water

or synthetic seawater (SSW) as soon as the voltage dropped from 4.2V to about 2.5V. This was done to set the voltage drop temperature, which served as a TR warning signal. Immersion in both liquids stopped TR development by lowering the temperature of the cells below the point of ignition. However, DI water kept the structure intact, while SSW led to rapid electrolytic discharge and serious corrosion after about 1.5 hours. The writers found three steps of TR, each with its own temperature and voltage pattern. They came to the conclusion that SOC was a key factor in starting internal short circuits around 100°C. Notably, nail penetration tests showed that even after submersion, leftover energy still posed risks of re-ignition.[34]

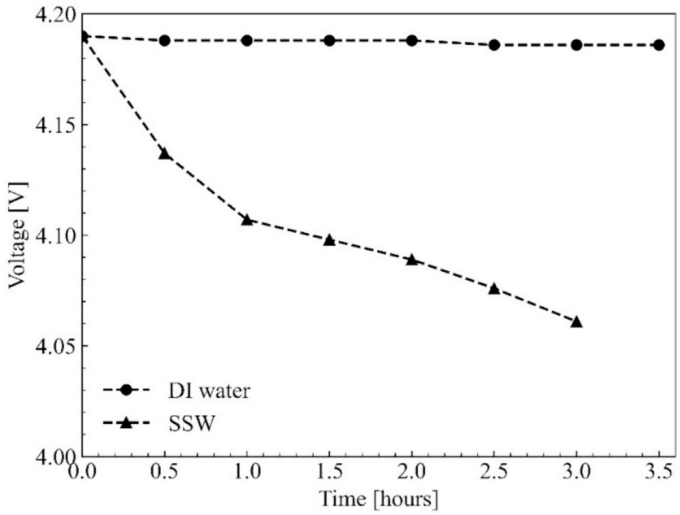

Figure 24 Voltage changes of fully charged lithium-ion battery (LIB) submerged in DI water and synthetic seawater (SSW).[34]

2.6 Hazard Level and Fire Test Observations

Zhou et al. studied how thermal runaway (TR) spreads in stacked lithium iron phosphate (LFP) battery cells in both horizontal and vertical directions. Two sets of four 3.2-V LFP prismatic cells (100% SOC) were put in a fire chamber, and three cells were mounted about 10 cm above it on wire mesh to make it look like a stacked battery cabinet. An external 500-W surface heater set off the TR in the first lower cell. To make sure there was a flame combustion (because LFP cells usually only vent white smoke and don't self-ignite), an igniter was turned on at the time of safety venting to light the gases that were released. The next step was watched by thermocouples and voltage sensors on each cell (1 Hz sampling) that recorded temperature jumps and voltage drops that marked the start of the safety vent (SV) and the transient (TR). Nine thermocouples placed in the space between the modules measured the temperature spread across the vertical flame, and video cameras recorded the burning process so that it could be studied.

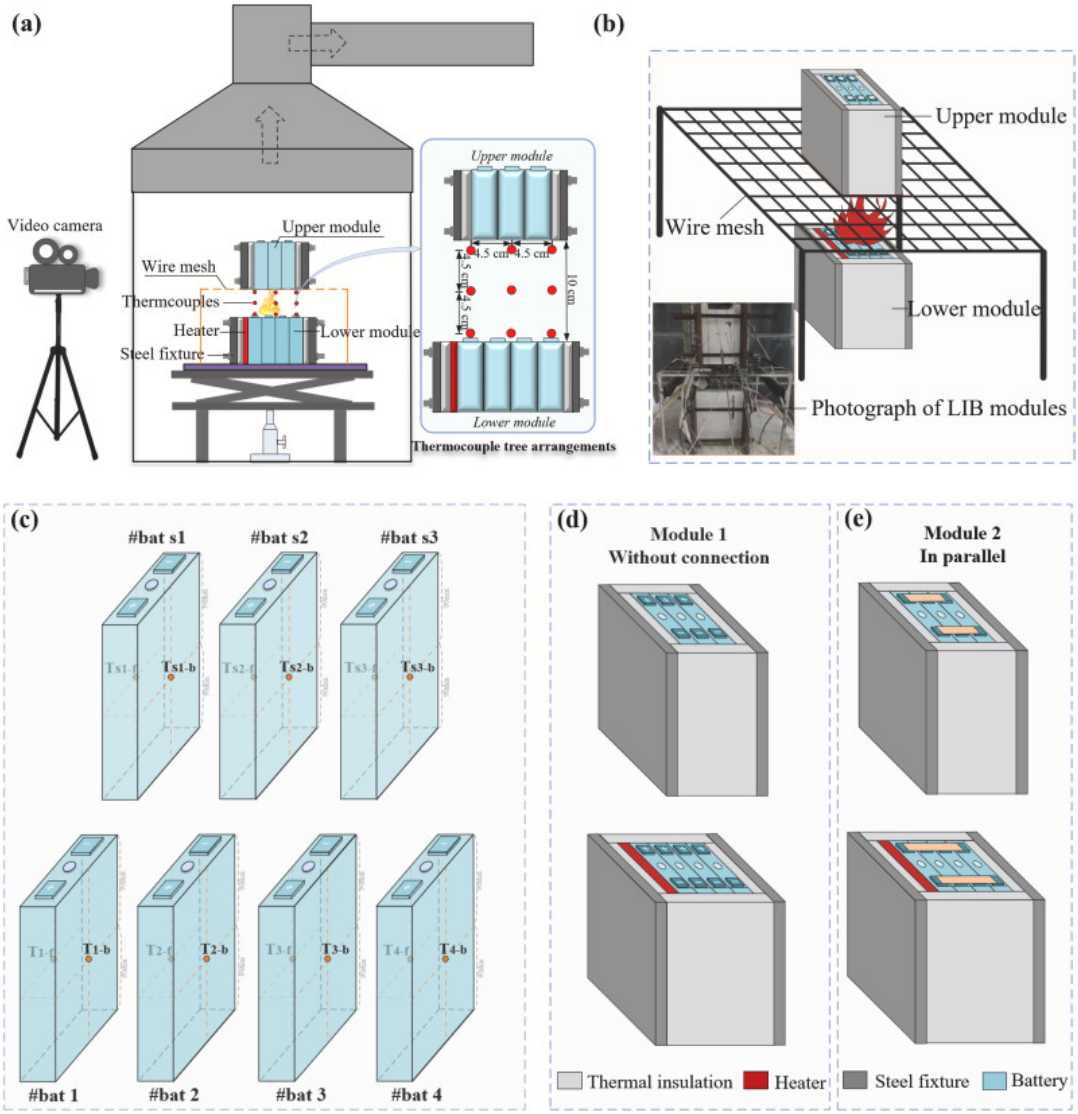

Figure 25 Schematic of the experimental setup: (a) experimental platform of TR propagation tests; (b) layout of the battery modules; (c) thermocouple arrangements of batteries; (d) configuration of the module without connection; (e) configuration of the module in parallel. [35]

According to Zhou et al.'s tests, horizontal (within-module) TR propagation was mainly caused by heat transfer between cells that were very close together. This created a chain reaction that went from one battery to the next. On the other hand, heat moved vertically to the upper module mostly through convection and radiation. Flames and hot gases rising from the burning lower cells heated the bottom of the upper module (a "ceiling jet" effect), and the rising plume (like a chimney draft) quickly warmed the upper cells. So, when the upper module cells were involved, several LFP cells went into TR almost at the same time, with stronger flames and higher peak temperatures (about 548 °C in the upper cells vs. about 423 °C in the lower cells). Notably, each lower-cell combustion only raised the temperatures of the upper-module cells by about 30–40°C, which wasn't enough to cause TR on its own.

However, the heat from the successive horizontal failures finally caused the upper cells to run away. This caused the upward spread to happen much faster and more severely. The upper module gave off about twice as much heat energy as the lower module (490.7 kJ vs. 217.7 kJ) and burned in a "extreme" way.[35]

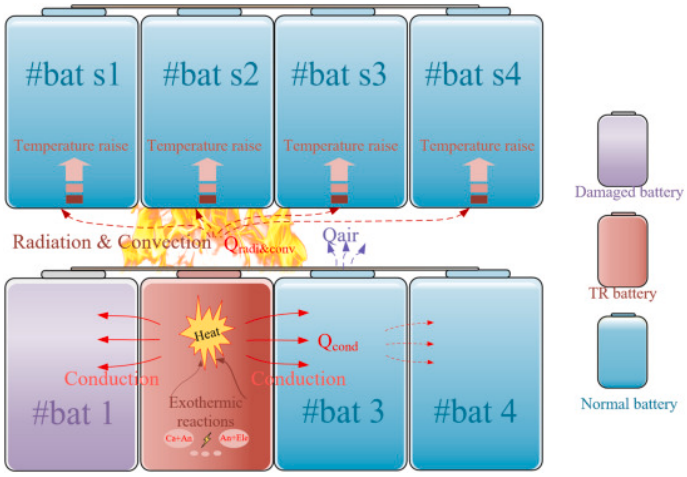

Figure 26 TR propagation along horizontal and vertical directions for battery modules. [35]

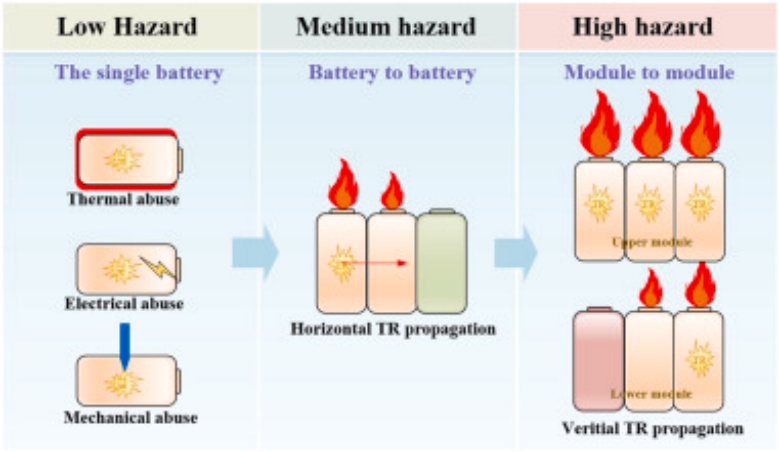

Figure 27 The developmental sequence of TR in energy storage systems.[35]

Another full-scale experiment to study how a 50 Ah lithium iron phosphate (LFP) battery module behaved in a fire when exposed to radiant heat. They focused on measuring the heat release rate (HRR) and total heat release (THR) using oxygen consumption calorimetry. The HRR-time curve (Figure 28) shows that large-format prismatic cell modules have a complex combustion process with multiple peaks. After a heating delay of about 700 to 800 seconds, the first major HRR peak (~56.1 kW) marks the start of venting and the first flame ignition. Next, there are sharp peaks at 166 kW, 288 kW, and 314 kW at about 1350 seconds, which show that each cell or submodule is

involved and the jet flame is ejected. After the radiant burner was turned off after about 1500 seconds, the module continued to burn very hot, with two more steps of combustion reaching their highest points at 170 kW and 190 kW, respectively, before slowly dying out. There was a peak in the red THR curve, which shows that the combustion took about 3000 seconds and released 269.5 MJ of heat. [36]

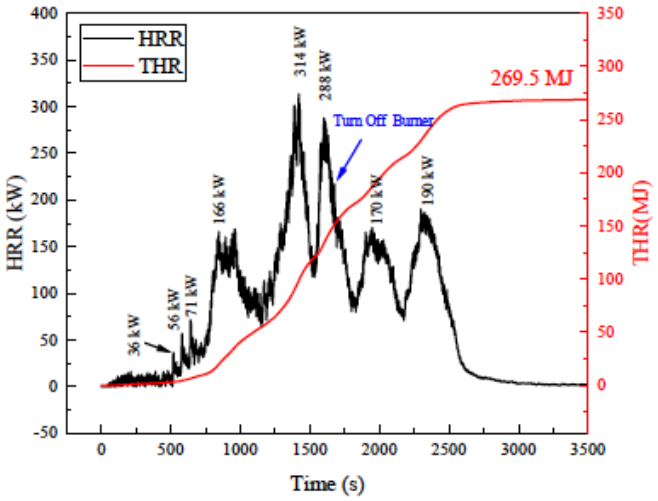

Figure 28 HRR and THR variations for LIB pack at different combustion states.[36]

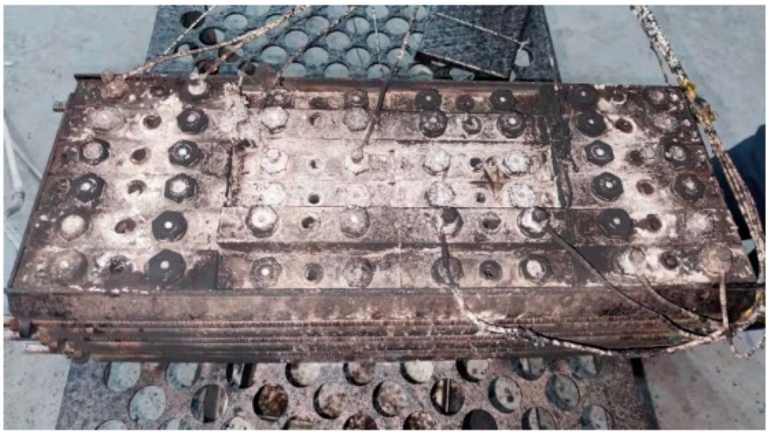

Figure 29 Picture of the LIB pack after the combustion test.[36]

2.7 DNV Guidelines on Battery Room Design and Failure Modes

One important safety design limit that is now in place is a limit on how much energy a single battery compartment can hold. In 2023, Det Norske Veritas (DNV), a well-known classification society, changed its rules to limit the amount of energy that can be stored in a single battery room to 5 MWh. This 5 MWh level is the minimum, and any higher level needs extra safety measures to get approval. DNV's class rules say that installations of up to about 25 MWh in a single battery space are only allowed if better fire protection and risk reduction systems are put in place.

After a 2019 battery fire on the ferry MF Ytterøyningen and a subsequent fire aboard MS Brim, investigators discovered that existing standards were inadequate and that "traditional extinguishing systems have limited effect" on Li-ion battery fires. In response, the Norwegian government made safety recommendations that called for "compensatory measures" to protect passengers and crew in case of a battery fire. These represent regulatory measures at the governmental level, which influence national safety requirements.

Now, any installation that uses more than 5 MWh of energy in one place must have special equipments for fire protection, cooling, and venting. For example, rules say that a battery room above the threshold must have an automatic fire-extinguishing system that can inert the air, as well as a water-based sprinkler or spray to keep things cool all the time. Flooding with an inert gas like nitrogen or CO_2 will take away the oxygen from a lithium-ion fire. Water mist will absorb heat to stop the fire from starting again and keep it from getting out of control.[37]

At the same time as these new rules, battery makers and ship designers have been making energy storage systems (ESS) bigger while also adding the safety features that are needed. The Corvus Blue Whale ESS is a good example of this. It's a next-generation marine battery system that can be used in installations with a total capacity of more than 10 MWh. [38] The Blue Whale was made just for big vessels, like cruise ships, Ro-Pax ferries, and offshore support vessels, that need a lot of energy to run without polluting the air. These kinds of systems can provide 20-25 MWh of power per ship. In fact, the world's first fully electric offshore vessel, the eCSOV, will have a 25 MWh Blue Whale battery, which is the biggest lithium-iron-phosphate (LFP) maritime battery deployment to date.[39] This 25 MWh Blue Whale installation has been approved by DNV after demonstrating compliance with the latest class rules. [40]

2.7.1 Thermal Runaway Prevention

The main goal of DNV's class rules is to stop and control thermal runaway in lithium-ion batteries. The battery management system (BMS) is very important. It needs to monitor the cells conditions (temperature, voltage, and current). This keeps batteries working in safe ranges and avoid triggering thermal runaway. In the design, physical barriers and module design are expected to limit propagation if a cell does fail. Ideally, a single cell's failure should not spread to neighbouring cells ("module shall inhibit propagation from cell to cell"). A failure in one cell should not affect cells nearby. The rules say that the event must be contained, even if propagation isn't completely stopped. For example, during a thermal incident, the outside of a battery module should stay below about 130 °C, and no flames should escape. The rules try to protect the rest of the battery system and give crews time to respond before a small failure turns into a bigger fire by keeping any thermal runaway to the smallest level possible (cell or module).

2.7.2 Ventilation and Explosion Relief

DNV class rules specify that there must be good ventilation so that any gas that leaks out of a broken battery (like hydrogen or electrolyte vapor) can be quickly removed from the area. The rules require a minimum ventilation rate of 6 (ACH) in the battery room. This fast exchange of air lowers the levels of flammable gases and gets rid of them, keeping them well below explosive levels.

DNV's class rules also cover the worst-case scenarios by requiring explosion relief measures. The battery space must safely vent the pressure if the flammable gas does catch fire so that the structure isn't damaged. It is best to use explosion venting panels that open at a low pressure (about 0.05 bar gauge). These panels let off pressure at about 50 mbar (millibar), which keeps any deflagration in the battery room from building to a dangerous level. The overpressure is vented to a safe area outside.[32]

2.7.3 Fire Detection and Suppression

DNV's safety rules also prioritize early fire detection and effective suppression to manage a battery fire if it occurs. The goal is to catch a thermal event early and cool the batteries down so that the fire doesn't spread. In the battery space, you usually need conventional smoke detectors or other early fire sensors for quick detection of any cells burning or overheating. When

something is detected, the response systems (alarms, changes to ventilation, and actions by the BMS) kick in to handle the situation.

To quickly cool the batteries and put out the flames, a fixed fire extinguishing system (usually water-based, like a water mist or sprinkler system) is usually needed. Water-based suppression is preferred because of its cooling capacity. The class rules make sure there is enough water or suppressant available, since a battery fire can last a long time and start up again if it isn't cooled down enough. The class rules say that if a fire gets too big for the suppression system to handle (for example, if it involves more than one battery module), it may become uncontrollable. In that case, the priority changes to saving lives (evacuating people).[32]

In summary, DNV's battery safety rules are based on three pillars: thermal runaway prevention, ventilation, and fire suppression. Each one deals with a different hazard such as cells getting too hot, gas leaking, and fire. But they all have the same goal: to lower the chances of batteries failing. DNV's class rules include design measures (like propagation-resistant modules and vent panels) and system requirements (like gas ventilation rates, detectors, and extinguishing systems). The main goal is to protect the ship and crew by stopping any battery incident as soon as possible and keeping it as small as possible.

3 First Principles (Physics Based) Modelling Approach

This chapter presents a method that is both structured and generalizable for modeling the thermal behavior and fire propagation of lithium-ion battery energy storage systems (BESS) being used in marine applications.

For analysis, a hierarchical framework is used instead of full models of specific systems to show how thermal runaway (TR) events happen in real marine battery systems. The investigation begins with the smallest component, which is the battery cell or module, and then progresses to the rack level, and finally reaches the entire battery room. At each stage, important thermal parameters are measured and tracked over time, these include the rate of heat release (HRR), the total heat release (THR) and combustion duration.

The main goal is to figure out how thermal runaway starts and spreads from one module in a rack to another and from one rack in a battery room to another. By doing so, we are able to observe how the state of charge (SOC), the distance between racks, and the Battery room size play a role in determining the rate at which a fire spreads, the point at which secondary racks begin to burn, and the amount of heat battery room steel walls experience. The end result is an estimation of the time at which structural boundaries, such as steel bulkheads, might become excessively hot and start melt.

This modeling system is set up in Excel by utilizing a combination of empirical scaling laws, data from fire tests that have been published in the literature. The primary assumptions, simplifications, and physical laws that govern the process are outlined in this chapter. In addition to that, it provides a step-by-step guide that can be utilized with any battery configuration.

Module Fire Modeling → Rack Fire Propagation → Room-Level Simulation

3.1 Overall Modeling Strategy

The method begins at the level of the battery module and then progresses upwards to the rack and room levels to illustrate the progression of fire throughout the building. The model does not assume that the ignition point with in rack is always the same; rather, it considers many different ignition positions in a battery rack, such as fires that begin at the bottom, the middle, or the top, and it records how heat release, combustion duration, and thermal runaway (TR) spread throughout the system.

There are three primary steps throughout the modeling process:

Module Level Fire Behavior As shown in (Fig. 30) First, we determine a realistic heat release curve for one module. This is based on data from fire tests that were published in the literature such as FM Global fire test [4] , which shows that only a portion of the battery's total energy is released when it is exposed to fire. Using reduction factors from experiments, the module's theoretical energy is turned into an estimated THR for both chemical and convective transfer. Then, the normalized HRR curve is adjusted to match the expected THR, combustion time, and peak HRR of the module. This makes an HRR series that is time-resolved for one module.

Rack Level Fire Propogation As shown in (Fig. 30) Once we know the HRR series for one module, we can model how the fire spreads amongst modules that are stacked on top of each other in a rack. The thermal runaway could begin at the top, the middle, or the bottom of the rack, depending on the situation. Based on where the ignition is, the model figures out how much heat needs to be released off before the next module is ignited. Time delays and energy threshold are utilized, and scaling variables are utilized to alter the duration of time that the higher or lower modules burn, as well as the peak HRR. The result is a stacked, time shifted HRR series for the whole rack that shows how the fire spreads up and down.

Room Level Fire Simulation As shown in (Fig. 31) The next stage is to determine how horizontal propagation happens between racks in a battery room when the whole HRR and THR output of one rack has been estimated. According to the FM Global [4] , when one rack burns, it causes the racks that are nearby to receive heat. We use the idea that the flame source is in the middle of the burning rack to figure out the radiative heat flux at different heights and distances. If the heat flux that another rack receives exceeds a certain level, then it is believed that rack will enter TR after a short period of time. Depending on how the room is set up, this pattern goes on across the room.

Parameters like state of charge (SOC) and inter-rack spacing are adjustable inputs in the model. When SOC levels are higher, fires burn hotter and spread faster. When racks are further apart, it may take longer for fires to spread, or they may not start at all. Based on how long and how much energy is in the space, the model also guesses when the steel structure would start to deteriorate or melt.

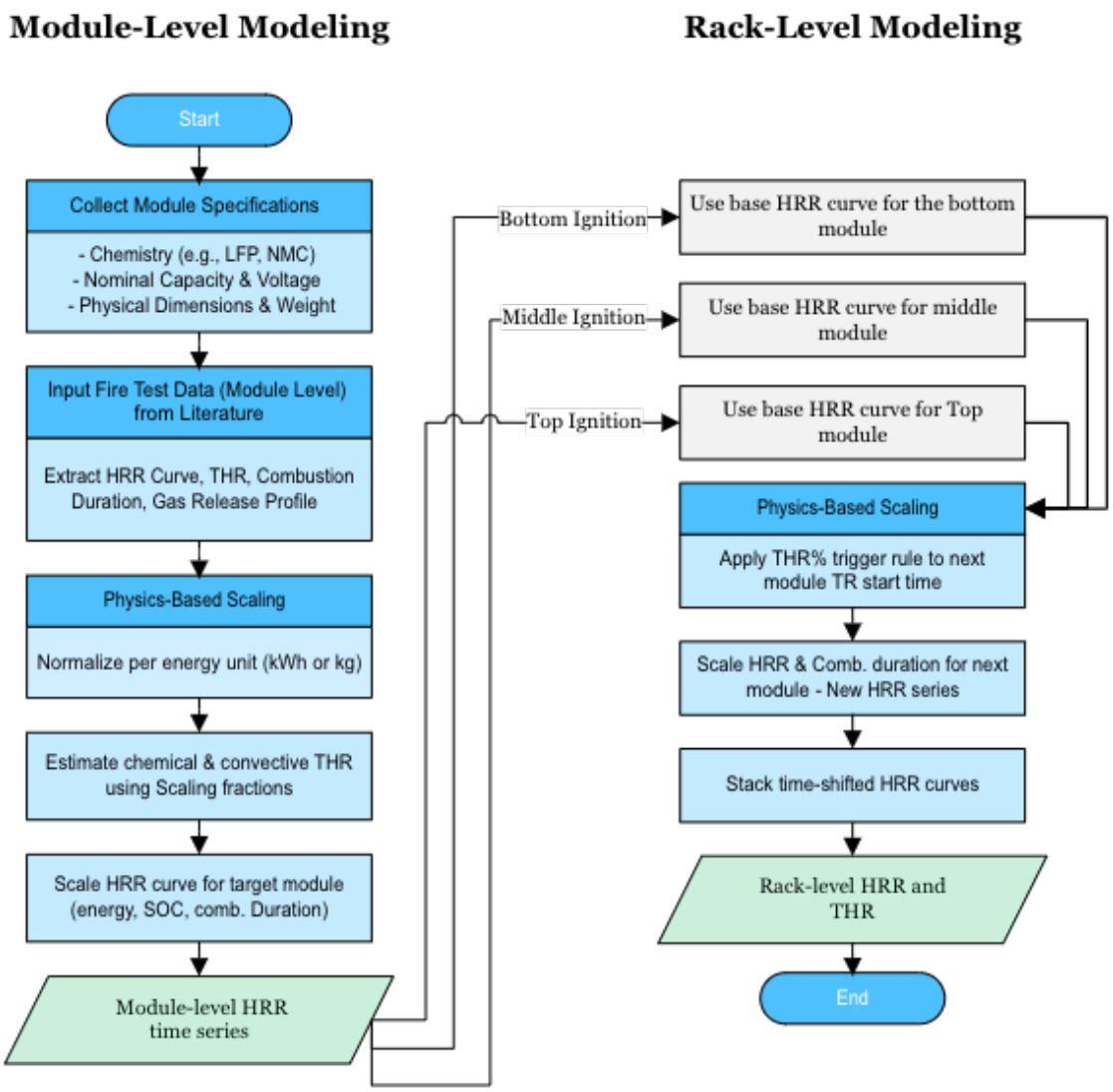

Figure 30 Methodology Overview for Fire Propagation Modeling Module and Rack Level

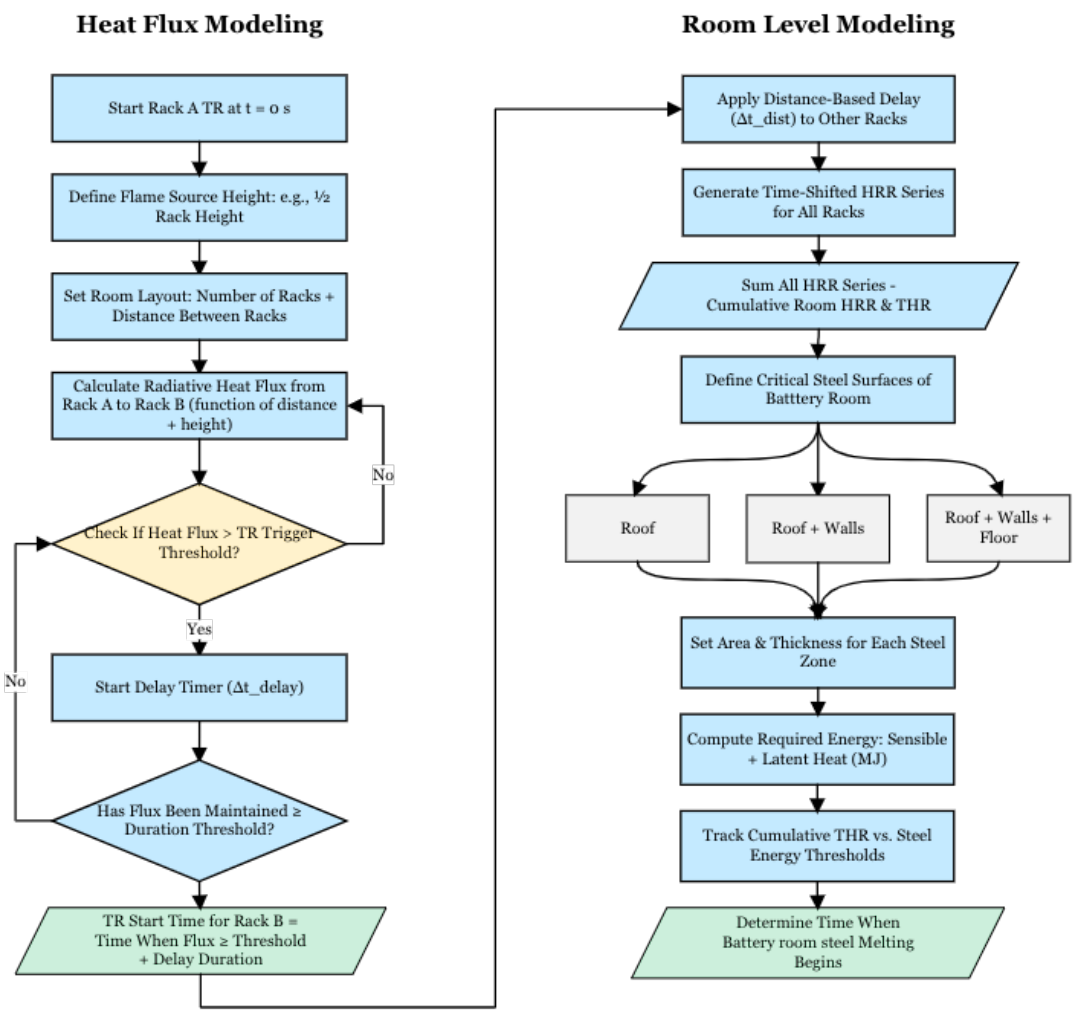

Figure 31 Methodology Overview for Fire Propagation Modeling Heat Flux and Battery Room

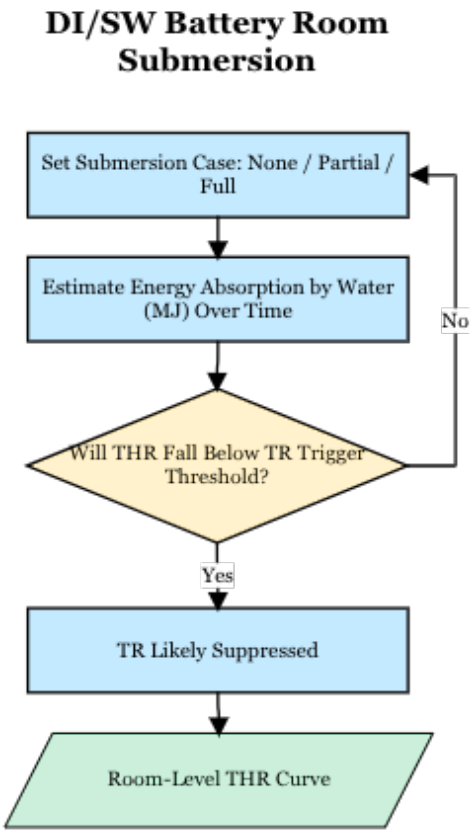

Figure 32 Methodology Overview for Fire Propagation Modeling Battery Room Submerssion

Assumptions and Physical Principles

Thermal runaway (TR) is a harmful chain reaction that can happen in a battery when it becomes too hot. The materials inside the battery start to break down if the heat inside builds up faster than it can get out. This lets out gases that can catch fire, and if the temperature is high enough, the gases can catch fire, which can cause flames, jets of flame, and more heat release. When TR starts in one portion of a battery, it can spread to other parts, making the fire bigger.

This model says that thermal runaway goes through these essential steps:

1. The first module gets hotter and hotter
2. Gases that catch fire are let out
3. The gasses catch fire, making a flame and heat.
4. That heat moves to nearby racks or modules.
5. If they get hot enough, new modules might catch fire.

This model is based on a few important fire science principles:

Heat Release Rate (HRR)
This is the rate at which energy is released during combustion. It's measured in kilowatts (kW). HRR is the main indicator of fire intensity.

Total Heat Release (THR)
This is the total amount of energy that the fire let off. It's the cumulative area under the HRR curve over the burning duration (t), which is usually given in megajoules (MJ). If the total THR is known, the HRR curve can be scaled to fit the desired peak and duration.

$$\mathrm{THR} = \int_0^{t_{\mathrm{end}}} \mathrm{HRR}(t)\ dt \qquad (1)$$

This is used to scale experimental HRR shapes to larger modules.

Radiative Heat Transfer
Fire emits heat through radiation, which can heat up other racks without direct contact. The model uses radiative heat flux to estimate when a neighbouring rack might goes into thermal runaway. [4]

$$q'' = \frac{\chi_r \cdot Q}{4\pi r^2} \qquad (2)$$

where q'' is the chemical HRR, and χ_r is the radiative fraction. The $1/r^2$ dependence follows directly from the conservation of radiant power over a spherical surface (inverse-square law), as presented in standard fire radiation theory [41]. The radiative fraction χ_r is taken from FM Global module- and rack-scale fire tests, which reported values of 0.3–0.4 for prismatic LFP modules.[4]

Heat Flux Threshold
This is the minimum amount of radiative heat (kW/m²) that must hit a surface for a long enough time to cause thermal runaway in another rack.

It is assumed that the fire does not release all of the energy that is stored in a set of batteries. According to the results of fire experiments in literature Chapter 2, only a small fraction of the chemical energy that is theoretically present is converted into heat.

Furthermore, the model assumes that the amount of heat released from the module below (or above) is determined by vertical propagation within a rack, and that the amount of radiative heat flux received determines horizontal propagation between racks. To ignite, a neighbouring rack it must first

receive an adequate amount of energy or flux, which is delayed by a period of time that accounts for the resistance to ignition. [41]

3.2 Module Level TR Propagation and HRR Estimation

To simulate thermal runaway in battery rooms, an accurate estimate of the heat release profile of a single battery module is required. This section describes a generalized method for estimating a module's heat release rate (HRR) curve and total heat release (THR). The method makes use of data derived from full-scale fire tests on lithium iron phosphate (LFP) battery systems comparable to the module under consideration.

The modelling approach assumes that the total energy released during a module fire is made up of two components as discussed in Chapter 2: chemical energy stored in the battery's combustible materials (such as plastics and electrolyte), and electrical energy stored as usable charge. These two contributions are added together to get an estimate of the module's theoretical total energy generated through combustion. Nonetheless, experimental fire tests have repeatedly shown that not all of this energy is released during combustion. In the real world, the observed heat release is the result of only a small fraction of the total energy available. To accurately represent the conditions that exist in the real world, correlation factors derived from empirical research are used.

3.2.1 Module Total Heat Release Scaling

The modelling process starts with estimating the module's composition. The module is based on the standard lithium-ion battery design and contains a variety of materials such as electrolyte and plastic separators. Each material is assigned a known heat of combustion (ΔH_a), typically expressed in MJ/kg. To calculate each combustible component's energy contribution, multiply its mass by its respective heat of combustion. [4]

$$E_{\text{chem}} = m_{\text{electrolyte}} \cdot \Delta H_{c,\text{electrolyte}} + m_{\text{plastic}} \cdot \Delta H_{c,\text{plastic}} \quad (3)$$

Furthermore, the electrical energy is included by converting the module's rated energy from kilowatt-hours (kWh) to megajoules (MJ), using the following relation:

$$E_{\text{electrical}} = E_{\text{kWh}} \times 3.6 \quad (4)$$

The total combustion energy is then calculated as:

$$E_{\text{total}} = E_{\text{chem}} + E_{\text{electrical}} \quad (5)$$

After calculating the theoretical total energy release, correction factors are used to estimate the realistic partitioning of chemical and convective THR seen in real fires. According to FM Global's large-scale ESS fire experiments [4] chemical THR accounts for 51% of total energy release, while convection accounts for 36%. In Eq. (6), they are given as empirical coefficients (k_1 and k_2) rather than numerical constants since the exact fractions can vary depending on battery chemistry, system design, and fire scenario. The values given here are for $LiFePO_4$ prismatic cell systems, and other chemistries (e.g., NMC or LCO) can have different partitioning factors.

$$\mathrm{THR}_{\mathrm{chem}} = k_1 \cdot E_{\mathrm{total}}, \quad \mathrm{THR}_{\mathrm{conv}} = k_2 \cdot E_{\mathrm{total}} \tag{6}$$

3.2.2 Module Combustion Duration Scaling

Combustion duration was scaled according to the square root of the ratio of target to reference THR. This assumption avoids the overestimation that would result from linear scaling, since larger fires burn more intensely due to increased flame feedback and radiative transfer. Fire dynamics theory [42] and large-scale FM Global ESS tests [4] both confirm that burn duration increases sub linearly with energy.

This method compares the total heat release (THR) of a known reference test module to that of the target module. The scaling factor is determined by calculating the ratio of these two energy values and taking its square root. This factor is then multiplied by the reference module's known burn duration to determine the new system's combustion duration.

$$\mathrm{Duration}_{\mathrm{target}} = \mathrm{Duration}_{\mathrm{reference}} \times \sqrt{\frac{\mathrm{THR}_{\mathrm{target}}}{\mathrm{THR}_{\mathrm{reference}}}} \tag{7}$$

This square-root relationship is the physical principle that burning time increases sublinearly with energy due to larger fires forming stronger flame feedback and radiative heat transfer, speeding up combustion.

3.2.3 Module Peak HRR Scaling

To estimate the peak Heat Release Rate (HRR) for a battery module when the total heat released (THR) is known, we use a simple scaling approach based on an existing HRR curve from a literature. First, we take the shape of the reference HRR curve, which depicts how heat is released over time, and adjust its height by changing the peak HRR value. This adjustment is made to ensure that the area under the scaled curve, which represents total energy released, matches the battery's known THR. In practice, each point on the original HRR curve is multiplied by a scaling factor proportional to the target

and reference peak HRR values. We adjust the peak HRR until all heat release values over time (HRR × time step) equal the desired THR. This method allows us to generate a realistic HRR curve for larger or different batteries without having to conduct additional experiments.

Equation to scale HRR

$$\mathrm{HRR}_{\mathrm{scaled}} = \mathrm{HRR}_{\mathrm{original}} \times \left(\frac{\mathrm{Peak\ HRR}_{\mathrm{target}}}{\mathrm{Peak\ HRR}_{\mathrm{reference}}} \right) \tag{8}$$

Equation to calculate THR

$$\mathrm{THR} = \sum_{i=1}^{n} \mathrm{HRR}_i \times \Delta t \tag{9}$$

3.2.4 Module HRR vs Combustion Duration Curve

After determining the THR and Combustion Duration, the next step is to generate the HRR curve over time. Given that experimental HRR data from modules is available in the literature, the normalized HRR curve can be extracted. In most cases, this curve will show several flame events, including a delay in ignition, a peak fire intensity, and a gradual decay. The model does not create a new curve from scratch; rather, it keeps the shape of the experimental HRR curve and scales it to match the target module's estimated THR and combustion duration.

After that, the HRR curve is scaled vertically to determine the peak HRR that is desired, and then it is scaled horizontally to correspond with the anticipated combustion time. All of this scaling is determined by the following relation:

$$\mathrm{THR} = \int_0^{t_{\mathrm{end}}} \mathrm{HRR}(t)\ dt \tag{10}$$

HHR Curve Time Scaling

The time scaling factor is used to adjust the total duration of the fire's combustion process. If it is expected that the target module will burn for a longer period than the reference module, the curve will be stretched along the time direction. This represents the time scaling factor.

$$S_t = \frac{t_{\mathrm{target}}}{t_{\mathrm{ref}}} \tag{11}$$

Where,

t_{target} is the estimated combustion duration of the new module t_{ref} is the total duration of the reference fire test. Each time point in the reference HRR series is scaled by this factor to generate the corresponding time point for the target module.

Each point on the reference time axis is stretched using:

$$t_{\text{scaled}} = t_{\text{ref}} \cdot S_t \tag{12}$$

HRR Curve (Amplitude) Scaling
Once the time series is adjusted, the HRR amplitude must also be scaled to reflect the desired peak HRR. This is done using the HRR scaling factor Sq , calculated as:

$$S_q = \frac{Q_{\text{target,peak}}}{Q_{\text{ref,peak}}} \tag{13}$$

Where:
$Q_{\text{target,peak}}$ peak is the peak heat release rate (HRR) of the module to be modeled $Q_{\text{ref,peak}}$ is the peak HRR from the reference fire test. This scaling factor is multiplied by each HRR data point in the reference curve to generate the HRR profile for the new module.

The scaled HRR value at time t is:

$$\text{HRR}_{\text{scaled}}(t) = \text{HRR}_{\text{ref}}\left(\frac{t}{S_t}\right) \cdot S_q \tag{14}$$

This ensures that the area under the scaled HRR curve integrates to match the expected THR:

$$\int_0^{t_{\text{target}}} \text{HRR}_{\text{scaled}}(t)\ dt = \text{THR}_{\text{target}} \tag{15}$$

Finally, the HRR curve that was generated is used as the input for the modeling steps that are performed at the rack-level and room-level. It serves as the basis for the simulation of thermal runaway propagation and is used for evaluating aspects such as the duration of the flame, the timing of the trigger for neighboring modules, and the total energy load in the battery room. The model is able to maintain its adaptability to a variety of module sizes, designs, and Battery chemical compositions e.g NMC, NCA. The following table gives an overview of how to get the scaled HRR curve:

Input Values	
Peak HRR	= [to be calculated]
Combustion Time	$t_{\text{target}} = t_{\text{ref}} \times \sqrt{\frac{\text{THR}_{\text{target}}}{\text{THR}_{\text{ref}}}}$
Ref Peak HRR	= given
THR_target	= given
THR_ref	$\text{THR}_{\text{ref}} = \sum(\text{HRR}_{\text{ref}} \times \Delta t)$

Known		To Find		
Time (Sec)	**Ref HRR (kW)**	**Time (Scaled)**	**Scaled HRR (kW)**	**Energy Segment (kJ)**
t_{ref}	HRR_{ref}	$t_{\text{scaled}} = t_{\text{ref}} \cdot S_t$	$\text{HRR}_{\text{target}}(t) = \text{HRR}_{\text{ref}}(t) \times \left(\frac{\text{Peak HRR}_{\text{target}}}{\text{Peak HRR}_{\text{ref}}}\right)$	$E_{\text{segment},i} = \text{HRR}_i \times \Delta t$

Table 2 Input parameters for scaled HRR calculation. Reference values and equations used for HRR and THR Curve scaling.

3.2.5 SOC-Dependent Scaling

The state of charge (SOC) of a battery module has a significant impact on both thermal runaway behavior and fire intensity. As the state of charge (SOC) of the battery decreases, so does the amount of chemical energy available within it, which has a direct impact on fire dynamics. Modules with a high state of charge (SOC) tend to produce more violent and intense fires, with higher peak heat release rates (HRR) and faster firing times. Modules with a lower SOC, on the other hand, burn slower and with less intensity, resulting in longer fire durations and a lower total heat rise (THR). SOC is treated as an input parameter in the model, influencing the scaling of THR, peak HRR, and combustion duration. The model alters the shape and magnitude of the HRR curve in response to general trends observed in experimental studies. Higher SOC values result in steeper and more intense HRR curves, whereas lower SOC values result in broader, flatter curves with slower fire growth.

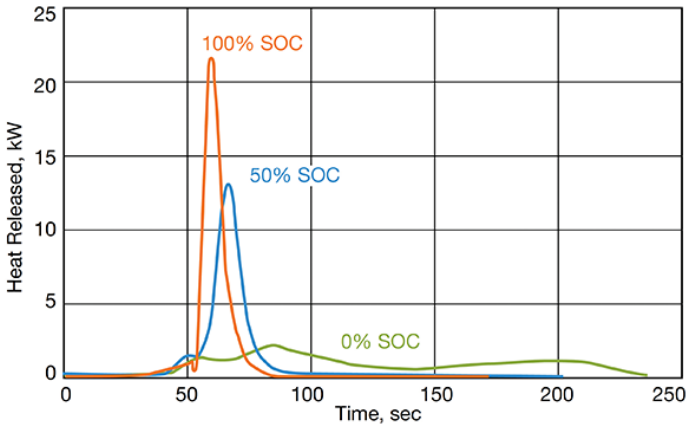

Figure 33 Heat release rate (HRR) during the combustion of a 7.7 Wh Li-ion cell at 0%, 50%, and 100% SOC[43]

Table 3 Battery SOC Scaling Summary

SOC Level	THR	Peak HRR	Combustion Duration	Fire Behavior Description
SOC (100%)	High	High	Short	Rapid and intense combustion, with the greatest release of energy
SOC (75%)	Moderate–High	Moderate–High	Moderate	Not as strong, but still energetic and quick-burning
SOC (50%)	Moderate	Moderate	Longer	Fire growth is slower, and it releases less energy.
SOC (25%)	Low	Low	Extended	Weak combustion, slow spread, and not much of a fire risk.
SOC (0%)	Very Low	Minimal or None	Long or negligible	It's not likely that the fire will last long; it may not start a thermal runaway.

3.3 Rack-Level Thermal Runaway Propagation and HRR Estimation

After modeling the heat release behavior of a single battery module, the next step is to create the HRR profile for a battery rack containing all of the modules. A rack is made up of several modules stacked vertically above one another. Thermal runaway (TR) can spread to neighboring modules depending on the dynamics of the flame, gas venting, heat transfer, and the module's structural configuration. This section describes how the rack-level HRR curve is created by simulating the propagation of thermal runaway from one module to the next within the rack.

One of the most important ideas is that not all of the modules in a rack will ignite simultaneously. Instead, once thermal runaway (TR) begins in a single module (the base case), adjacent modules will enter thermal runaway if a specific trigger condition is met. This condition is defined by the total heat released by the module that came before it.

3.3.1 Triggering Rule for Next Module

The threshold condition is defined as a specific percentage of total heat released by the base module that is currently burning. During the simulation, the cumulative THR curve is tracked over time, and the time when the trigger threshold is crossed is recorded. This time value determines when the subsequent module's combustion process begins.

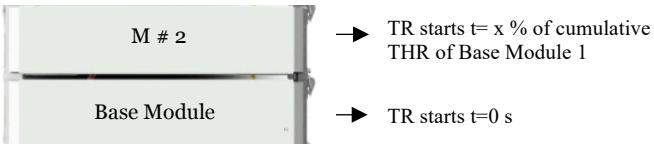

3.3.2 Generating HRR for the Next Module

Starting from the base module's combustion duration (as discussed in section 3.2.2), the duration for Module 2 is obtained by scaling it up or down depending on the thermal runaway propagation direction. With this new combustion duration, we then adjust the module's THR, since Module 2 will not have exactly the same duration or energy release as the base module. Using the updated THR and combustion duration, the two-step approach described in Chapter 3.2 is applied to generate a new HRR data series for Module 2. Finally, this HRR curve is assigned a delayed start time, as determined using the ignition delay procedure described in section 3.3.1.

1. Scaling of time based on the estimated amount of time required for combustion for the new module
2. Scaling of the amplitude based on the newly determined peak HRR

3.4 Propagation Scenarios: Bottom-Up, Middle-Out, Top-Down

There are different locations on the rack where thermal runaway can begin, and the behavior of the propagation varies depending on the direction:

3.4.1 Bottom-Up Propagation Scenario

In the bottom-up scenario, thermal runaway begins in the lowest module on the battery rack as shown in Fig. 34 and progresses upward in a sequential manner to higher modules. In this modeling approach, the first module, located at the bottom, serves as the reference scenario, and the behavior of the heat release from that module determines the fire's baseline shape, duration, and intensity. After a delay, the modules above it experience thermal runaway. This delay is defined by a predetermined fraction of the total heat release (THR) from the module directly beneath it. When the fractional THR is attained, the subsequent module's ignition is activated.

Each new module's HRR curve is created by scaling the reference curve (as discussed in section 3.3.2) with a module specific peak HRR factor and temporal scaling factor. After scaling, the curve is time-shifted to account for the ignition delay, which is caused by the triggering THR condition. The stacking of time-shifted HRR curves from bottom to top produces a realistic rack-level fire profile with overlapping fires, increased intensity, and shorter burn periods.

Table 4 Bottom-Up Propagation – Scaling Strategy Summary

Parameter	**Scaling Approach[44]**
Trigger Condition	THR-based threshold (e.g., 5–10% of previous module's THR)[44]
Start Delay	Time when triggering threshold is reached
Peak HRR	Scaled upward from one module to the next
Combustion Duration	Scaled downward (shorter) for upper modules - faster burning
THR	Slightly decreasing across modules

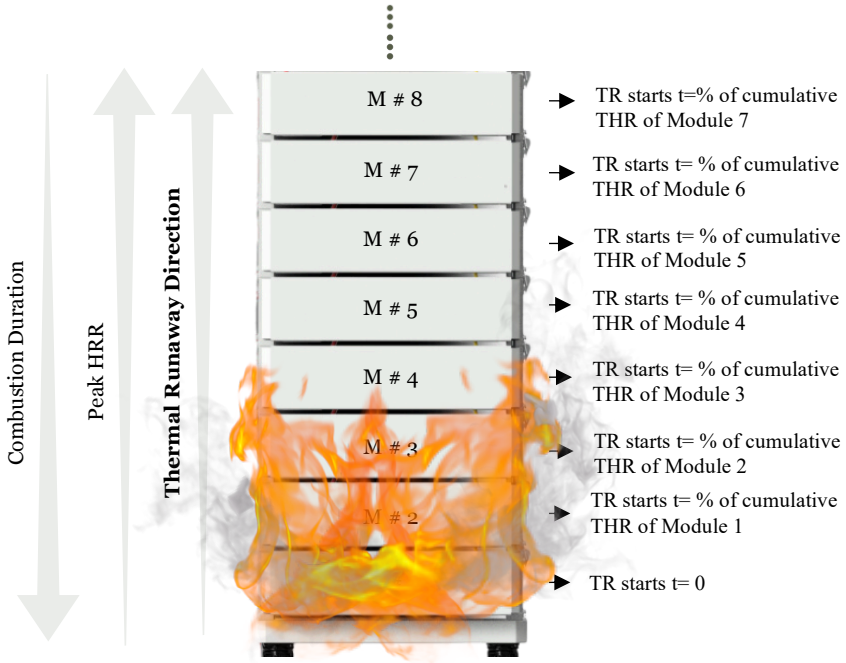

Figure 34 Bottom-Up Propagation Scenario

3.4.2 Middle-Out Propagation Scenario

The middle-out scenario involves the onset of thermal runaway in a module located in the centre of the battery rack as shown in Fig. 35. The fire spreads in two ways from this ignition point: upward to the top module and downward to the bottom module. Both directions are being propagated simultaneously.

First, the middle module is designated as the reference case in the modeling logic. The baseline HRR curve is then created by combining the middle module's total heat rate (THR), combustion duration, and peak HRR. The next modules are activated whenever a present percentage of the cumulative THR has been released from the module that came before them in their respective directions. This applies to both upward and downward branches.[44]

Table 5 Middle-Out Propagation – Scaling Strategy Summary

Parameter	Scaling Approach
Ignition Logic	TR initiates in a middle and propagates both upward/downward
Trigger Condition	THR-based threshold from the adjacent module
Start Delay	Calculated for each direction based on local trigger thresholds
Peak HRR	Scaled for upward and downward paths (higher upward)
Combustion Duration	Decreases for upward modules, can be longer downward
THR	Decreases slightly along both directions or kept constant

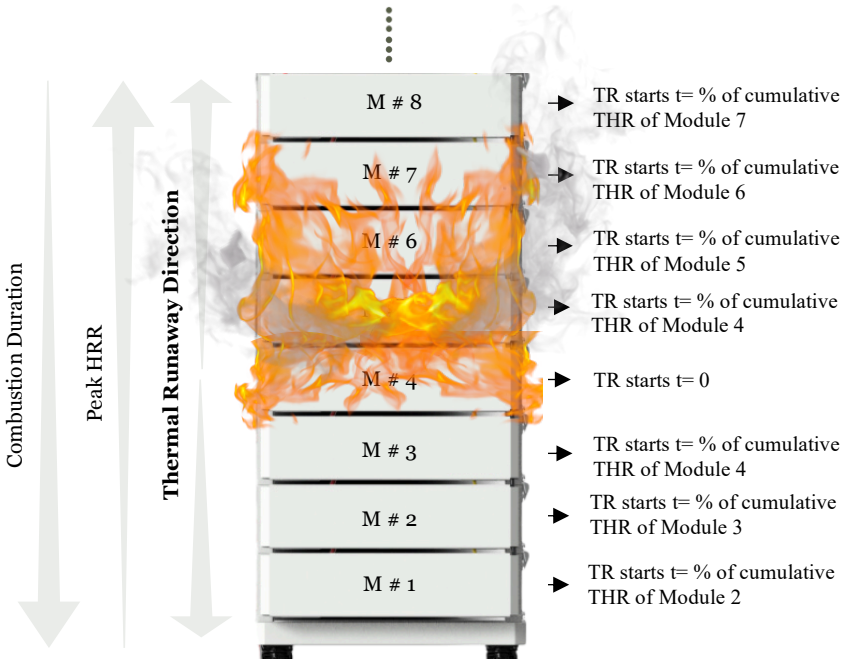

Figure 35 Middle-Out Propagation Scenario

3.4.3 Top-Down Propagation Scenario

In the top-down scenario, thermal runaway begins in the battery rack's top-most module and spreads downward toward the base. Unlike bottom-up propagation, downward spread runs opposed to natural convection, making heat transmission to lower modules slower and less efficient. As a result, the fire growth pattern differs in both timing and scale dynamics.

In this modeling method, the top module serves as the reference scenario. It describes the baseline heat release rate (HRR) curve in terms of shape, duration, and peak intensity. Once a certain fraction of the upper module's accumulated THR has been released, the module below ignites. This threshold is used consistently across layers to calculate ignition delays, and the start time for each succeeding module is established by measuring when the THR % is achieved in the module immediately above.

Because the downward spread encounters opposing buoyant forces and reduces direct flame contact, each lower module ignites later and burns less brightly than the one above. As a result, the model employs a scaling-down technique in which the maximum HRR steadily drops for each lower module. At the same time, the combustion duration is somewhat increased, indicating a slower ignition and longer combustion process at the bottom of the rack.[44]

Table 6 Top-Down Propagation – Scaling Strategy Summary

Parameter	Scaling Approach
Ignition Logic	Fire initiates at the top module and spreads downward
Trigger Condition	THR threshold from the module directly above
Start Delay	Tracking when each module receives required heat
Peak HRR	Scaled downward progressively from top to bottom
Combustion Duration	Scaled upward for lower modules, simulating slower burning
THR	Slight decrease toward bottom modules
HRR Curve	Based on top module’s curve; each one scaled and time-shifted

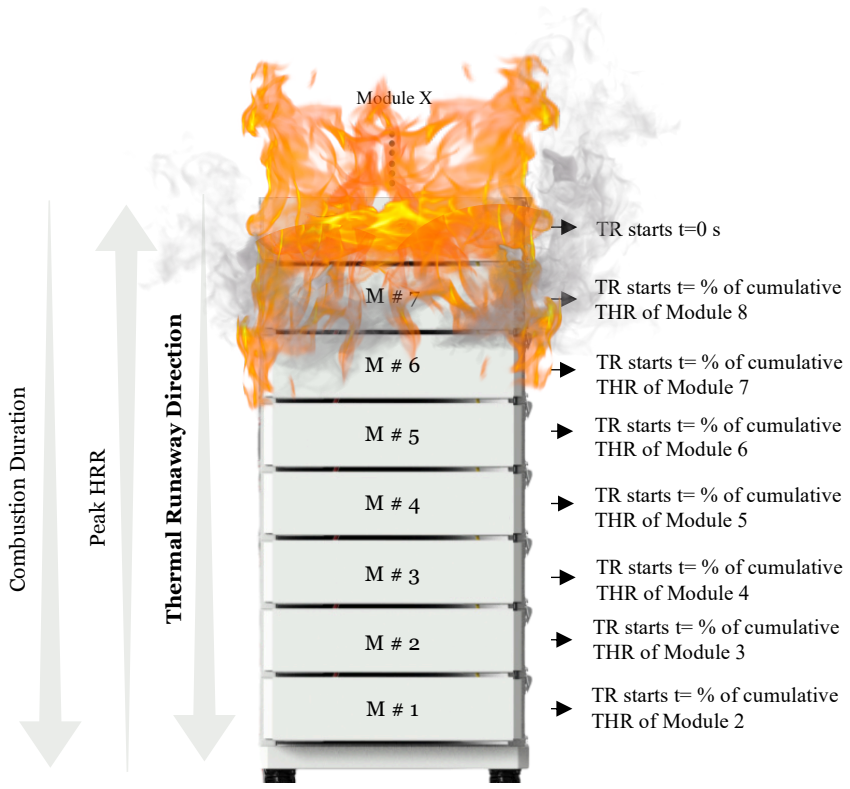

Figure 36 Top-Down Propagation Scenario

3.5 Room Level Thermal Runaway Propagation

Estimating the Ignition Time of Adjacent Racks Using Heat Flux

After modeling the heat release behavior of a single battery rack experiencing thermal runaway (TR), our next step is to evaluate the possibility of horizontal fire propagation to surrounding racks. In this method, the whole heat output from a burning rack is considered and a point heat source is estimated to be located in the center 1/2 H of the height of rack. Because of this simplification, we can model the radiative heat flux that reach adjacent racks at varying heights while also considering for the gap between racks.

This flux based on conventional radiation and convection equations that account for variables such as flame temperature, distance between racks, and radiative proportion of total heat output. The analysis identifies whether the incident heat flux exceeds a crucial level required to begin TR for each module located in the rack adjacent to it.

Once a module has accumulated enough cumulative heat to reach this threshold it begins TR. Except for this we also have additional delay accounts for thermal inertia, the effects of local suppression, and the time necessary for

gas creation and venting. Following this delay, the module is considered to have thermal runaway, and a new HRR curve is generated for that rack based on the new start time we have identifies from the heat flux.

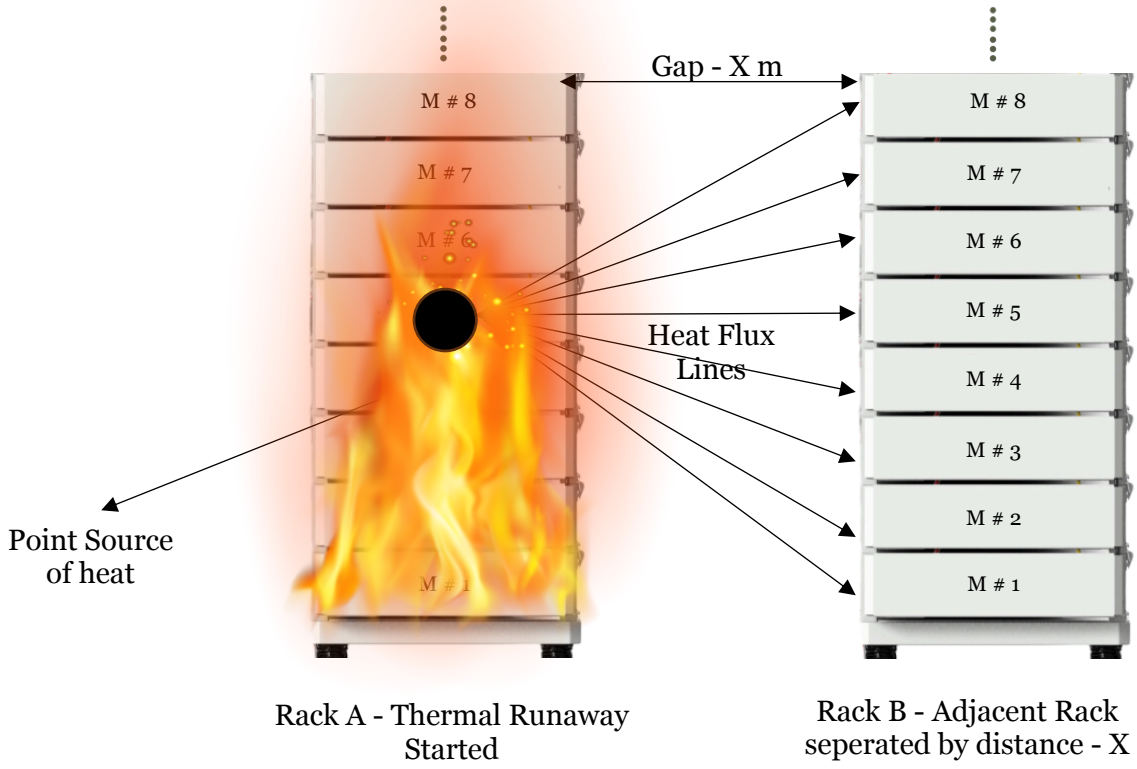

Figure 37 Estimating the Ignition Time of Adjacent Racks Using Heat Flux

Assumptions and Inputs

As described in the previous section, we first use heat flux (the amount of heat that reaches another surface) to determine how long it takes to activate the second rack once the first one catches fire. This delay provides a starting point. Once we know the time, we can determine when the other racks in the room will catch fire.

When a battery fire (thermal runaway) occurs in one rack, it might cause heat to spread to the others. However, this does not happen all at once; it takes some time for the heat to spread to the other racks, causing them to catch fire. To determine when each nearby rack will go into thermal runaway, we must first determine its distance from the rack where the fire began. We accomplish this by examining the position of each rack in the room (as if it were

on a map). Once we have the distance, we can apply a simple rule: the farther the rack is, the longer it takes the fire to reach it. For example, if the rule states that it takes 30 seconds for fire to travel one meter and a rack is two meters away, we expect it to catch fire after sixty seconds. The entire battery room is divided into two rows, and we repeat this process for each rack by measuring the distance it is from the first rack that caught fire. The delay is then used to create the fire curve (HRR curve) for each rack, which depicts how the fire spreads around the room over time. This delay is determined by how near or far apart the racks are, therefore changing the spacing affects how quickly or slowly the fire spreads.

Room Configuration The battery room has many racks spaced at regular intervals (e.g., 1.2 m apart). The X and Y coordinates of each rack are defined, and one rack is chosen as the ignition rack from where the TR initiated. The thermal runaway is supposed to start at t=0

Distance Based Delay Estimation The distance between racks is calculated using the Pythagorean theorem (Eq. 16), which gives the Euclidean distance between two rack centers in a 2D floor layout. This is a first-principles geometric relation, appropriate because racks are arranged on a rectangular floor plan, and the center-to-center distance defines the effective heat transfer path.

$$d = \sqrt{(x_2 - x_1)^2 + (y_2 - y_1)^2} \tag{16}$$

The delay time to trigger TR in an adjacent rack is then:

$$t_{\text{delay}} = d \times \delta_{\text{per meter}} \tag{17}$$

where $\delta_{\text{per meter}}$ is the delay time per meter (Distance of desired rack from the base rack) (e.g., 8125 s/m).

The delay time is then assumed proportional to this distance (Eq. 17). This linear relation is an empirical simplification: it comes from the ignition delay calculated earlier in this chapter based on radiative heat flux thresholds. Once this delay factor is established, it is applied to other racks in the battery room by multiplying with the distance found from (Eq. 16).

The ignition time of the new rack is:

$$t_{\text{ignition}} = t_{\text{start, base rack}} + t_{\text{delay}} \tag{18}$$

Directionality of Flame and Ignition Module Selection

Depending on the location in the base rack where TR began, the model assumes that the ignition in the subsequent rack will take place at a particular module:

The ignition location within a rack determines how flames impinge on adjacent racks. Three cases are considered in the model: ignition starting from the bottom, the top, or the middle of a rack. This assumption is based on visual observations from experimental videos of full-scale rack fire tests (e.g., FM Global). When ignition occurred at the bottom of a rack, flames rose upward and impinged on the neighboring rack from the top. When ignition began at the top, flames spread downward, so the neighboring rack was exposed from the top as well. Finally, when ignition occurred in the middle, flames and hot gases struck the neighboring rack at the same mid-level. These observed flame propagation patterns are reflected in the model, which assigns the ignition height of adjacent racks based on the location of ignition in the base rack.[45]

Room Level Heat Release Output

The room-level HRR is obtained by summing the HRR curves of all racks, each shifted by its ignition time (Eq. 19). This superposition approach is consistent with the fact that HRR is an extensive property: the total is simply the sum of contributions from each burning rack.

$$HRR_{\text{room}}(t) = \sum_{i=1}^{n} HRR_i\left(t - t_{\text{ignition},i}\right) \tag{19}$$

Similarly, the total cumulative heat release is:

$$THR_{\text{room}}(t) = \sum_{i=1}^{n} \int_0^t HRR_i\left(t - t_{\text{ignition},i}\right)\, d \tag{20}$$

In Eqs. (19)-(20), n denotes the number of racks in the battery room. Each rack contributes its own HRR curve, HRR_i which is shifted in time by its ignition delay $t_{\text{ignition},i}$. The room-level HRR, $HRR_{\text{room}}(t)$, is obtained by summing these contributions (Eq. 19). The corresponding cumulative total heat release, $THR_{\text{room}}(t)$, is obtained by integrating each rack's HRR over time and summing the results (Eq. 20).

3.6 Consequences of Thermal Runaway: Structural Steel Melting

When assessing the battery room's safety, one of the most important questions to ask is whether the cumulative heat release from battery thermal runaway (TR) events can cause structural steel elements, such as the walls, ceiling, and frames, to melt. This section describes the methodology used to compare the total energy input from combustion (Total Heat Release, or THR) to the energy required to melt structural steel. The goal of this investigation is to determine whether the thermal energy in the room exceeds the critical melting threshold, and when this occurs.

The approach relies on computing the energy required to heat and melt the structural steel components in the room. This total melting energy comprises two parts:

1. Sensible heat to raise the temperature of the steel from ambient (20 °C) to its melting point (approximately 1500 °C), and
2. Latent heat required to perform the phase transition from solid to liquid at constant temperature.

The cumulative thermal energy from battery fires (THR) is then compared against this threshold to assess structural risk.

Step 1: Calculating Steel Mass
The steel structure in the battery room includes vertical wall plating, ceiling/deck plating, horizontal stringers, and vertical frames. The total steel volume
V_{steel} is the sum of individual component volumes:

$$V_{\text{steel}} = V_{\text{wall}} + V_{\text{ceiling}} + V_{\text{deck}} + V_{\text{frames}} + V_{\text{stringers}} \quad (21)$$

The total steel mass m_{steel} is then calculated by:

$$m_{\text{steel}} = \rho_{\text{steel}} \cdot V_{\text{steel}} \quad (22)$$

Where $\rho_{\text{steel}} = 7850\, kg/m3$ is the density of shipbuilding steel.[46]

Figure 38 shows a typical ship hull structure with internal bulkheads and deck plating. These structural steel components serve as the load-bearing boundaries of compartments like battery rooms, as well as the areas exposed to heat during a thermal runaway event.[47]

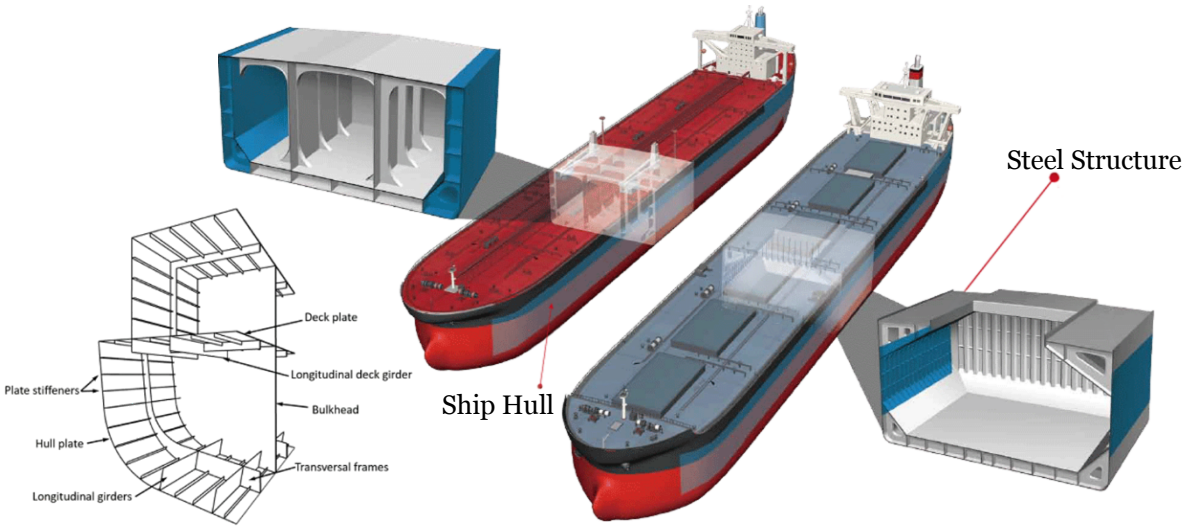

Figure 38 Ship structural steel layout (hull, deck, and bulkheads)

Step 2: Sensible Heat Calculation
Sensible heat is the energy required to raise the steel's temperature from ambient (T0 = 20°C)to its melting point (Tm = 1500°C) [48]

$$Q_{\text{sensible}} = m_{\text{steel}} \cdot c \cdot \Delta T \tag{23}$$

Where c = 0.46 kJ/kg·K (specific heat capacity of steel, assumed constant). [49]

Step 3: Latent Heat Calculation
Once the steel reaches its melting point, an additional energy input is required to melt it:

$$Q_{\text{latent}} = m_{\text{steel}} \cdot L \tag{24}$$

Where L=272 kJ/kg is the latent heat of fusion for steel.[50]

Step 4: Total Melting Energy
The total energy required to raise the steel to its melting point and melt it is the sum of the sensible and latent heat:

$$Q_{\text{total, melt}} = Q_{\text{sensible}} + Q_{\text{latent}} = m_{\text{steel}} \cdot (c \cdot \Delta T + L) \tag{25}$$

This value represents the energy threshold against which we will compare the battery room's total heat release.

Step 5: Comparing to Battery Room THR
The cumulative THR of the battery room is calculated by adding the THR of all racks experiencing thermal runaway while accounting for staggered ignition and propagation. When THR Qroom(t) exceeds the steel melting threshold Qtotal, structural failure is likely to occur.

The condition is:

$$\text{If} \quad Q_{\text{room}}(t) \geq Q_{\text{total, melt}}, \quad \text{then melting onset occurs at time } t \tag{26}$$

Step 6: Final Calculation
To complete the analysis, we track the cumulative THR over time and compare it to the threshold.

$$\int_0^{t_{\text{melt}}} \dot{Q}(t)\ dt \geq Q_{\text{total, melt}} \tag{27}$$

Where:
Q d(t) is the total heat release rate (HRR) from the room at time t, tmelt is the predicted onset of steel melting.

3.7 Design and Workflow of the Spread sheet Simulation Tool

In the last part of the methodology, the spreadsheet simulation tool for modeling thermal runaway situations in large marine battery systems is shown. The tool integrates data from experimental fire tests, battery specifications, and propagation dynamics to estimate the heat release rate (HRR), total heat release (THR), combustion duration, and impact on battery room integrity. It is made to be modular, scalable, and flexible so that it can be used with different case studies and room layouts. This makes it useful for conceptual design and early-stage fire safety evaluation.

STEP 1: Input & Configuration Block

This is the entry point where the user provides all the key simulation parameters. These values drive all subsequent calculations in the Excel tool.
User Inputs:

1. Battery module type (e.g., Corvus Blue Whale)
2. Battery Chemistry (LFP/NMC)
3. Module Nominal voltage and Capacity
4. Battery room capacity (e.g., 5-25 MWh)
5. Ignition location (bottom, middle, top module)
6. Ignition type - Rack Number (corner or center of the room)
7. State of charge (SOC) in %
8. Distance between racks
9. Area of Inetrest (Battery room Roof, Walls, Floor)
10. Submersion scenario (none, partial, full)

Rack 1 / Rack 7	Rack 2 / Rack 8	Rack 3 / Rack 9	Rack 4 / Rack 10	Rack 5 / Rack 11	Rack 6 / Rack 12

Module and Rack Specifications

Parameter	Value	Unit	Description
Battery Chemistry	NMC		or the battery room. Choose either LFP (Lithium Iron Phosphate) or NM
Room Capacity	5000	kWh	Editable: Total energy capacity for battery room
Module Mass	395	kg	From datasheet
Module Nominal Voltage	80	V	From Corvus datasheet
Module Capacity	628	Ah	From Corvus datasheet
Module Energy	50,24	kWh	Energy = Voltage × Capacity / 1000
Ignition Rack #:	1		
Modules per Rack	9	-	Fixed for Corvus rack (vertical stack)
Distance Between Racks	1	m	Editable: space between adjacent racks
Vacant Margin (each wall)	0,8	m	Editable: space around room (walls, ceiling, floor)
TR Threshold (kW/m²)	60		This is the heat flux threshold limit, set to indicate when a
heat flux remains - s (Delay)	1500		
Module Length	1,165	m	Corvus module length (rack depth)
Module Width	0,905	m	Corvus module width (rack width)
Module Height	0,238	m	Corvus module height (stacked vertically)
Modules Required	99,52229299	-	Total modules to meet required capacity
Racks Required	12	-	Total racks required (rounded up)
Rack Length	0,8	m	Same as module length
Rack Width	1,165	m	Same as module width
Rack Height	2,142	m	9 modules stacked vertically
Select SOC	100 %		Select the State of Charge (SOC) of the batteries in the room.
Select TR Initiation Point	Bottom		ation in the rack where thermal runaway begins (e.g., bottom/middle/
Select Area to Melt	Only Roof		uctural region considered for melting analysis (e.g., only roof, walls, et
TR - Start Time of Rack B - s	5000	1h 23m	Time when thermal runaway reaches Rack B
Melting Start Time (s)	3900	1h 5m	Time when thermal runaway reaches Rack B
Post-Melt Start Time (s)	4300	1h 11m	Time when melting has fully progressed
Melting Duration (s)	400	0h 6m	Total time during which structural steel is melting
THR Battery Room (GJ)	241,0525655	GJ	Total thermal energy released in the room (in GJ)
Melting After water Submersion	4100		Indicates if steel melting still occurred after water suppression

Battery Room Flooding Configuration

Water Type	Sea Water		Type of water used for submersion, e.g., Sea Water or DI Water
Water Flow Rate (m³/min)	8	(m³/min)	Rate at which water fills the battery room, in cubic meters per minute
Fill Start Time	4500	(s)	Time (in seconds) after ignition when water starts filling the room
Select Fill %	100 %		arget water level (as % of total room volume) to simulate partial/full fil
Decay Factor After Fill	0,03 %		nential decay constant applied to reduce THR after water submersion b
Corrosion Start Time (s)	9900	(s)	nential decay constant applied to reduce THR after water submersion b

Structural Steel Heat Load Summary

Parameter	Value	Unit	Description
Steel Mass	6577,16018	kg	Total structural steel mass
Specific Heat (c)	0,46	kJ/kg·K	Specific heat capacity of steel
Temperature Rise (ΔT)	1480	K	From 20°C to 1500°C
Latent Heat of Fusion	272	kJ/kg	Energy to melt 1 kg of steel at 1500°C
Sensible Heat per kg	680,8	kJ/kg	c × ΔT
Total Sensible Heat	6396758	kJ	Steel mass × sensible heat/kg
Total Latent Heat	25556696,527	kJ	Steel mass × latent heat/kg
Total Energy to Melt Steel	8952455	kJ	Sensible + latent heat
Heat Absorption Efficiency	70 %	η	Fraction of the total fire heat release rate (HRR) that is absorbed by

Battery Room Steel Specification Table

Component	Value	Unit	Description	Source Link
Room Length	4,93	m	ngth = racks per row × (rack length + spacing) + marg	
Room Width	12,03	m	2 rows of racks + spacing + margins	
Room Height	3,742	m	Rack height + top/bottom margin	
Room Volume	221,9	m³		
Steel Grade	E	-	High-strength arctic-grade ship steel	Source
Steel Density	7850	kg/m³	Density of shipbuilding mild steel	Source
Wall Plating Thickness	0,008	m	Typical wall steel thickness (8 mm)	Source
Deck/Ceiling Plating Thickness	0,012	m	Typical deck/ceiling plating thickness (12 mm)	Source
Frame Member Count	5	count	Estimated vertical frames inside the room	
Frame Cross-Section Area	0,002	m²	Cross-sectional area of each frame (flat bars, T-	
Stringer Count	6	count	Estimated horizontal stringers	
Stringer Cross-Section Area	0,003	m²	ectional area of each stringer Stringer (L-bar)150×1	
Total Melting Section Volume	0,7116948	m³		
Wall Area	126,92864	m²	Total area of all 4 vertical walls	
Ceiling Area	59,3079	m²	area of floor	
Deck Area	59,3079	m²	area of floor	
Frame Volume	0,03742	m³	Volume of vertical frame steel	
Stringer Volume	0,08874	m³	Volume of horizontal stringer steel	
Total Steel Volume	0,83785548	m³	Total structural steel volume	
Total Steel Mass	6,577116018	T	Total steel mass of the structure	

Results Summary - Battery Room

Scenario	Bottom	Middle	Top	Bottom	Middle	Top
TR - Start Time of Rack B - s	5000	5450	8600	1h 23m	1h 30m	2h 23m
Melting Start Time (s)	3900	4300	5450	1h 5m	1h 11m	1h 30m
Post-Melt Start Time (s)	4300	4950	6000	1h 11m	1h 22m	1h 40m
Melting Duration (s)	400	650	550	0h 6m	0h 10m	0h 9m
THR Battery Room (GJ)	241,05	254,91	235,26	-	-	-
Melting After water Submersion	4100	4500	Melting not triggered	-	-	-
Peak HRR - kW	17273	15760	14823	-	-	-
Combustion Duration (s)	34811	38780	54959	9h 40m	10h 46m	15h 15m
TR - Start Time of Rack B - s	5000	5450	8600	1h 23m	1h 30m	2h 23m

Figure 39 The input sheet contains all model parameters including steel mass, room geometry, and ignition scenarios.

STEP 2: Cell → Module Scaling

This part of the model takes known thermal runaway behavior of a single prismatic LFP cell (e.g., HRR curve, combustion energy, duration) and scales it up to the full module level based on the number of cells per module and their configuration (series/parallel).
For example, the Corvus Blue Whale module contains:

1. 75 prismatic LFP cells (25S3P)
2. Each cell: ~672 Wh, 210 Ah
3. Total module energy: ~50.24 kWh
4. The tool scales:
5. Peak HRR
6. Total Heat Release (THR)
7. Combustion duration by either direct energy ratio scaling or calibrated empirical multipliers (based on FM Global test data).

The next step converts single-cell thermal runaway data into module-level heat release profiles. Using cell-level heat release rate (HRR) and total heat release (THR) values extracted from literature (e.g., Wang et al., 2017) and calibrated against FM Global's large-scale fire test data, the tool multiplies these by the number of active cells within the module. For the Corvus Blue Whale module, this includes 75 prismatic $LiFePO_4$ cells arranged in a 25S3P configuration. The scaling accounts for both energy content and SOC-dependent combustion behavior. The combustion duration and flame dynamics are also adjusted based on the total chemical energy and experimental trends. The result is a module-level HRR curve used in downstream rack-level aggregation.

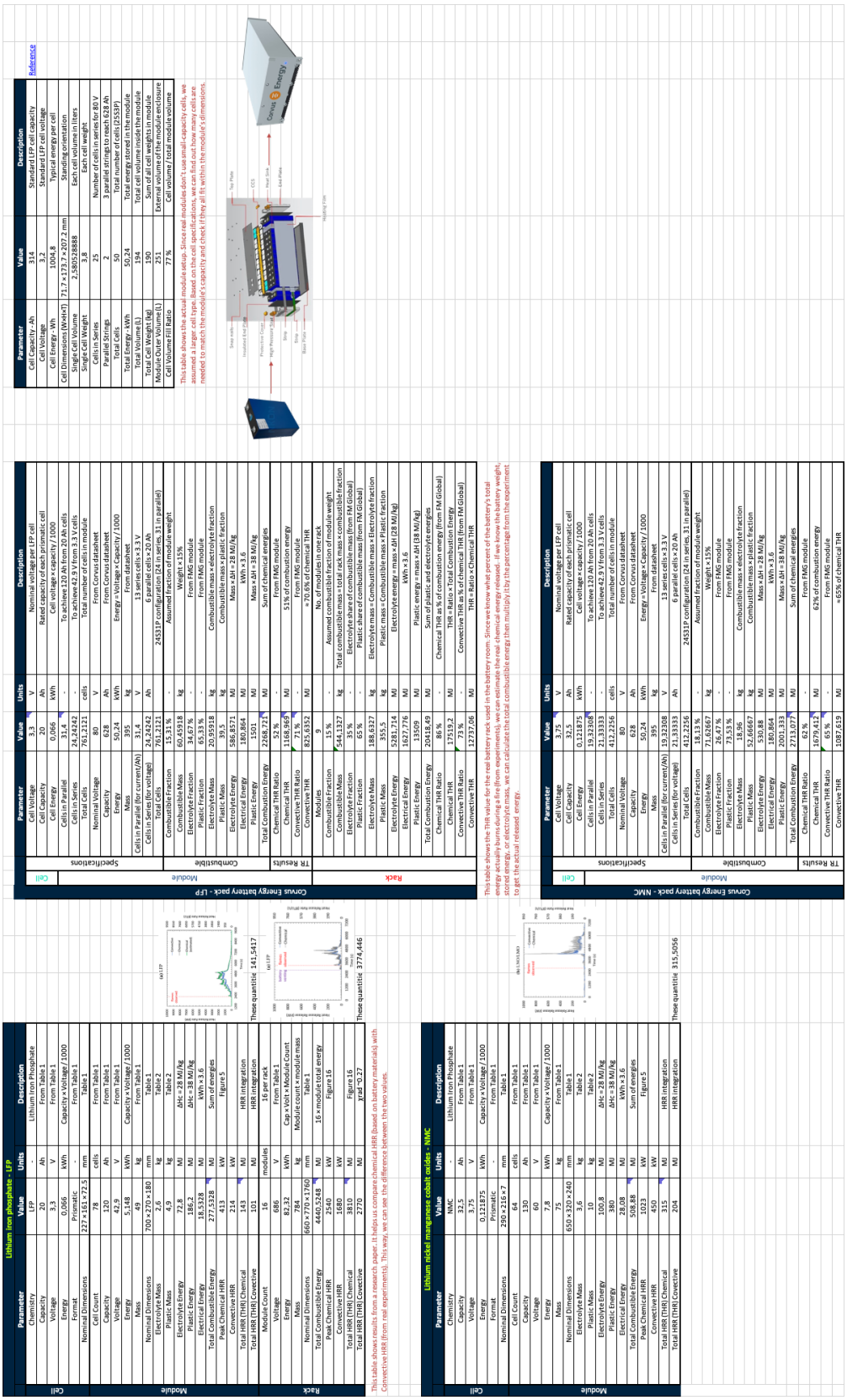

Figure 40 FM Global rack test data scaled to the Corvus module for THR and combustion duration estimation.

STEP 3: Module → Rack Scaling

This step sums up the HRR and THR contributions from individual modules to generate a rack-level fire profile.
You can customize:

1. Number of modules per rack (default: 9 for Corvus Blue Whale)
2. Which modules ignite and when (based on propagation logic)
3. Ignition direction (bottom-up, top-down, middle-out)

It outputs:

1. Combined HRR curve for the entire rack
2. Rack-level THR
3. Total combustion duration of the rack fire

The tool then aggregates the module-level thermal behavior to form rack-level heat release profiles. For each rack, the number of modules and their respective ignition times are specified. The user can define ignition order based on physical location (e.g., bottom-up, top-down, or middle-out). This allows simulation of realistic fire propagation paths through the rack. The model computes the cumulative rack HRR and THR curves by summing active module profiles while accounting for overlap in combustion and delay in ignition. This step captures the influence of module arrangement and ignition pattern on total rack combustion energy, flame behavior, and duration.

Module	THR (MJ)	Duration (s)	Peak HRR (kW)	Start Delay (s)	t_peak	End Time	THR Scaling	Duration Scaling	Peak HRR Scaling	Fraction of THR	Triggering HRR	Start Time	End	Duration
1	1679	9564	1249	0	840	9564	1	1	1			0h 0m	2h 39m	2h 39m
2	1664,3	9085,7	1439	400	4943	9486	0,991	0,95	1,2	0,7 %	11,8	0h 6m	2h 38m	2h 31m
3	1642,5	8990,0	1873	650	5145	9640	0,978	0,94	1,5	0,4 %	7,7	0h 10m	2h 40m	2h 29m
4	1620,6	8894,4	2123	650	5097	9544	0,965	0,93	1,7	0,1 %	1,2	0h 10m	2h 39m	2h 28m
5	1598,8	8798,8	2747	700	5099	9499	0,952	0,92	2,2	0,1 %	1,3	0h 11m	2h 38m	2h 26m
6	1578,6	8703,1	3372	750	5102	9453	0,94	0,91	2,7	0,1 %	1,7	0h 12m	2h 37m	2h 25m
7	1556,8	8607,5	2997	800	5104	9407	0,927	0,9	2,4	0,1 %	2,1	0h 13m	2h 36m	2h 23m
8	1536,7	8511,8	2498	850	5106	9362	0,915	0,89	2	0,1 %	1,8	0h 14m	2h 36m	2h 21m
9	1511,5	8416,2	2123	900	5108	9316	0,9	0,88	1,7	0,1 %	1,5	0h 15m	2h 35m	2h 20m
		1684,8				1930,02				2366,625			2677,5	

																														Peak HRR - kW	THR - MJ
	Module 1				Module 2				Module 3				Module 4				Module 5				Module 6				Module 7				Module 8				Module 9				Rack/Pack	
Time (s)	HRR (kW)	THR (MJ)	Comm. HRR (MJ)	% of THR	HRR (kW)	THR (MJ)	Comm. HRR (MJ)	% of THR	HRR (kW)	THR (MJ)	Comm. HRR (MJ)	% of THR	HRR (kW)	THR (MJ)	Comm. HRR (MJ)	% of THR	HRR (kW)	THR (MJ)	Comm. HRR (MJ)	% of THR	HRR (kW)	THR (MJ)	Comm. HRR (MJ)	% of THR	HRR (kW)	THR (MJ)	Comm. HRR (MJ)	% of THR	HRR (kW)	THR (MJ)	Comm. HRR (MJ)	% of THR	Total HRR (kW)	THR - KJ
0	3,0			0%	0			0%	0			0%	0			0%	0			0%	0			0%	0			0%	0			0%	3,0	0
50	17,0	0,5	0,5	0%	0	0	0	0%	0	0	0	0%	0	0	0	0%	0	0	0	0%	0	0	0	0%	0	0	0	0%	0	0	0	0%	17,0	500
100	30,0	1,2	1,7	0%	0	0	0	0%	0	0	0	0%	0	0	0	0%	0	0	0	0%	0	0	0	0%	0	0	0	0%	0	0	0	0%	30,0	1175
150	36,0	1,7	3,3	0%	0	0	0	0%	0	0	0	0%	0	0	0	0%	0	0	0	0%	0	0	0	0%	0	0	0	0%	0	0	0	0%	36,0	1650
200	38,0	1,9	5,2	0%	0	0	0	0%	0	0	0	0%	0	0	0	0%	0	0	0	0%	0	0	0	0%	0	0	0	0%	0	0	0	0%	38,0	1850
250	38,0	1,9	7,1	0%	0												0	0	0	0%	0	0	0	0%	0	0	0	0%	0	0	0	0%	38,0	1900
300	37,0	1,9	9,0	1%	0												0	0	0	0%	0	0	0	0%	0	0	0	0%	0	0	0	0%	37,0	1875
350	35,0	1,8	10,8	1%	0												0	0	0	0%	0	0	0	0%	0	0	0	0%	0	0	0	0%	35,0	1800
400	30,0	1,6	12,4	1%	4												0	0	0	0%	0	0	0	0%	0	0	0	0%	0	0	0	0%	33,6	1715
450	25,0	1,4	13,8	1%	36												0	0	0	0%	0	0	0	0%	0	0	0	0%	0	0	0	0%	61,0	2365
500	21,0	1,2	14,9	1%	43												0	0	0	0%	0	0	0	0%	0	0	0	0%	0	0	0	0%	64,2	3130
550	18,0	1,0	15,9	1%	46												0	0	0	0%	0	0	0	0%	0	0	0	0%	0	0	0	0%	63,6	3195
600	16,0	0,9	16,7	1%	46												0	0	0	0%	0	0	0	0%	0	0	0	0%	0	0	0	0%	61,6	3130
650	18,0	0,9	17,6	1%	44												0	0	0	0%	0	0	0	0%	0	0	0	0%	0	0	0	0%	72,0	3340
700	19,0	0,9	18,5	1%	42												7	0	0	0%	0	0	0	0%	0	0	0	0%	0	0	0	0%	163,6	5890
750	21,0	1,0	19,5	1%	36												66	2	2	0%	8	0	0	0%	0	0	0	0%	0	0	0	0%	246,3	10247,1
800	22,0	1,1	20,6	1%	30												79	4	6	0%	81	2	2	0%	7	0	0	0%	0	0	0	0%	341,0	14682,5
850	24,0	1,2	21,7	1%	25												84	4	10	0%	97	4	7	0%	72	2	2	0%	6	0	0	0%	429,6	19265
900	25,0	1,2	23,0	1%	22												84	4	14	0%	103	5	12	0%	86	4	6	0%	60	2	2	0%	502,7	23307,5
950	28,0	1,3	24,3	1%	19												81	4	18	1%	103	5	17	0%	91	4	11	0%	72	3	5	0%	51	1	2	0%	557,4	26502,5
1000	33,0	1,5	25,8	2%	22												77	4	22	1%	100	5	22	1%	91	5	15	0%	76	4	9	0%	61	3	4	0%	555,9	27832,5
1050	39,0	1,8	27,6	2%	23												66	4	26	1%	95	5	27	1%	89	5	20	1%	76	4	13	0%	65	3	7	0%	531,7	27190
1100	53,0	2,3	29,9	2%	25												55	3	29	1%	81	4	31	1%	84	4	24	1%	74	4	16	1%	65	3	11	0%	504,0	25892,5
1150	67,0	3,0	32,9	2%	26												46	3	31	1%	68	4	35	1%	72	4	28	1%	70	4	20	1%	63	3	14	1%	469,6	24340
1200	77,0	3,6	36,5	2%	29												40	2	33	1%	57	3	38	1%	60	3	31	1%	60	3	23	1%	60	3	17	1%	432,8	22560
1250	85,0	4,1	40,6	2%	30												35	2	35	1%	49	3	41	1%	50	3	34	1%	50	3	26	1%	51	3	20	1%	407,8	21015
1300	89,0	4,4	44,9	3%	34												42	2	37	1%	49	2	43	1%	38	2	36	1%	36	2	28	1%	36	2	22	1%	383,9	19792,5
1350	87,0	4,4	49,3	3%	40												46	2	39	1%	51	2	46	1%	43	2	38	1%	32	2	30	1%	31	2	24	1%	398,8	19567,5
1400	84,0	4,3	53,6	3%	64												48	2	42	1%	57	3	48	1%	46	2	40	1%	36	2	32	1%	27	1	25	1%	433,3	20852,5
1450	74,0	4,0	57,5	3%	80												53	3	44	1%	59	3	51	1%	50	2	43	1%	38	2	33	1%	31	1	26	1%	465,6	22522,5
1500	64,0	3,5	61,0	4%	92	4	41	2%	42	2	33	1%	48	2	38	1%	55	3	47	1%	65	3	54	1%	53	3	45	1%	42	2	35	1%	32	2	28	1%	492,9	23962,5
1550	57,0	3,0	64,0	4%	102	5	45	2%	50	2	36	2%	56	3	41	2%	62	3	50	1%	68	3	58	1%	58	3	48	1%	44	2	38	1%	36	2	30	1%	531,0	25597,5
1600	52,0	2,7	66,7	4%	107	5	51	3%	59	3	38	2%	66	3	44	2%	73	3	53	2%	76	4	61	1%	60	3	51	1%	48	2	40	1%	37	2	32	1%	577,2	27705
1650	46,0	2,5	69,2	4%	104	5	56	3%	80	3	42	2%	90	4	48	2%	86	4	57	2%	89	4	65	2%	67	3	54	1%	50	2	42	1%	43	2	34	1%	654,6	30795
1700	40,0	2,2	71,3	4%	101	5	61	3%	101	5	46	2%	114	5	53	2%	117	5	62	2%	105	5	70	2%	79	4	58	2%	66	3	45	2%	48	2	36	1%	769,9	35612,5
1750	35,0	1,9	73,2	4%	89	5	66	3%	116	5	52	2%	131	6	59	2%	147	7	69	2%	143	6	76	2%	127	5	63	2%	78	4	49	2%	56	3	38	2%	922,0	42297,5
1800	32,0	1,7	74,9	4%	77	4	70	4%	128	6	58	2%	145	7	66	2%	169	8	77	2%	208	9	85	2%	161	7	70	2%	106	5	53	2%	66	3	41	2%	1091,2	50330
1850	30,0	1,6	76,4	5%	68	4	74	4%	134	7	64	3%	151	7	73	3%	187	9	86	3%	230	11	96	2%	185	9	79	2%	134	6	59	2%	90	4	45	2%	1208,6	57495
1900	29,0	1,5	77,9	5%	62	3	77	4%	131	7	71	3%	148	7	81	3%	191	9	91	3%	240	12	108	3%	204	10	89	2%	154	7	67	2%	114	5	50	2%	1273,4	62050
1950	29,0	1,5	79,4	5%	55	3	80	4%	126	6	77	3%	143	7	88	3%	185	9	104	3%	235	12	120	3%	214	10	99	3%	170	8	75	2%	131	6	57	2%	1287,2	64015
2000	30,0	1,5	80,8	5%	48	3	82	4%	111	6	83	4%	109	6	94	4%	163	9	113	3%	227	12	131	3%	209	11	110	3%	178	9	83	3%	145	7	63	3%	1218,7	62647,5
2050	35,0	1,6	82,5	5%	42	2	85	4%	96	5	89	4%	97	5	99	4%	141	8	121	4%	200	11	142	3%	202	10	120	3%	174	9	92	3%	148	7	71	3%	1134,0	58817,5
2100	39,0	1,9	84,3	5%	38	2	87	4%	86	5	93	4%	88	5	104	4%	125	7	127	4%	173	9	151	4%	178	9	129	4%	148	8	100	3%	143	7	78	3%	1017,9	53797,5
2150	42,0	2,0	86,3	5%	36	2	88	5%	78	4	97	4%	78	4	108	4%	114	6	133	4%	154	8	160	4%	154	8	138	4%	128	7	107	4%	126	7	85	3%	909,9	48195
2200	44,0	2,2	88,5	5%	35	2	90	5%	69	4	101	4%	68	4	112	4%	101	5	139	4%	140	7	167	4%	125	7	145	4%	114	6	113	4%	109	6	91	4%	805,0	42872,5
2250	40,0	2,1	90,6	5%	35	2	92	5%	53	3	104	4%	60	3	115	4%	88	5	143	4%	124	7	173	4%	110	6	150	4%	104	5	119	4%	97	5	96	4%	710,3	37882,5
2300	34,0	1,9	92,4	5%	36	2	94	5%	48	3	106	4%	54	3	118	4%	77	4	148	4%	95	5	179	4%	96	5	156	4%	92	5	124	4%	88	5	100	4%	620,3	33265
2350	29,0	1,6	94,0	6%	47	2	96	5%	45	2	109	5%	51	3	121	5%	70	4	151	4%	86	5	183	4%	84	5	160	4%	80	4	128	4%	78	4	105	4%	570,8	29777,5
2400	27,0	1,4	95,4	6%	50	2	98	5%	44	2	111	5%	49	3	123	5%	66	3	155	5%	81	4	188	5%	77	4	164	4%	70	4	132	4%	60	3	108	4%	523,5	27357,5
2450	26,0	1,3	96,7	6%	53	3	101	5%	44	2	113	5%	49	2	126	5%	64	3	158	5%	78	4	192	5%	72	4	168	5%	64	3	135	5%	54	3	111	4%	504,1	25690
2500	27,0	1,3	98,1	6%	48	3	103	5%	45	2	115	5%	51	3	128	5%	66	3	161	5%	78	4	196	5%	70	4	171	5%	58	3	138	5%	51	3	113	4%	493,9	24950
2550	29,0	1,4	99,5	6%	41	2	106	5%	53	2	118	5%	60	3	131	5%	77	4	165	5%	81	4	200	5%	70	3	175	5%	58	3	141	5%	49	3	116	5%	516,7	25265
2600	31,0	1,5	101,0	6%	35	2	107	6%	59	3	120	5%	66	3	134	5%	86	4	169	5%	95	4	204	5%	72	4	178	5%	60	3	144	5%	49	2	118	5%	552,2	26722,5
2650	33,0	1,6	102,6	6%	32	2	109	6%	63	3	124	5%	75	4	137	5%	92	4	173	5%	105	5	209	5%	94	4	183	5%	70	3	147	5%	51	3	121	5%	615,5	29192,5
2700	37,0	1,8	104,3	6%	31	2	111	6%	66	3	127	5%	68	4	141	5%	97	5	178	5%	113	5	214	5%	101	5	187	5%	78	4	151	5%	60	3	124	5%	650,7	31655
2750	43,0	2,0	106,3	6%	32	2	112	6%	60	3	130	5%	58	3	144	5%	88	5	183	5%	119	6	220	5%	106	5	193	5%	84	4	155	5%	71	3	127	5%	661,0	32792,5
2800	48,0	2,3	108,6	6%	35	2	114	6%	51	3	133	6%	49	3	147	5%	75	4	187	5%	92	5	225	5%	96	5	198	5%	88	4	159	5%	75	4	131	5%	608,5	31737,5
2850	52,0	2,5	111,1	7%	37	2	116	6%	44	2	135	6%	46	2	149	6%	64	3	190	6%	82	4	230	6%	82	4	202	5%	80	4	163	5%	68	4	134	5%	550,3	28970
2900	57,0	2,7	113,8	7%	40	2	118	6%	41	2	137	6%	44	2	151	6%	59	3	193	6%	73	4	233	6%	70	4	206	6%	58	3	167	6%	58	3	137	5%	499,0	26232,5
2950	60,0	2,9	116,7	7%	44	2	120	6%	39	2	139	6%	46	2	154	6%	57	3	196	6%	70	4	237	6%	65	3	209	6%	54	3	170	6%	49	3	140	6%	484,8	24595
3000	63,0	3,1	119,8	7%	52	2	122	6%	41	2	141	6%	49	2	156	6%	59	3	199	6%	73	4	241	6%	62	3	212	6%	52	3	172	6%	46	2	142	6%	497,0	24545
3050	123,0	4,7	124,5	7%	58	3	125	6%	47	2	143	6%	53	3	159	6%	68	3	202	6%	78	4	244	6%	65	3	216	6%	54	3	175	6%	44	2	145	6%	589,3	27157,5
3100	288,0	10,2	134,7	8%	62	3	128	7%	50	2	146	6%	56	3	161	6%	73	4	206	6%	84	4	248	6%	74	3	219	6%	58	3	178	6%	46	2	147	6%	788,6	34447,5
3150	452,0	18,5	153,1	9%	68	3	131	7%	56	3	148	6%	63	3	164	6%	81	4	210	6%	89	4	253	6%	79	4	223	6%	62	3	181	6%	53	2	149	6%	1003,2	44795
3200	795,0	31,2	184,3	11%	72	4	135	7%	65	3	151	6%	73	3	168	6%	95	4	214	6%	100	5	258	6%	89	4	227	6%	66	3	184	6%	56	3	152	6%	1410,0	60330
3250	1248,0	51,1	235,4	14%	76	4	138	7%	72	3	155	7%	82	4	172	6%	106	5	219	6%	116	5	263	6%	103	5	232	6%	74	4	187	6%	63	3	155	6%	1939,0	83725
3300	1017,0	56,6	292,0	17%	343	10	149	8%	78	4	158	7%	88	4	176	7%	114	6	225	7%	140	6	269	7%	115	5	237	6%	96	4	192	6%	73	3	158	6%	2065,7	100117,5
3350	676,0	42,3	334,3	20%	542	22	171	9%	86	4	163	7%	102	5	181	7%	125	6	231	7%	154	7	277	7%	125	6	243	7%	104	5	197	7%	82	4	162	6%	1995,6	101332,5
3400	480,0	28,9	363,2	22%	954	37	208	11%	90	4	167	7%	107	5	186	7%	132	6	237	7%	162	8	285	7%	137	7	250	7%	114	5	202	7%	88	4	167	7%	2264,3	106497,5
3450	541,0	25,5	388,8	23%	1498	61	270	14%	95	5	172	7%	209	8	194	7%	139	7	244	7%	170	8	293	7%	144	7	257	7%	120	6	208	7%	97	5	171	7%	3011,8	131902,5
3500	598,0	28,5	417,2	25%	1220	68	338	17%	185	7	179	8%	486	17	211	8%	271	10	254	7%	332	13	305	7%	151	7	264	7%	126	6	214	7%	107	5	176	7%	3476,1	162197,5
3550	523,0	28,0	445,3	26%	811	51	388	20%	429	15	194	8%	768	31	243	9%	629	22	276	8%	772	28	333	8%	686	21	285	8%	246	9	223	7%	209	8	184	7%	5074,5	213765
3600	447,0	24,3	469,5	28%	576	35	423	22%	678	28	222	9%	1352	53	296	11%	1748	59	336	10%	1228	50	383	9%	1085	44	330	9%	572	20	244	8%	486	17	202	8%	8164,9	330985
3650	456,0	22,6	492,1	29%	649	31	454	24%	1193	47	268	11%	2122	87	382	14%	2746	112	448	13%	2147	84	467	11%	1908	75	404	11%	904	37	281	9%	768	31	233	9%	12891,8	526417,5
3700	505,0	24,0	516,1	31%	718	34	488	25%	1872	77	345	15%	1729	96	479	18%	2237	125	573	17%	3370	138	605	15%	2995	123	527	14%	2496	85	366	12%	1552	53	286	11%	17273,2	754125
3750	519,0	25,6	541,7	32%	628	34	522	27%	1526	85	430	18%	1149	72	551	21%	1487	93	666	20%	2746	153	758	18%	2441	136	663	18%	2034	113	479	16%	2122	87	373	15%	14650,8	798100

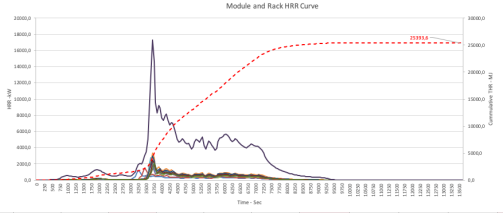

Figure 41 Time-resolved heat-release-rate (HRR) datasets used in the model, including reference, scaled, and cumulative curves with ignition delay.

STEP 4: Rack → Room Aggregation and Spatial Propagation

This stage calculates total battery room-level fire behavior by:

1. Summing HRR and THR from all racks undergoing thermal runaway
2. Applying propagation delays between racks based on distance and ignition type
3. Incorporating spatial layout (e.g., racks in rows, corner vs. center ignition)
4. Allowing full or partial ignition scenarios (e.g., only 4 of 12 racks burn)

The propagation timing can be:

1. Manual (user-defined)
2. Automatic (based on radiative heat flux models like FM Global's MPS radiation model)

This step yields:

1. Total room HRR curve
2. Total THR
3. Overall fire duration
4. Time-resolved rack ignition sequence

In this stage, the model scales thermal behavior from rack to room level. The user defines how many racks are involved in the thermal runaway event, and the spatial configuration (e.g., total racks in room, inter-rack distance, and ignition point). The tool calculates the ignition delay between racks based on either user-defined values or automatic estimates using heat flux correlations (e.g., the FM Global MPS model). The resulting total room-level HRR and THR curves represent the full energy release scenario under the defined layout and propagation logic. This enables realistic modeling of partial room involvement, directional fire spread, and worst-case cascading effects across multiple racks.

Figure 42 Time-resolved heat release rate (HRR) curves for sequential rack ignition in the battery room, including ignition delays, rack contributions, and cumulative room HRR.

STEP 5: Structural Impact Analysis (Steel Melting & Cooling Effects)

This stage evaluates the impact of the fire on the battery room's steel structure, specifically:

1. Calculates incident heat flux on walls, roof, and floor over time (based on flame height and HRR)

Checks when local temperature exceeds steel melting thresholds

1. Wall, roof, floor thresholds are treated separately

Allows toggling of seawater or freshwater submersion:

1. None
2. Partial (e.g., lower 1 m)
3. Full (entire rack submerged)

It outputs:

1. Melting status and time for each surface
2. Temperature vs. time profiles
3. Cooling impact curves (if submersion selected)

The final physical modeling step assesses how the fire affects the structural integrity of the battery room. The tool estimates heat flux on the steel walls, roof, and floor based on calculated flame height, combustion power, and rack position. Using known steel melting thresholds, the model checks when structural elements are likely to fail. Users can simulate cooling scenarios by toggling partial or full seawater submersion, which affects flame quenching and temperature decay. The tool outputs time-to-melt estimates and plots for structural response, helping evaluate passive safety and mitigation strategies under different fire conditions.

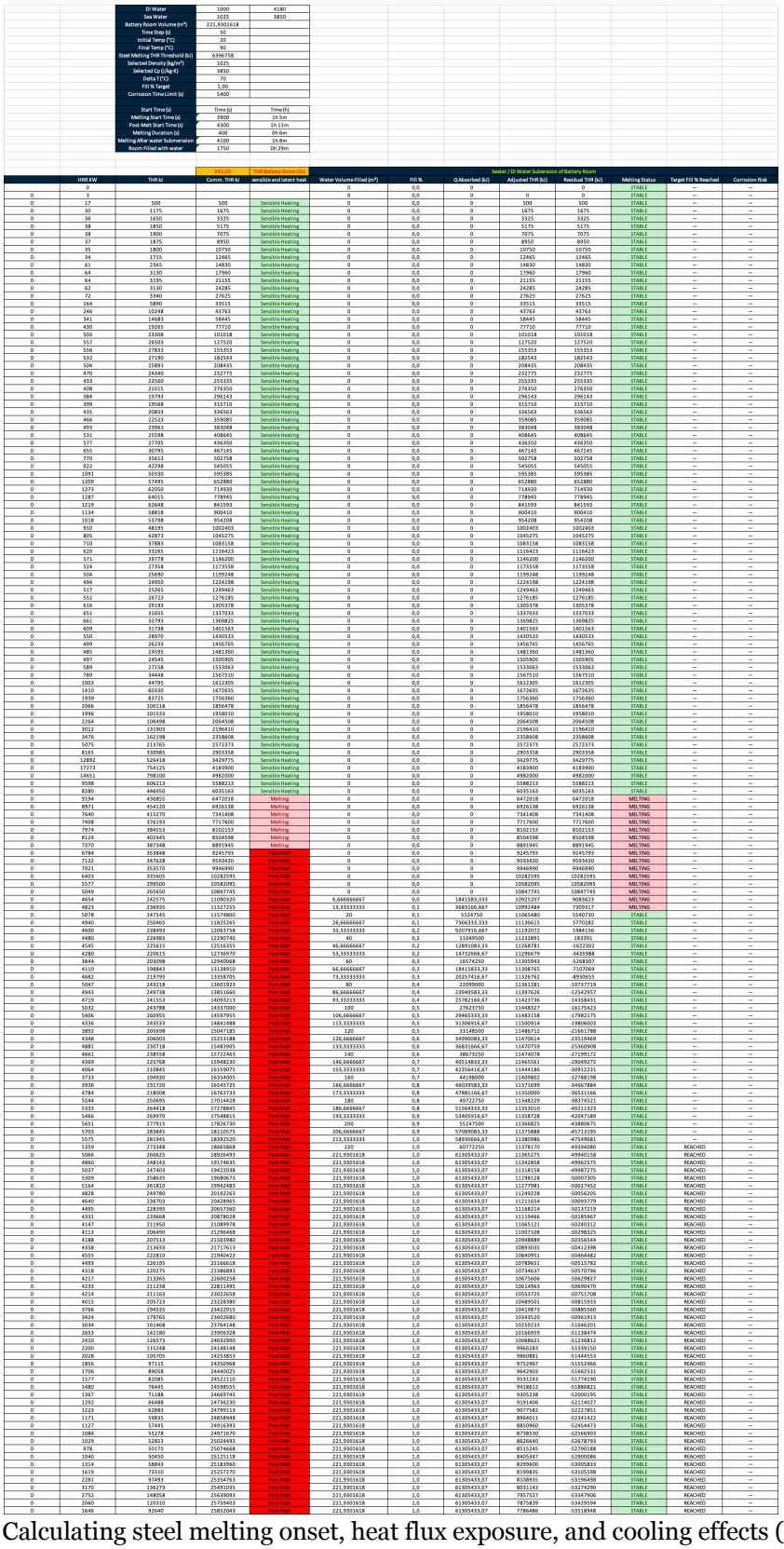

Di Water	1000
Sea Water	1025
Battery Room Volume (m³)	221,9301618
Time Step (s)	50
Initial Temp (°C)	20
Final Temp (°C)	90
Steel Melting THR Threshold (kJ)	6396758
Selected Density (kg/m³)	1025
Selected Cp (J/kg·K)	3850
Delta T (°C)	70
Fill % Target	1,00
Corrosion Time Limit (s)	5400

	Time (s)	Time (h)
Start Time (s)		
Melting Start Time (s)	3900	1h 5m
Post-Melt Start Time (s)	4300	1h 11m
Melting Duration (s)	400	0h 6m
Melting After water Submersion	4100	1h 8m
Room Filled with water	1750	0h 29m

			241,05	THR Battery Room (kJ)		Sealer / Di Water Submersion of Battery Room					
	HRR kW	THR kJ	Comm. THR kJ	sensible and latent heat	Water Volume Filled (m³)	Fill %	QAbsorbed (kJ)	Adjusted THR (kJ)	Residual THR (kJ)	Melting Status	Target Fill % Reached	Corrosion Risk
0	0				0	0,0	0	0	0	STABLE	—	—
0	3				0	0,0	0	0	0	STABLE	—	—
0	17	500	500	Sensible Heating	0	0,0	0	500	500	STABLE	—	—
0	30	1175	1675	Sensible Heating	0	0,0	0	1675	1675	STABLE	—	—
0	36	1650	3325	Sensible Heating	0	0,0	0	3325	3325	STABLE	—	—
0	38	1850	5175	Sensible Heating	0	0,0	0	5175	5175	STABLE	—	—
0	38	1900	7075	Sensible Heating	0	0,0	0	7075	7075	STABLE	—	—
0	37	1875	8950	Sensible Heating	0	0,0	0	8950	8950	STABLE	—	—
0	35	1800	10750	Sensible Heating	0	0,0	0	10750	10750	STABLE	—	—
0	34	1715	12465	Sensible Heating	0	0,0	0	12465	12465	STABLE	—	—
0	61	2365	14830	Sensible Heating	0	0,0	0	14830	14830	STABLE	—	—
0	64	3130	17960	Sensible Heating	0	0,0	0	17960	17960	STABLE	—	—
0	64	3195	21155	Sensible Heating	0	0,0	0	21155	21155	STABLE	—	—
0	62	3130	24285	Sensible Heating	0	0,0	0	24285	24285	STABLE	—	—
0	72	3340	27625	Sensible Heating	0	0,0	0	27625	27625	STABLE	—	—
0	164	5890	33515	Sensible Heating	0	0,0	0	33515	33515	STABLE	—	—
0	246	10248	43763	Sensible Heating	0	0,0	0	43763	43763	STABLE	—	—
0	341	14683	58445	Sensible Heating	0	0,0	0	58445	58445	STABLE	—	—
0	430	19265	77710	Sensible Heating	0	0,0	0	77710	77710	STABLE	—	—
0	503	23308	101018	Sensible Heating	0	0,0	0	101018	101018	STABLE	—	—
0	557	26503	127520	Sensible Heating	0	0,0	0	127520	127520	STABLE	—	—
0	556	27833	155353	Sensible Heating	0	0,0	0	155353	155353	STABLE	—	—
0	532	27190	182543	Sensible Heating	0	0,0	0	182543	182543	STABLE	—	—
0	504	25892	208435	Sensible Heating	0	0,0	0	208435	208435	STABLE	—	—
0	470	24340	232775	Sensible Heating	0	0,0	0	232775	232775	STABLE	—	—
0	433	22560	255335	Sensible Heating	0	0,0	0	255335	255335	STABLE	—	—
0	408	21015	276350	Sensible Heating	0	0,0	0	276350	276350	STABLE	—	—
0	384	19793	296143	Sensible Heating	0	0,0	0	296143	296143	STABLE	—	—
0	399	19568	315710	Sensible Heating	0	0,0	0	315710	315710	STABLE	—	—
0	435	20853	336563	Sensible Heating	0	0,0	0	336563	336563	STABLE	—	—
0	466	22523	359085	Sensible Heating	0	0,0	0	359085	359085	STABLE	—	—
0	493	23963	383048	Sensible Heating	0	0,0	0	383048	383048	STABLE	—	—
0	531	25598	408645	Sensible Heating	0	0,0	0	408645	408645	STABLE	—	—
0	577	27705	436350	Sensible Heating	0	0,0	0	436350	436350	STABLE	—	—
0	655	30795	467145	Sensible Heating	0	0,0	0	467145	467145	STABLE	—	—
0	770	35613	502758	Sensible Heating	0	0,0	0	502758	502758	STABLE	—	—
0	922	42298	545055	Sensible Heating	0	0,0	0	545055	545055	STABLE	—	—
0	1091	50330	595385	Sensible Heating	0	0,0	0	595385	595385	STABLE	—	—
0	1209	57495	652880	Sensible Heating	0	0,0	0	652880	652880	STABLE	—	—
0	1273	62050	714930	Sensible Heating	0	0,0	0	714930	714930	STABLE	—	—
0	1287	64015	778945	Sensible Heating	0	0,0	0	778945	778945	STABLE	—	—
0	1233	62648	841593	Sensible Heating	0	0,0	0	841593	841593	STABLE	—	—
0	1134	58818	900410	Sensible Heating	0	0,0	0	900410	900410	STABLE	—	—
0	1018	53798	954208	Sensible Heating	0	0,0	0	954208	954208	STABLE	—	—
0	910	48195	1002403	Sensible Heating	0	0,0	0	1002403	1002403	STABLE	—	—
0	805	42873	1045275	Sensible Heating	0	0,0	0	1045275	1045275	STABLE	—	—
0	710	37883	1083158	Sensible Heating	0	0,0	0	1083158	1083158	STABLE	—	—
0	620	33265	1116423	Sensible Heating	0	0,0	0	1116423	1116423	STABLE	—	—
0	571	29778	1146200	Sensible Heating	0	0,0	0	1146200	1146200	STABLE	—	—
0	524	27358	1173558	Sensible Heating	0	0,0	0	1173558	1173558	STABLE	—	—
0	504	25690	1199248	Sensible Heating	0	0,0	0	1199248	1199248	STABLE	—	—
0	494	24950	1224198	Sensible Heating	0	0,0	0	1224198	1224198	STABLE	—	—
0	517	25265	1249463	Sensible Heating	0	0,0	0	1249463	1249463	STABLE	—	—
0	552	26723	1276185	Sensible Heating	0	0,0	0	1276185	1276185	STABLE	—	—
0	616	29193	1305378	Sensible Heating	0	0,0	0	1305378	1305378	STABLE	—	—
0	651	31655	1337033	Sensible Heating	0	0,0	0	1337033	1337033	STABLE	—	—
0	661	32793	1369825	Sensible Heating	0	0,0	0	1369825	1369825	STABLE	—	—
0	609	31738	1401563	Sensible Heating	0	0,0	0	1401563	1401563	STABLE	—	—
0	550	28970	1430533	Sensible Heating	0	0,0	0	1430533	1430533	STABLE	—	—
0	499	26233	1456765	Sensible Heating	0	0,0	0	1456765	1456765	STABLE	—	—
0	485	24595	1481360	Sensible Heating	0	0,0	0	1481360	1481360	STABLE	—	—
0	497	24545	1505905	Sensible Heating	0	0,0	0	1505905	1505905	STABLE	—	—
0	589	27158	1533063	Sensible Heating	0	0,0	0	1533063	1533063	STABLE	—	—
0	789	34448	1567510	Sensible Heating	0	0,0	0	1567510	1567510	STABLE	—	—
0	1003	44795	1612305	Sensible Heating	0	0,0	0	1612305	1612305	STABLE	—	—
0	1410	60330	1672635	Sensible Heating	0	0,0	0	1672635	1672635	STABLE	—	—
0	1939	83725	1756360	Sensible Heating	0	0,0	0	1756360	1756360	STABLE	—	—
0	2066	100118	1856478	Sensible Heating	0	0,0	0	1856478	1856478	STABLE	—	—
0	1996	101533	1958010	Sensible Heating	0	0,0	0	1958010	1958010	STABLE	—	—
0	2264	106498	2064508	Sensible Heating	0	0,0	0	2064508	2064508	STABLE	—	—
0	3012	131903	2196410	Sensible Heating	0	0,0	0	2196410	2196410	STABLE	—	—
0	3476	162198	2358608	Sensible Heating	0	0,0	0	2358608	2358608	STABLE	—	—
0	5075	213765	2572373	Sensible Heating	0	0,0	0	2572373	2572373	STABLE	—	—
0	8165	330985	2903358	Sensible Heating	0	0,0	0	2903358	2903358	STABLE	—	—
0	12892	526418	3429775	Sensible Heating	0	0,0	0	3429775	3429775	STABLE	—	—
0	17273	754125	4183900	Sensible Heating	0	0,0	0	4183900	4183900	STABLE	—	—
0	14651	798100	4982000	Sensible Heating	0	0,0	0	4982000	4982000	STABLE	—	—
0	9598	606213	5588213	Sensible Heating	0	0,0	0	5588213	5588213	STABLE	—	—
0	8280	446950	6035163	Sensible Heating	0	0,0	0	6035163	6035163	STABLE	—	—
0	9194	436855	6472018	Melting	0	0,0	0	6472018	6472018	MELTING	—	—
0	8971	454120	6926138	Melting	0	0,0	0	6926138	6926138	MELTING	—	—
0	7640	415270	7341408	Melting	0	0,0	0	7341408	7341408	MELTING	—	—
0	7408	376193	7717600	Melting	0	0,0	0	7717600	7717600	MELTING	—	—
0	7974	384553	8102153	Melting	0	0,0	0	8102153	8102153	MELTING	—	—
0	8124	402445	8504598	Melting	0	0,0	0	8504598	8504598	MELTING	—	—
0	7370	387348	8891945	Melting	0	0,0	0	8891945	8891945	MELTING	—	—
0	6784	353848	9245793	Post-Melt	0	0,0	0	9245793	9245793	MELTING	—	—
0	7122	367628	9593420	Post-Melt	0	0,0	0	9593420	9593420	MELTING	—	—
0	7021	353570	9946990	Post-Melt	0	0,0	0	9946990	9946990	MELTING	—	—
0	6403	335605	10282595	Post-Melt	0	0,0	0	10282595	10282595	MELTING	—	—
0	5577	299300	10582095	Post-Melt	0	0,0	0	10582095	10582095	MELTING	—	—
0	5049	265650	10847745	Post-Melt	0	0,0	0	10847745	10847745	MELTING	—	—
0	4654	242575	11090320	Post-Melt	6,666666667	0,0	1841583,333	10925207	9083623	MELTING	—	—
0	4823	236935	11327255	Post-Melt	13,33333333	0,1	3683166,667	10992484	7309317	MELTING	—	—
0	5078	247545	11574800	Post-Melt	20	0,1	5524750	11065480	5540730	STABLE	—	—
0	4940	250465	11825265	Post-Melt	26,66666667	0,1	7366333,333	11136615	3770282	STABLE	—	—
0	4600	238493	12063758	Post-Melt	33,33333333	0,2	9207916,667	11192072	1984156	STABLE	—	—
0	4480	226983	12290740	Post-Melt	40	0,2	11049500	11232891	183391	STABLE	—	—
0	4545	225615	12516355	Post-Melt	46,66666667	0,2	12891083,33	11268781	-1622302	STABLE	—	—
0	4280	220615	12737070	Post-Melt	53,33333333	0,2	14732666,67	11296679	-3435988	STABLE	—	—
0	3844	203098	12940068	Post-Melt	60	0,3	16574250	11305943	-5268307	STABLE	—	—
0	4110	198843	13138910	Post-Melt	66,66666667	0,3	18415833,33	11308765	-7107069	STABLE	—	—
0	4682	219795	13358705	Post-Melt	73,33333333	0,3	20257416,67	11326762	-8930655	STABLE	—	—
0	5047	243218	13601923	Post-Melt	80	0,4	22099000	11361281	-10737719	STABLE	—	—
0	4943	249738	13851660	Post-Melt	86,66666667	0,4	23940583,33	11397626	-12542957	STABLE	—	—
0	4719	241553	14093213	Post-Melt	93,33333333	0,4	25782166,67	11423736	-14358431	STABLE	—	—
0	5032	243788	14337000	Post-Melt	100	0,5	27623750	11448327	-16175423	STABLE	—	—
0	5406	260955	14597955	Post-Melt	106,6666667	0,5	29465333,33	11483158	-17982175	STABLE	—	—
0	4336	243533	14841488	Post-Melt	113,3333333	0,5	31306916,67	11500914	-19806003	STABLE	—	—
0	3892	205898	15047185	Post-Melt	120	0,5	33148500	11480712	-21667788	STABLE	—	—
0	4348	206003	15253188	Post-Melt	126,6666667	0,6	34990083,33	11470614	-23519469	STABLE	—	—
0	4881	230718	15483905	Post-Melt	133,3333333	0,6	36831666,67	11470759	-25360908	STABLE	—	—
0	4661	238558	15722463	Post-Melt	140	0,6	38673250	11474078	-27199172	STABLE	—	—
0	4369	225768	15948230	Post-Melt	146,6666667	0,7	40514833,33	11465561	-29049272	STABLE	—	—
0	4064	210865	16159075	Post-Melt	153,3333333	0,7	42356416,67	11444186	-30912231	STABLE	—	—
0	3733	194930	16354005	Post-Melt	160	0,7	44198000	11409802	-32788198	STABLE	—	—
0	3936	191720	16545725	Post-Melt	166,6666667	0,8	46039583,33	11371099	-34668984	STABLE	—	—
0	4784	218008	16763733	Post-Melt	173,3333333	0,8	47881166,67	11350000	-36531166	STABLE	—	—
0	5244	250695	17014428	Post-Melt	180	0,8	49722750	11348229	-38374521	STABLE	—	—
0	5333	264418	17278845	Post-Melt	186,6666667	0,8	51564333,33	11353010	-40211323	STABLE	—	—
0	5466	269970	17548815	Post-Melt	193,3333333	0,9	53405916,67	11358728	-42047189	STABLE	—	—
0	5651	277915	17826730	Post-Melt	200	0,9	55247500	11366825	-43880675	STABLE	—	—
0	5703	283845	18110575	Post-Melt	206,6666667	0,9	57089083,33	11375888	-45713195	STABLE	—	—
0	5575	281945	18392520	Post-Melt	213,3333333	1,0	58930666,67	11380986	-47549681	STABLE	—	—
0	5359	273348	18665868	Post-Melt	220	1,0	60772250	11378170	-49394080	STABLE	REACHED	—
0	5066	260625	18926493	Post-Melt	221,9301618	1,0	61305433,07	11365275	-49940158	STABLE	REACHED	—
0	4860	248143	19174635	Post-Melt	221,9301618	1,0	61305433,07	11342858	-49962575	STABLE	REACHED	—
0	5037	247403	19422038	Post-Melt	221,9301618	1,0	61305433,07	11318158	-49987275	STABLE	REACHED	—
0	5309	258635	19680673	Post-Melt	221,9301618	1,0	61305433,07	11298128	-50007305	STABLE	REACHED	—
0	5164	261810	19942483	Post-Melt	221,9301618	1,0	61305433,07	11277981	-50027452	STABLE	REACHED	—
0	4828	249780	20192263	Post-Melt	221,9301618	1,0	61305433,07	11249228	-50056205	STABLE	REACHED	—
0	4640	236703	20428965	Post-Melt	221,9301618	1,0	61305433,07	11211654	-50093779	STABLE	REACHED	—
0	4495	228395	20657360	Post-Melt	221,9301618	1,0	61305433,07	11168214	-50137219	STABLE	REACHED	—
0	4331	220668	20878028	Post-Melt	221,9301618	1,0	61305433,07	11119446	-50185967	STABLE	REACHED	—
0	4147	211950	21089978	Post-Melt	221,9301618	1,0	61305433,07	11065121	-50240312	STABLE	REACHED	—
0	4113	206490	21296468	Post-Melt	221,9301618	1,0	61305433,07	11007108	-50298325	STABLE	REACHED	—
0	4188	207113	21503580	Post-Melt	221,9301618	1,0	61305433,07	10948889	-50356544	STABLE	REACHED	—
0	4358	213633	21717213	Post-Melt	221,9301618	1,0	61305433,07	10893035	-50412398	STABLE	REACHED	—
0	4555	222810	21940023	Post-Melt	221,9301618	1,0	61305433,07	10840951	-50464482	STABLE	REACHED	—
0	4693	226195	22166618	Post-Melt	221,9301618	1,0	61305433,07	10788651	-50515782	STABLE	REACHED	—
0	4318	220275	22386893	Post-Melt	221,9301618	1,0	61305433,07	10734637	-50570796	STABLE	REACHED	—
0	4237	213365	22600258	Post-Melt	221,9301618	1,0	61305433,07	10675696	-50629827	STABLE	REACHED	—
0	4233	211238	22811495	Post-Melt	221,9301618	1,0	61305433,07	10614963	-50690470	STABLE	REACHED	—
0	4314	211163	23022658	Post-Melt	221,9301618	1,0	61305433,07	10553725	-50751708	STABLE	REACHED	—
0	4015	205723	23228380	Post-Melt	221,9301618	1,0	61305433,07	10489501	-50815933	STABLE	REACHED	—
0	3766	194335	23422915	Post-Melt	221,9301618	1,0	61305433,07	10419873	-50883560	STABLE	REACHED	—
0	3424	179765	23602680	Post-Melt	221,9301618	1,0	61305433,07	10343520	-50961913	STABLE	REACHED	—
0	3034	161468	23764148	Post-Melt	221,9301618	1,0	61305433,07	10259233	-51046201	STABLE	REACHED	—
0	2653	142180	23906328	Post-Melt	221,9301618	1,0	61305433,07	10168959	-51138474	STABLE	REACHED	—
0	2410	126573	24032900	Post-Melt	221,9301618	1,0	61305433,07	10068621	-51236812	STABLE	REACHED	—
0	2200	115248	24148148	Post-Melt	221,9301618	1,0	61305433,07	9962183	-51339150	STABLE	REACHED	—
0	2028	105705	24253853	Post-Melt	221,9301618	1,0	61305433,07	9860881	-51444553	STABLE	REACHED	—
0	1856	97115	24350968	Post-Melt	221,9301618	1,0	61305433,07	9752967	-51552466	STABLE	REACHED	—
0	1706	89058	24440025	Post-Melt	221,9301618	1,0	61305433,07	9642903	-51662531	STABLE	REACHED	—
0	1577	82085	24522110	Post-Melt	221,9301618	1,0	61305433,07	9531243	-51774190	STABLE	REACHED	—
0	1480	76445	24598555	Post-Melt	221,9301618	1,0	61305433,07	9418812	-51886821	STABLE	REACHED	—
0	1367	71188	24669743	Post-Melt	221,9301618	1,0	61305433,07	9305238	-52000195	STABLE	REACHED	—
0	1292	66488	24736230	Post-Melt	221,9301618	1,0	61305433,07	9191406	-52114027	STABLE	REACHED	—
0	1223	62883	24799113	Post-Melt	221,9301618	1,0	61305433,07	9077382	-52227851	STABLE	REACHED	—
0	1171	59835	24858948	Post-Melt	221,9301618	1,0	61305433,07	8964011	-52341422	STABLE	REACHED	—
0	1127	57445	24916393	Post-Melt	221,9301618	1,0	61305433,07	8850960	-52454473	STABLE	REACHED	—
0	1084	55278	24971670	Post-Melt	221,9301618	1,0	61305433,07	8738530	-52566903	STABLE	REACHED	—
0	1029	52823	25024493	Post-Melt	221,9301618	1,0	61305433,07	8626640	-52678793	STABLE	REACHED	—
0	978	50175	25074668	Post-Melt	221,9301618	1,0	61305433,07	8515245	-52790188	STABLE	REACHED	—
0	1040	50450	25125118	Post-Melt	221,9301618	1,0	61305433,07	8405347	-52900086	STABLE	REACHED	—
0	1314	58843	25183960	Post-Melt	221,9301618	1,0	61305433,07	8299600	-53005833	STABLE	REACHED	—
0	1619	73310	25257270	Post-Melt	221,9301618	1,0	61305433,07	8199835	-53105598	STABLE	REACHED	—
0	2281	97493	25354763	Post-Melt	221,9301618	1,0	61305433,07	8108935	-53196498	STABLE	REACHED	—
0	3170	130273	25493035	Post-Melt	221,9301618	1,0	61305433,07	8031143	-53274290	STABLE	REACHED	—
0	2752	148058	25639093	Post-Melt	221,9301618	1,0	61305433,07	7957527	-53347906	STABLE	REACHED	—
0	2060	120310	25759403	Post-Melt	221,9301618	1,0	61305433,07	7875839	-53429594	STABLE	REACHED	—
0	1646	92640	25852043	Post-Melt	221,9301618	1,0	61305433,07	7786486	-53518948	STABLE	REACHED	—

Figure 43 Calculating steel melting onset, heat flux exposure, and cooling effects (none, partial, or full submersion).

STEP 6: Outputs and Visualization Module

This module automatically generates graphs and visual summaries of simulation results. It pulls computed data from earlier steps and visualizes:

1. HRR curves (per module, rack, and room)
2. THR totals
3. Fire duration
4. Steel melting timelines
5. Propagation charts

Sensitivity visuals:

1. Radar/spider charts (effect of SOC, rack distance, etc.)

It also includes:

1. Conditional formatting for warnings (e.g., “Steel melts at T = xxx s”)
2. Toggle buttons or dropdowns for scenario switching.

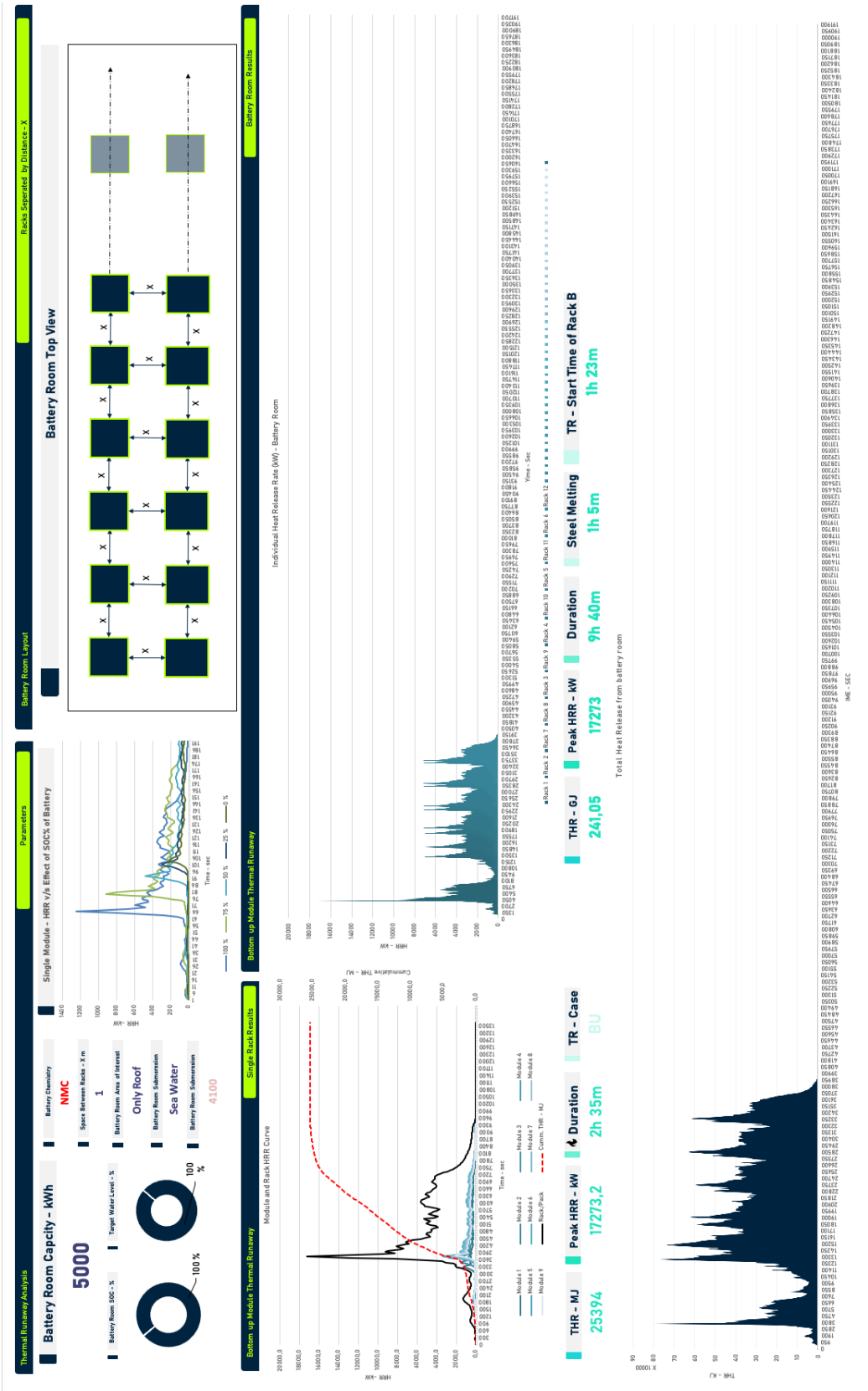

Figure 44 the visualization module compiles results into HRR/THR curves, structural response charts, and sensitivity plots for design evaluation

The simulation tool concludes with an integrated output dashboard that visualizes the results of each scenario. HRR and THR curves are plotted for individual modules, racks, and the entire battery room, enabling easy comparison across scenarios. Structural failure predictions are displayed in time-series charts showing the onset of melting in various surfaces. Sensitivity analysis results are visualized through tornado charts (ranking parameter influence) and radar/spider charts (multi-variable effects on key outputs). Conditional formatting highlights critical thresholds such as excessive flame height, unacceptable heat flux, or late rack ignition. These visual tools support intuitive interpretation of the fire dynamics and facilitate fast design decisions during conceptual ship safety planning.

4 Validation Case: Corvus Blue Whale ESS

Corvus Energy is a leading supplier of marine battery systems for hybrid and all-electric vessels.[51] Its product lines include the Orca, Dolphin, Marlin, Moray, and Blue Whale ESS, which are all optimized for specific maritime applications.[52] The Corvus Blue Whale was created specifically for high-energy, low-power applications in large vessels like ferries, cruise ships, and offshore support vessels. It uses lithium iron phosphate ($LiFePO_4$, LFP) prismatic cells and features passive single-cell thermal runaway isolation, as well as fail-safe protection circuits for over-temperature and over-voltage events.[53]

This validation study focuses on the Corvus Blue Whale ESS, which produces 48.23 kWh of energy per module with a nominal voltage of 80 V and a total capacity of 628 Ah. The system has a continuous discharge rate of 0.7C, making it ideal for long-duration, emission-free operations like port stays or transit at low loads. [38]DNV and RINA have class-approved the Blue Whale system, indicating that it is suitable for maritime use. [54]

While the Corvus specification sheet does not specify the exact cell model or configuration, modeling assumptions were required to proceed. Based on the energy, voltage, and chemistry, this thesis assumes that each module has 75 prismatic LFP cells arranged in a 25S3P configuration. Each cell is expected to deliver approximately 672 Wh (3.2 V, 210 Ah), which is comparable to commercially available high-capacity prismatic LFP cells.[55]

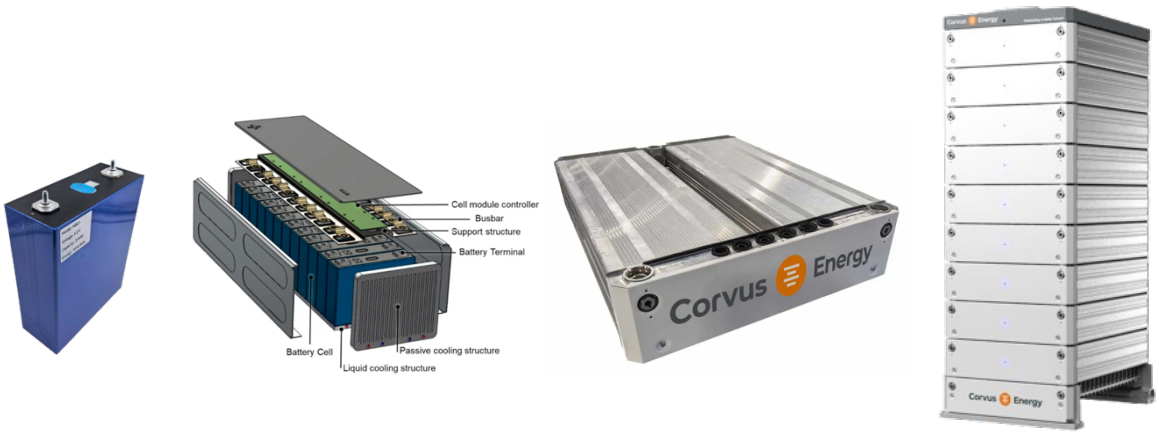

Figure 45 Battery Cell to Rack Structure in Corvus Marine ESS

Specification	Value
Battery Cell Chemistry	Lithium Iron Phosphate ($LiFePO_4$)
Single Module Capacity	628 Ah
Single Module Energy	48.23 kWh
Module Voltage	80 VDC
C-Rate (Peak)	1C / 1C for 20 minutes
C-Rate (Continuous)	0.7C / 0.7C
Module Dimensions (L x W x H)	1165 x 905 x 238 mm
Module Weight	395 kg
Volumetric Energy Density	192 Wh/L
Specific Energy	122 Wh/kg
Cooling Method	Forced air

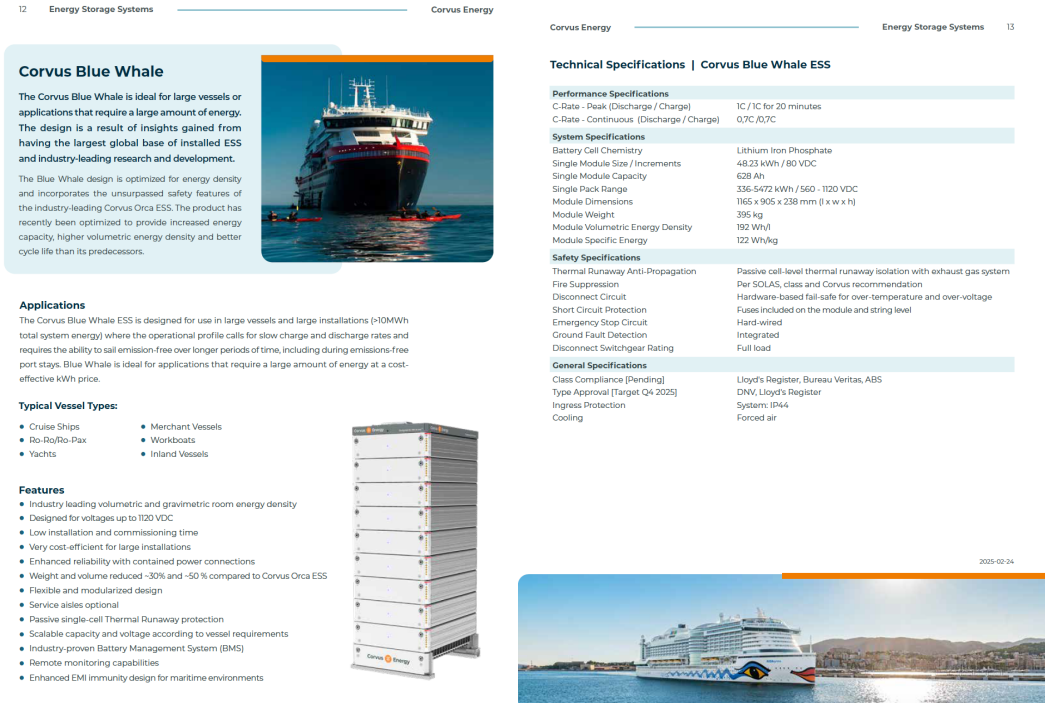

Figure 46 Technical Specifications of Corvus Blue Whale Battery Module and Rack

4.1 Cell Configuration Assumption

To estimate the internal configuration of the Blue Whale module, we selected the EVE MB31 prismatic LFP cell as a representative cell model. [56] This cell is a Grade A 3.2 V, 314 Ah lithium iron phosphate cell with a single stud terminal, selected for its close match with Corvus's known voltage specification and its suitability for high-energy marine battery modules.

To achieve the module's specified output of 80 V and 628 Ah, a configuration of 25 cells in series is required to meet the voltage requirement.

$$25\ cells\ \times\ 3.2\ V\ =\ 80\ V \tag{28}$$

To reach a total module capacity of 628 Ah, and since each EVE cell is 314 Ah, we need two parallel strings:

$$314\ Ah\ \times\ 2\ =\ 628\ Ah \tag{29}$$

Therefore, the total number of cells in the module is:

$$25\ (series)\times\ 2\ (parallel)=\ 50\ cells\ per\ module \tag{30}$$

According to manufacturer data, each cell has a volume of 2.58 liters and weighs 3.8 kg. This gives a total cell volume of 129 liters and a total mass of 190 kilograms. However, refined volume and weight estimates from the Excel model show:

Therefore, the total number of cells in the module is:

Table 7 Cell Configuration and Calculation of Total Cells per Module

Parameter	Value	Description
Cell Capacity - Ah	314	Standard LFP cell capacity
Cell Voltage	3,2	Standard LFP cell voltage
Cell Energy - Wh	896	Typical energy per cell
Cell (T x W x H)	71× 173.7 × 207.2 mm	Standing orientation
Single Cell Volume	2,58	Each cell volume in liters
Single Cell Weight	3,8	Each cell weight
Cells in Series	25	Number of cells in series for 80 V
Parallel Strings	2	2 parallel strings to reach 628 Ah
Total Cells	56	Total number of cells (25SP)
Total Energy - kWh	50,24	Energy stored in the module
Total Volume (L)	194	Cell volume inside the module
Total Cell Weight (kg)	213	Sum of all cell weights in module
Module Outer Volume (L)	251	Volume of the module enclosure
Cell Volume Fill Ratio	77 %	total module volume

4.2 Use of FM Global Experimental Data

To validate the thermal runaway model developed in this thesis, published experimental data from FM Global's full-scale fire tests [4] were used as the reference. These tests involved lithium iron phosphate (LFP) batteries constructed with prismatic cells.

The FM Global study calculated the total heat release of prismatic-cell LFP modules by considering both chemical combustion energy (electrolyte and plastic casing) and electrical energy (kWh converted to MJ). For a 5.2 kWh module, the estimated theoretical energy was: Using Eq. (3), (4) & (5)

1. Electrolyte (2.6 kg × 28 MJ/kg) = 73 MJ
2. Plastics (4.9 kg × 38 MJ/kg) = 188 MJ
3. Electrical energy (5.2 kWh × 3.6 MJ/kWh) = 18.7 MJ
4. Total theoretical energy = ~279 MJ per module

However, in real-world fire tests, the actual released energy was much lower:

1. Chemical THR = ~143 MJ (51% of theoretical)
2. Convective THR = ~101 MJ (36% of theoretical)

Supporting graphs illustrate this behavior. In the single-module HRR profile, the first flame event begins at ~3600 seconds, reaching ~400–500 kW. Heat Release Rate Profile of a Single LFP Module During Thermal Runaway

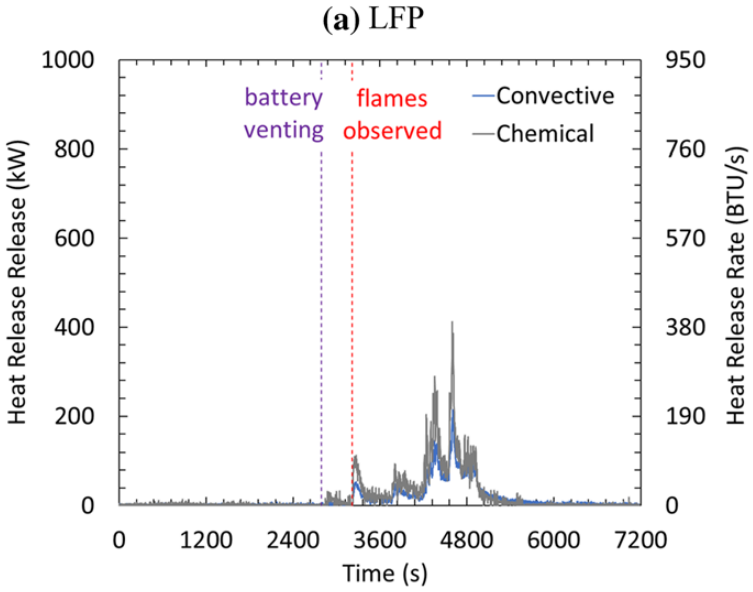

Figure 47 HRR Profile of a Single LFP Module [4]

Based on the FM Global study findings, the table summarizes the total energy content and fire behavior at the cell, module, and rack levels for lithium iron phosphate (LFP) battery systems.

The Appendix A contains additional results, detailed fire test data, and the FM Global-based model parameters used in the simulations.

4.3 Corvus Blue Whale Module: Combustion Energy and THR Estimation

To estimate the Corvus Blue Whale module's total heat release and combustion energy, an internal cell configuration based on standard LFP cells with a nominal voltage of 3.3 V and a capacity of 20 Ah is assumed. Notably, this is the same cell type as used in the FM Global fire test. To ensure consistency and accuracy in thermal runaway modeling, the Corvus Blue Whale module is assumed to be made up of the same 20 Ah LFP cells

4.3.1 Cell Configuration

To match the module's rated output of 628 Ah at 80 V, the following configuration is derived:

$$\text{Number of series cells}: 80\ V\ /\ 3.3\ V\ \approx\ 24$$
$$\text{Number of parallel strings}: 628\ Ah\ /\ 20\ Ah\ \approx\ 31$$
$$\text{Total cells per module}: 24\ \times\ 31\ =\ 744\ (\text{configuration}: 24s31p)$$

Combustible Mass Breakdown

$$\text{Based on FM Global's data, } 15.31\%\ \text{of the module's mass is combustible.}$$
$$\text{Combustible mass}: 395\ kg\ \times\ 0.1531\ =\ 60.46\ kg$$
$$\text{Electrolyte}\ (34.67\%): 60.46\ kg\ \times\ 0.3467\ =\ 20.96\ kg$$
$$\text{Plastic}\ (65.33\%): 60.46\ kg\ \times\ 0.6533\ =\ 39.50\ kg$$

Chemical and Electrical Energy

$$\text{Electrolyte energy}: 20.96\ kg\ \times\ 28\ MJ/kg\ =\ 586.86\ MJ$$
$$\text{Plastic energy}: 39.50\ kg\ \times\ 38\ MJ/kg\ =\ 1501\ MJ$$
$$\text{Total chemical energy}: 586.86\ +\ 1501\ =\ 2087.86\ MJ$$
$$\text{Electrical energy}: 50.24\ kWh\ \times\ 3.6\ MJ/kWh\ =\ 180.86\ MJ$$
$$\text{Total combustion energy}: 2087.86\ +\ 180.86\ =\ 2268.72\ MJ$$

Estimated Heat Release

Using Eq. (6)

$$\text{Chemical THR}\ (51\%): 0.51\ \times\ 2268.72\ =\ 1168.97\ MJ$$
$$\text{Convective THR}\ (70.6\%\ \text{of chemical}): 0.706\ \times\ 1168.97\ =\ 825.64\ MJ$$

4.3.2 Corvus Blue Whale Rack: THR Estimation for a 9-Module System

To simulate full rack behavior, a standard Corvus battery rack made up of 9 Blue Whale modules.

Rack Parameters

$$Rack\ energy: 9 \times 50.24\ kWh = 452.16\ kWh$$
$$Electrical\ energy: 452.16 \times 3.6 = 1627.78\ MJ$$
$$Rack\ mass: 9 \times 395\ kg = 3555\ kg$$

Combustible Mass and Breakdown

$$Combustible\ mass: 3555\ kg \times 0.15 = 533.25\ kg\ (rounded\ to\ 544.13\ kg)$$
$$Electrolyte\ (35\%): 544.13\ kg \times 0.35 = 188.63\ kg$$
$$Plastic\ (65\%): 544.13\ kg \times 0.65 = 355.50\ kg$$

Rack Combustion Energy

$$Electrolyte\ energy: 188.63\ kg \times 28\ MJ/kg = 5281.71\ MJ$$
$$Plastic\ energy: 355.5\ kg \times 38\ MJ/kg = 13{,}509\ MJ$$
$$Total\ chemical\ energy: 5281.71 + 13{,}509 = 18{,}790.71\ MJ$$
$$Total\ energy\ (incl.\ electrical): 18{,}790.71 + 1627.78 = 20{,}418.49\ MJ$$

Rack THR Estimation

$$Chemical\ THR\ (86\%): 0.86 \times 20{,}418.49 = 17{,}519.2\ MJ$$
$$Convective\ THR\ (73\%\ of\ chemical): 0.73 \times 17{,}519.2 = 12{,}737.06\ MJ$$

The Appendix A includes additional results and detailed model parameters for the Corvus Energy Blue Whale module and rack, which were used as inputs in the thermal runaway simulations.

4.3.3 Estimation of Combustion Duration and Peak (HRR)

FM Global's experiments included scenarios with:

1. A single module.
2. A 6-module cabinet.
3. A complete 16-module rack.

The duration of combustion was determined using the period of significant heat release. For example, in the single-module test, thermal runaway began around 3000 seconds and combustion ended around 5360 seconds, resulting in a total burn duration of: 2360s

Using Eq. (7)

$$THR\ ratio = Corvus\ Energy\ Module\ THR\ /\ FM\ Global\ Module\ THR$$
$$= 1168.97/143 \approx 8.18$$

$$Scaling\ factor\ = \sqrt{8.18}\ \approx\ 2.86$$
$$Corvus\ module\ Combustion\ Duration\ = 2360\ s\ \times\ 2.86\ \approx\ 6748\ s$$

The Appendix A contains scaling logic for estimating peak combustion duration for the Corvus Blue Whale module using experimental results from FM Global's 20 Ah LFP module tests.

4.3.4 Peak HRR Estimation via Curve Fitting

Square root scaling produced realistic combustion durations, linear scaling of peak HRR based on energy ratios resulted in unrealistically high values. This is due to the nonlinearity of flame dynamics and the localized combustion behavior found in large battery modules. As a result, a different method was used to calculate peak HRR while maintaining the experimental (FM Global) HRR curve shape.

The method relies on the relationship between Total Heat Release (THR) and the area under the HRR curve. Given what we already know:

1. THR for the Corvus module (826 MJ convective).
2. Total combustion duration (e.g., 6748 seconds).
3. Normalized HRR shape from FM Global data.

We applied curve scaling to fit the HRR curve. The methodology is as follows: The experimental HRR curve (for example, FMG single module) was normalized in shape. As explained in the Chapter 3, Section 3.2.3

1. Excel Solver was used to adjust the peak HRR (scaling factor) Eq. (8) while keeping the shape constant.
2. The solver reduced the difference between the area under the scaled curve (total heat released) and the target THR (from the previous section). Eq. (9)

This method preserves realistic flame dynamics while producing a physically consistent peak HRR that can be used directly in thermal modeling and structural fire analysis.

The HRR curve for the Corvus Blue Whale module was created using a validated curve-scaling method based on FM Global experimental fire test data. The normalized HRR curve shape from the FMG module test was replicated and scaled in two dimensions: time and amplitude. As explained in the Chapter 3, Section 3.2.2 to estimate the target combustion duration, time scaling Eq. (7) was applied by taking the square root of the THR ratio between the Corvus and reference modules. As explained in the Chapter 3, Section 3.2.4 Amplitude scaling Eq. (11), (12) & (13) was accomplished by fitting the HRR

peak value so that the integrated area under the curve corresponded to the THR calculated for the Corvus system.

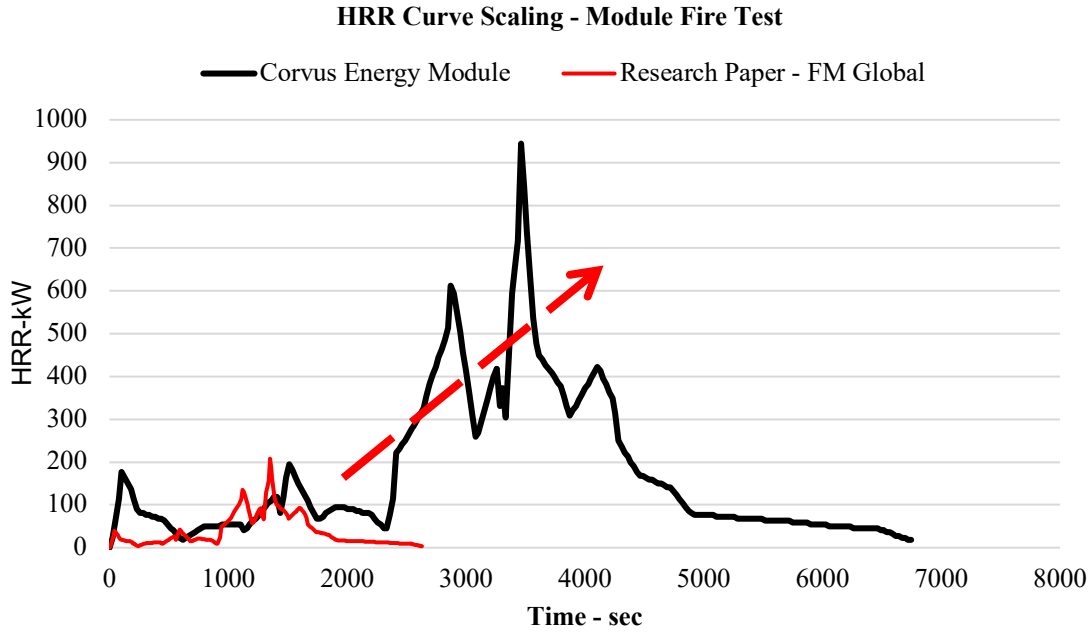

Figure 48 HRR vs. Combustion Duration: FM Global Module vs. Scaled Corvus Blue Whale Module

4.3.5 SOC Scaling strategy

To evaluate the impact of State of Charge (SOC) on thermal runaway behavior, scaling factors were applied to the baseline model (100% SOC) under lower SOC conditions. Because batteries with lower SOC contain less stored electrical energy and potentially less reactive material, the total heat release (THR) and peak heat release rate (HRR) are proportionately lower. Based on experimental trends and fire literature, a nonlinear scaling factor was assigned to each SOC level (e.g., 0.76 for 75% SOC, 0.515 for 50% SOC, and so on), as shown in Table 9. These factors were applied uniformly to THR, HRR, and combustion duration. As SOC decreases, combustion becomes less intense, but it may take longer to complete because the reduced heat generation causes slower thermal feedback. For example, 100% SOC has a peak HRR of 944 kW and a duration of ~6750 s, whereas 25% SOC has a lower peak (236 kW) but a longer burn time (~10,324 s).

Table 8 Corvus Energy Scaled parameters SOC levels

Corvus Energy Module	100 %(Base case)	75 %	50 %	25 %	0 %
THR - MJ	1168,9	935,1	701,3	584,4	467,5
Peak HRR - kW	944,38	717	486	236	170
Combustion Duration - s	6750	7894,6	8974,2	10323,7	10661,1

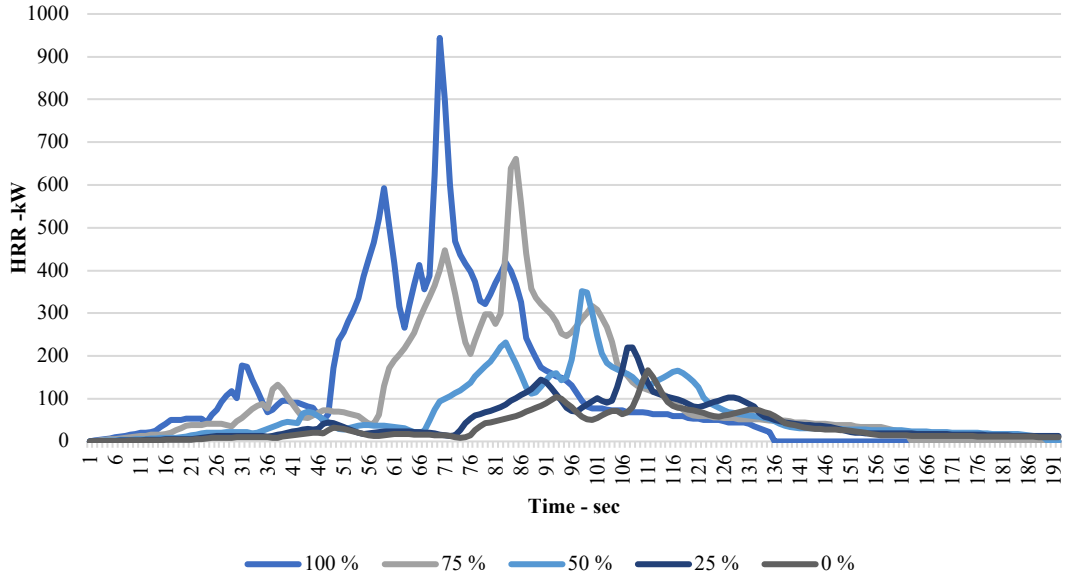

Figure 49 Heat release rate (HRR) as a function of battery state of charge (SOC).

4.4 Rack Level HRR and THR Estimation

4.4.1 Bottom-UP Thermal Runaway

In bottom-up scaling approach start delay for each module determines when thermal runaway occurs with respect to Module 1. The rack THR is calculated by adding the THR contributions of all nine modules. Similarly, the rack-level HRR curve is created by time-aligning each scaled module HRR curve based on its delay and duration, and then adding the instantaneous HRR values from all active modules at each time step.

Figure 50 Corvus Energy Rack with 9 Modules TR Initiated (Module 1)

To estimate the heat release rate (HRR) curves for modules after the first (e.g., Modules 2 and up in the rack), we start with known data from Module 1, for which the HRR profile has already been defined. Module 1 has a combustion duration of 6748 seconds and a total heat release (THR) of 1169 MJ.

We assume that Module 2 (the module directly above Module 1 in a bottom-up propagation scenario) ignites when a certain percentage of heat (THR) from Module 1 is released. In our model, we set the ignition threshold to 9% of Module 1's THR. By analyzing Module 1's HRR series, we can determine that the 9% energy release occurs at around 1700 seconds, which is then used to calculate the ignition start time for Module 2.

To calculate the end time of Module 2 combustion, we use a time-scaling factor of 0.95, implying that Module 2 burns slightly faster than Module 1 due to preheating and elevated temperatures. Thus, its combustion time is set to 95% of Module 1's.

Similarly, Module 2's peak HRR is scaled up by an amplitude factor of 1.2, assuming increased combustion behavior due to heat feedback. After determining the peak HRR, THR and new combustion duration for Module 2, we use time and amplitude scaling techniques to generate the complete HRR curve for Module 2. This is accomplished by stretching or compressing the Module 1 HRR series to fit the new duration and adjusting the intensity to match the new peak HRR.

Table 9 Scaled Combustion Parameters for Each Module Based on Module 1 Reference

Module	THR (MJ)	Duration (s)	Peak HRR (kW)	Start Delay (s)
1	1169	6748	944,3	0
2	1158,4	6410,1	1133,2	1700
3	1143,2	6342,6	1416,5	2150
4	1128,0	6275,2	1605,4	2250
5	1112,8	6207,7	2077,6	2400
6	1098,8	6140,2	2549,8	2550
7	1083,6	6072,7	2266,5	2700
8	1069,6	6005,3	1888,7	2850
9	1052,0	5937,8	1605,4	3000

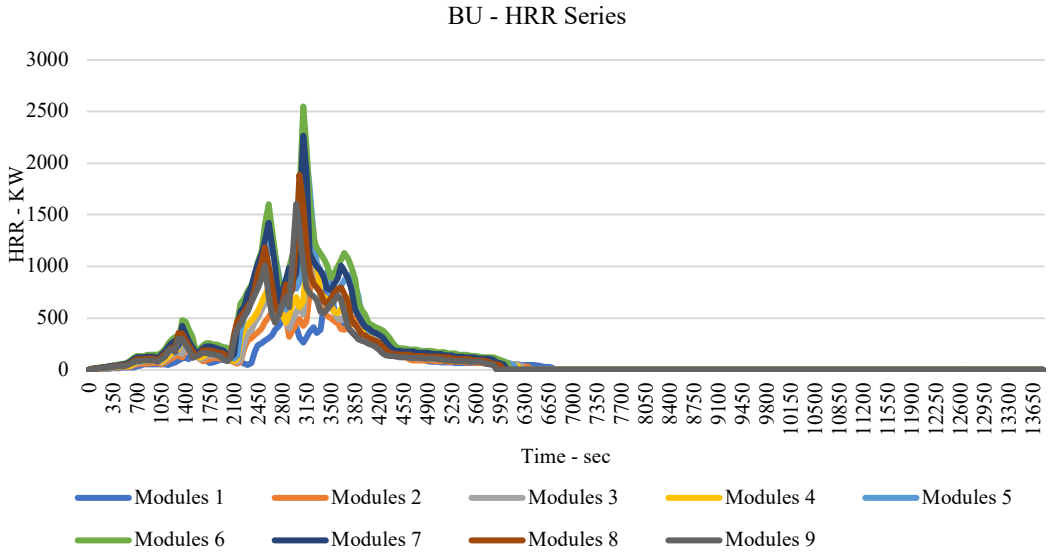

Figure 51 Delayed HRR profiles for 9 modules

The scaled HRR curve for Module 2 is then used as an input to generate the overall rack-level HRR. The same procedure is followed for each module in the rack, with adjustments made to ignition timing, combustion duration, and HRR scaling factors based on their relative position and assumed fire exposure.

Table 10 BU scaling factors, peak HRR, THR contribution, and combustion duration for a Corvus Blue Whale rack.

Module	THR (MJ)	Duration (s)	Peak HRR (kW)	Start Delay (s)	End Time	THR Scaling	Duration Scaling	Peak HRR Scaling	Fraction of THR
1	1169	6748	944	0	6748	1	1	1	-
2	1158	6410,2	1133	1700	8110	0,991	0,95	1,2	8,0 %
3	1143	6342,7	1417	2150	8493	0,978	0,94	1,5	0,4 %
4	1128	6275,2	1605	2250	8525	0,965	0,93	1,7	0,1 %
5	1112	6207,7	2078	2400	8608	0,952	0,92	2,2	0,1 %
6	1098	6140,3	2550	2550	8690	0,94	0,91	2,7	0,1 %
7	1083	6072,8	2267	2700	8773	0,927	0,9	2,4	0,1 %
8	1069	6005,3	1889	2850	8855	0,915	0,89	2	0,1 %
9	1052	5937,8	1605	3000	8938	0,9	0,88	1,7	0,1 %

The figure below shows the HRR profile for a Corvus Blue Whale battery rack made up of nine modules that are under thermal runaway in a sequential ignition scenario. The rack has a THR of approximately 17 GJ. The rack shows a gradual increase in HRR as flames spread from one module to the next. The peak HRR is around 8500 kW. The total combustion duration is 13,500 seconds (~3 hours and 45 minutes).

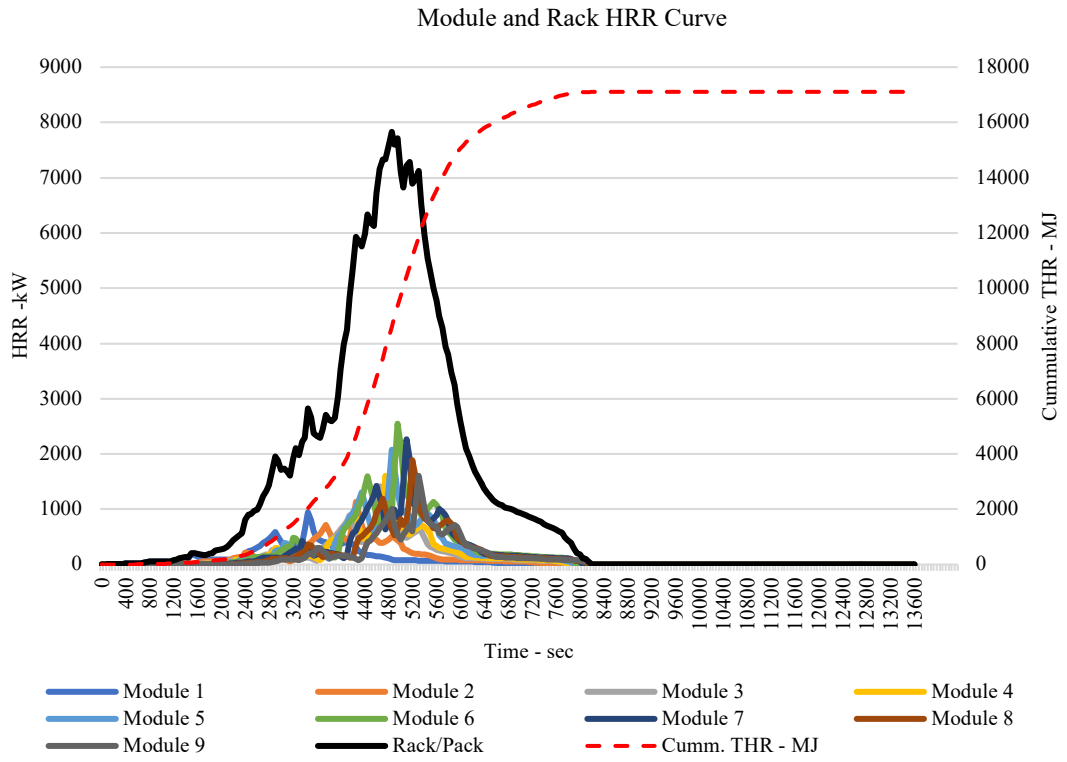

Figure 52 HRR Profiles Over Combustion Duration for Individual Modules and Full Rack

4.4.2 Rack-to-Rack Propagation Based on Radiative Heat Flux

To simulate the propagation of thermal runaway from Rack A to Rack B, a radiative heat flux model (using Eq. (2)) was developed using Rack A's HRR profile. FM Global's used the following approach to calculate heat flux at different distances from the flame source (derived from HRR via Heskestad's correlation). The threshold for thermal runaway initiation was set at 60 kW/m².

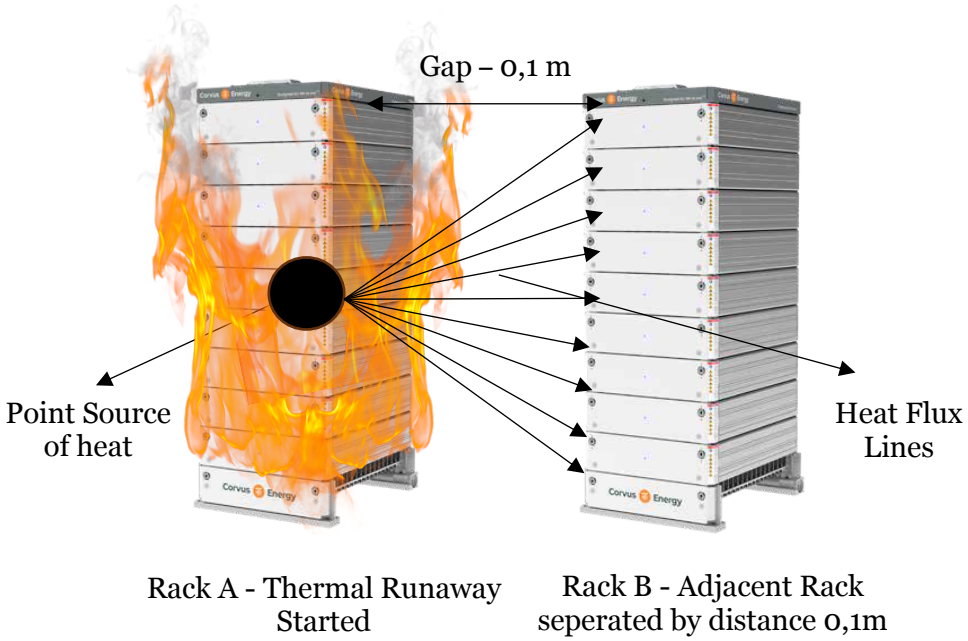

Figure 53 Radiative heat flux from Rack A flame to Rack B module faces.

The model calculates the incident heat flux over time for each module in Rack B as flames grow and decay in Rack A. The minimum ignition delay is recorded when any of the module's in rack B reaches the 60 kW/m² threshold. However, thermal runaway does not occur immediately at this threshold. An additional ignition delay of 3000 seconds is imposed to account for the time required for heat absorption, internal heating, and gas venting prior to ignition. This leads to a two-stage delay logic.

TR Trigger Time = Heat flux ≥ 60 kW/m². [57]
TR Start Time = TR Trigger Time + 3000 seconds. Eq. (18)

This logic is applied separately to each module in Rack B. The resulting TR start times are shown in the table below, with each module having a different

ignition time based on its vertical position and exposure to radiation from Rack A.

Radiative fraction (χ_r)	0,25
Distance between racks (d)	0,1
Heat source height (z_A)	1,071
TR Threshold (kW/m²)	60
heat flux remains - s (Delay)	3000
TR - Start Time of Rack B - s	3050

Module	TR - Start Time - s	TR - Start Time + Delay
1	4650	7650
2	3450	6450
3	2850	5850
4	2400	5400
5	50	3050
6	2400	5400
7	2850	5850
8	3450	6450
9	4650	7650

After finding the time-resolved heat flux distribution from Rack A, we assumed module with the highest heat flux is at top module of Rack B. For this scenario, a top-down thermal runaway propagation mode is assumed in Rack B. This approach differs from the previously modeled bottom-up case. In the top-down model, once the top module in Rack B reaches the radiative ignition threshold and experiences thermal runaway (with the applied delay), it becomes the new source of ignition for the lower modules. New scaling factors are applied to each module in Rack B to account for differences in flame spread direction (top-down vs. bottom-up).

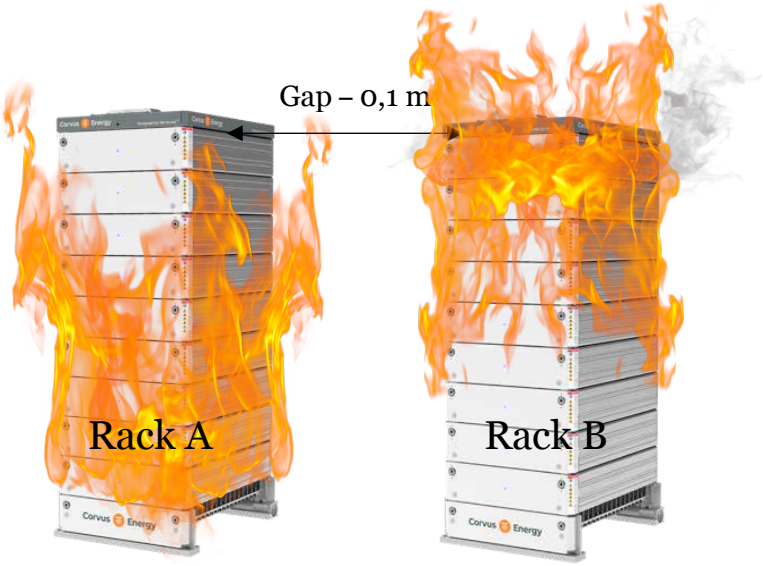

Figure 54 Thermal Runaway Propagation from Rack A (Bottom-Up) to Rack B (Top-Down Initiation)

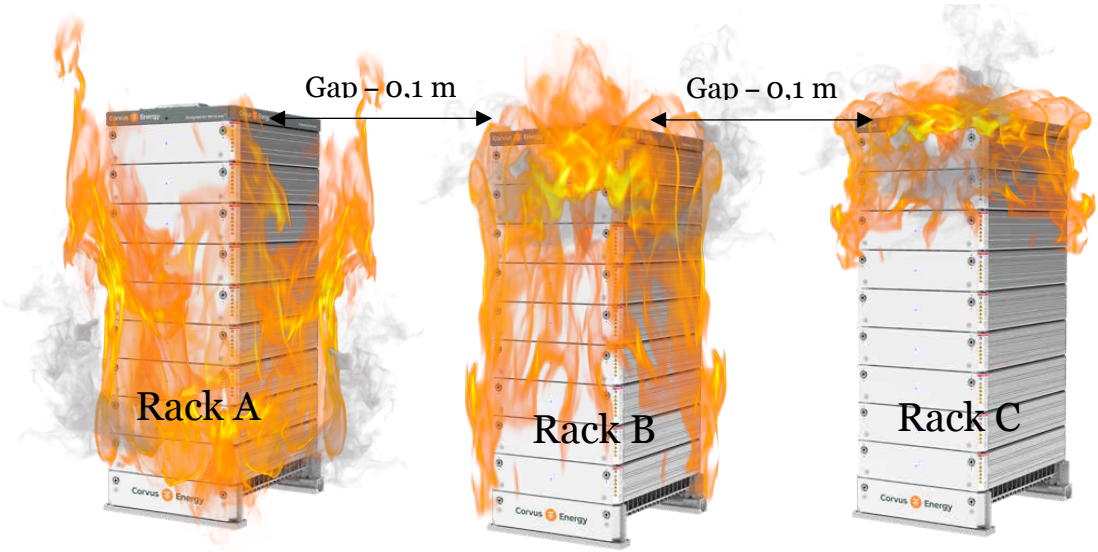

Figure 55 Thermal Runaway Propagation from Rack A (Bottom-Up) to Rack B (Top-Down Initiation) to Rack C (Top-Down Initiation)

The figure below shows the resulting HRR series for Racks A and B, which show Rack A's initial ignition and peak fire intensity, followed by Rack B's delayed onset and extended burning profile.

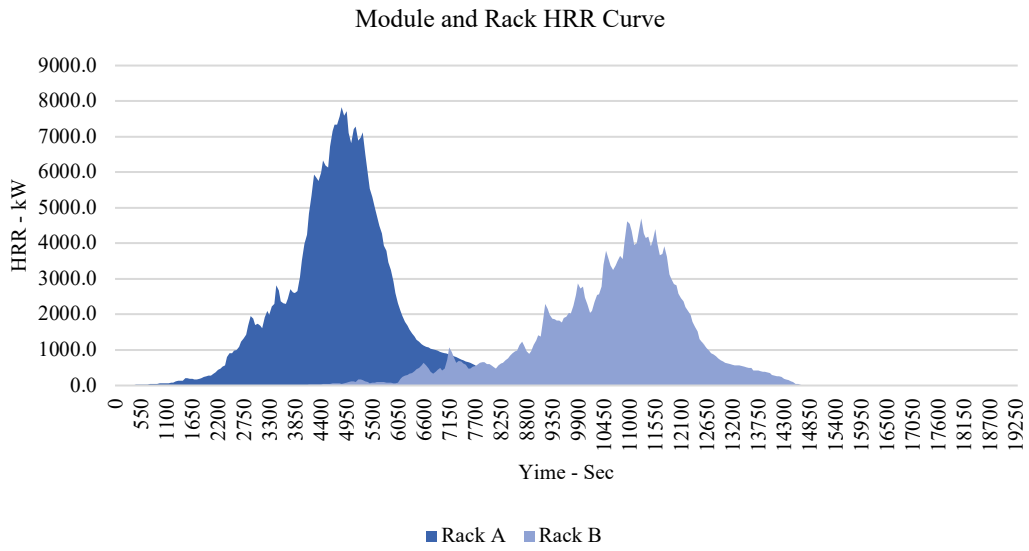

Figure 45: Rack-level HRR comparison for thermal runaway propagation from Rack A to Rack B under top-down ignition assumption.

4.4.3 Thermal Runaway Timing in a 5 MWh Battery Room

To simulate thermal runaway propagation in a full 5 MWh battery room, the model assumes 12 racks, each with 9 Corvus Blue Whale modules. With a module energy of 50.24 kWh, 12 racks are needed to achieve a total capacity of approximately 5 MWh. The racks are arranged in a 6-by-2 grid with defined X and Y spatial coordinates, which represent the physical layout and distance between racks.

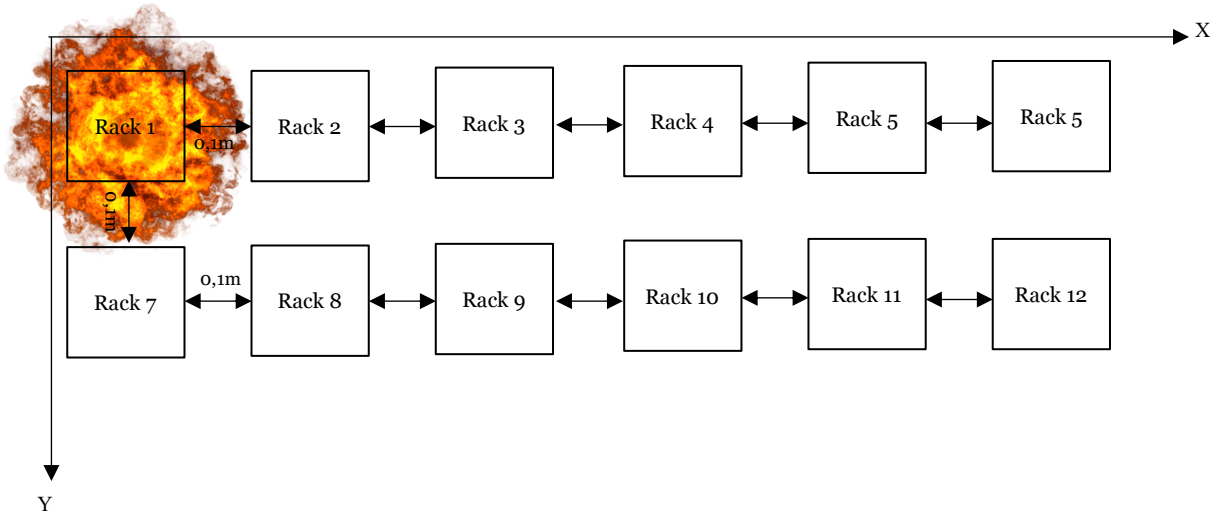

Thermal runaway occur in Rack 1, with fire spreading throughout the room. The delay before ignition for each subsequent rack is calculated using the distance from Rack 1 multiplied by a delay-per-meter factor of Rack B delay/Space between using Eq. (16), (17) & (18) Racks = 3050/0,1= 30,500

seconds/meter. The table displays the compiled and sorted start times for each rack, ranging from 0 seconds (Rack 1) to ~15,552 seconds (Rack 12).

This delay model allows for time-resolved superposition of HRR curves in each rack. The final HRR profile for the entire battery room is calculated by adding the delayed HRR series for all 12 racks, which were built from the previously scaled 9-module fire model. This produces a comprehensive HRR curve for the entire battery room, capturing the staggered onset of combustion throughout the spatial layout.

Table 11 Spatial coordinates, delay distances, and thermal runaway start times for all 12 racks in the 5 MWh battery room layout.

Total Racks (even):	**12**
Racks per row:	6
Spacing between racks (m):	0,1
Delay per meter (s):	30500
Ignition Rack #:	1
Ignition Start Time (s):	0

Rack	**No.**	**X**	**Y**	**Start_Time**	**Helper_Index**	**Sorted Time**	**Corresponding Rack**	**Start_Time**
Rack 1	1	0	0,0	0,0	0,0	0,0	Rack 1	0
Rack 2	2	0,1	0,0	3050,0	3050,0	3050,0	Rack 2	3050
Rack 3	3	0,2	0,0	6100,0	6100,0	3050,0	Rack 7	3050
Rack 4	4	0,3	0,0	9150,0	9150,0	4313,4	Rack 8	4313
Rack 5	5	0,4	0,0	12200,0	12200,0	6100,0	Rack 3	6100
Rack 6	6	0,5	0,0	15250,0	15250,0	6820,0	Rack 9	6820
Rack 7	7	0	0,1	3050,0	3050,0	9150,0	Rack 4	9150
Rack 8	8	0,1	0,1	4313,4	4313,4	9644,9	Rack 10	9645
Rack 9	9	0,2	0,1	6820,0	6820,0	12200,0	Rack 5	12200
Rack 10	10	0,3	0,1	9644,9	9644,9	12575,5	Rack 11	12575
Rack 11	11	0,4	0,1	12575,5	12575,5	15250,0	Rack 6	15250
Rack 12	12	0,5	0,1	15552,0	15552,0	15552,0	Rack 12	15552

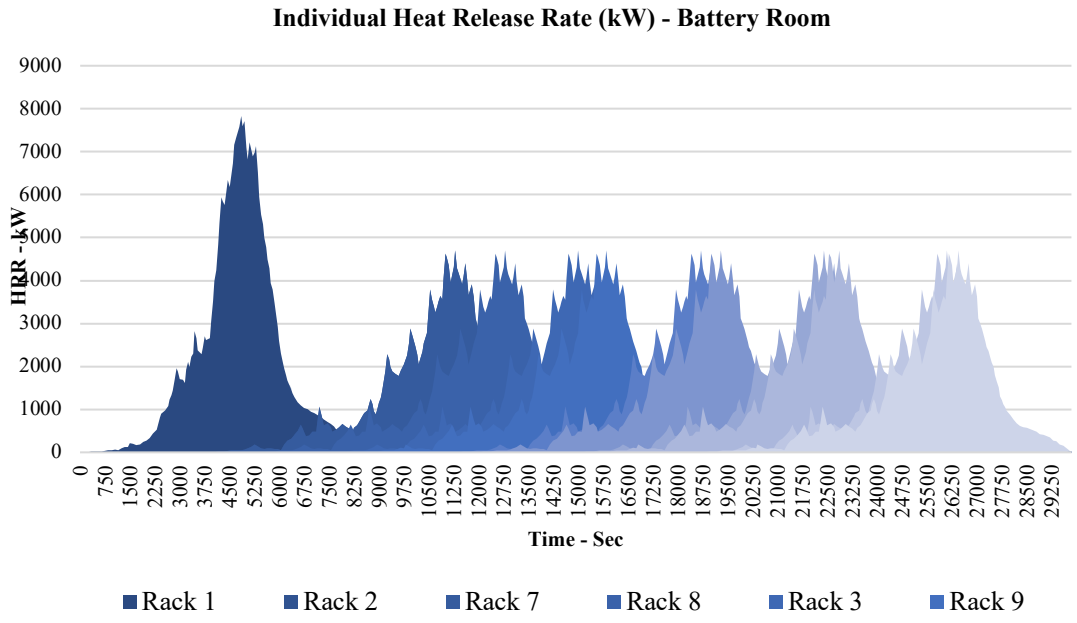

Figure 56 HRR profiles of individual racks in a 5 MWh battery room with staggered ignition.

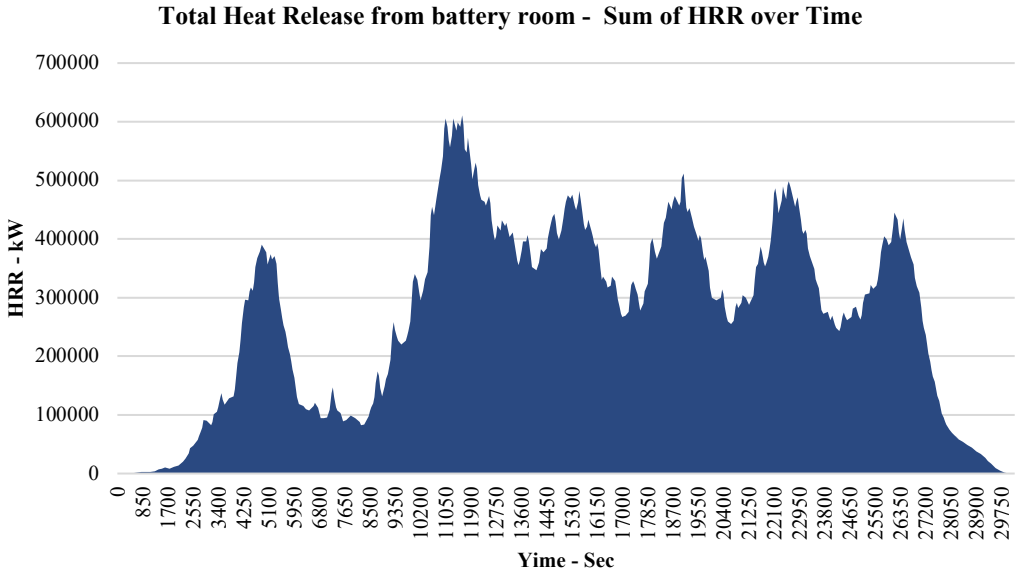

Figure 57 Total HRR from the full battery room

4.4.4 Structural Steel Melting Analysis – 5 MWh Battery Room

To evaluate the risk of structural failure during a thermal runaway event in a 5 MWh marine battery room, a heat balance analysis was performed on the ship steel structure of battery room. The room's modeled layout includes 12

Corvus racks measuring 4.03 m × 7.53 m × 3.74 m, as well as structural components like wall plating, ceiling plates, vertical frames, and horizontal stringers. The steel volume was calculated to be 1.166 m^3, with a total mass of approximately 9.15 tonnes (Walls + Roof). Eq. (21) & (22)

To estimate the energy required to melt this steel, two ther mal processes were considered.

1. Sensible heat: increasing steel temperature from ambient (20°C) to melting (~1500°C).
2. Latent heat of fusion: the energy needed to melt steel at a constant temperature.

Using a specific heat of 0.49 kJ/kg·K and latent heat of 272 kJ/kg, the total energy required to melt all structural steel was calculated as approximately 9.13 GJ (6.63 GJ sensible + 2.49 GJ latent). Eq. (23), (24) & (25)

By comparing the cumulative heat release curve (THR) from the room-level HRR data with this threshold, the point in time when melting begins can be identified. Eq. (27) In the bottom-up thermal runaway scenario (ignition from Rack 1 upward), the steel melts at around 5250 seconds and maintains full melting conditions for about 400 seconds. This is based on the intersection of cumulative THR and the energy required to reach 1500°C.

Additional thermal runaway supression scenarios were tested with seawater submersion. Despite a high peak HRR (13.7 MW) and total THR (~162 GJ), the heat flux to the steel structure was reduced enough to avoid melting.

Table 12 5 MWh Battery Room Specification and Steel requirement

Component	Value	Unit	Description
Room Length	4,03	m	Length = racks per row × (rack length + spacing) + margins
Room Width	7,53	m	2 rows of racks + spacing + margins
Room Height	3,742	m	Rack height + top/bottom margin
Room Volume	113,6	m^3	
Steel Grade	E	-	High-strength arctic-grade ship steel
Steel Density	7850	kg/m^3	Density of shipbuilding mild steel
Wall Plating Thickness	0,008	m	Typical wall steel thickness (8 mm)
Deck/Ceiling Plating Thickness	0,012	m	Typical deck/ceiling plating thickness (12 mm)
Frame Member Count	5	count	Estimated vertical frames inside the room
Frame Cross-Section Area	0,002	m^2	Cross-sectional area of each frame (flat bars, T-sections, or

			channels). Frame (T-bar) 150×10 web + 75×10 flange
Stringer Count	6	count	Estimated horizontal stringers
Stringer Cross-Section Area	0,003	m^2	Cross-sectional area of each stringer Stringer (L-bar) 150×150×10
Select Area to Melt	Wall + Roof		
Total Melting Section Volume	1,056	m^3	
Wall Area	86,51	m^2	Total area of all 4 vertical walls
Ceiling Area	30,3	m^2	area of floor
Deck Area	30,3	m^2	area of floor
Frame Volume	0,03	m^3	Volume of vertical frame steel
Stringer Volume	0,072	m^3	Volume of horizontal stringer steel
Total Steel Volume	1,166	m^3	Total structural steel volume
Total Steel Mass	9,154	T	Total steel mass of the structure

Table 13 Thermal properties, melting energy, and duration for steel in 5 MWh battery room

Structural Steel Heat Load Summary			
Parameter	Value	Unit	Description
Steel Mass	9154,914292	kg	Total structural steel mass
Specific Heat (c)	0,49	kJ/kg·K	Specific heat capacity of steel
Temperature Rise (ΔT)	1480	K	From 20°C to 1500°C
Latent Heat of Fusion	272	kJ/kg	Energy to melt 1 kg of steel at 1500°C
Sensible Heat per kg	725,2	kJ/kg	$c \times \Delta T$
Total Sensible Heat	6639144	kJ	Steel mass × sensible heat/kg
Total Latent Heat	2490136,687	kJ	Steel mass × latent heat/kg
Total Energy to Melt Steel	9129281	kJ	Sensible + latent heat

4.4.5 Summary of 5 MWh Battery Room Thermal Scenarios (100% SOC)

The result of the 5 MWh battery room simulations at 100% SOC Shown in table 15 is that, although all three ignition scenarios Bottom-Up, Middle-Out, and Top-Down give a comparable total heat release of about 160–172 GJ, the initiation time, severity, and burning distribution vary significantly. The Bottom-Up scenario sees thermal runaway propagate the quickest, with Rack B getting ignited at 3050 seconds and the onset of steel melting as soon as 5250 seconds. This case also produces the highest peak HRR at 13,737 kW but with shorter duration burning at around 24,500 seconds. In contrast, the Middle-Out case produces a more complex flame overlap pattern due to dual ignition

branches, resulting in intermediate peak intensity at 12,769 kW and longer burning duration at around 36,500 seconds. The Top-Down case propagates more slowly, with secondary ignition delayed to 8200 seconds, producing the lowest peak HRR at 10,046 kW but extending combustion to greater than 52,000 seconds. Steel melting is also delayed in this case to 7200 seconds due to the slower energy release. In each of the three cases, steel melting is not achieved when water submersion is applied, demonstrating its effectiveness as a mitigation measure. As discussed in Chapter 2 Section 2,6 our findings highlight the same, the sequence of ignition has a significant impact on peak fire intensity, structural vulnerability, and the time available for suppression and containment measures, with Bottom-Up posing the most immediate structural risk.

See Appendix A for detailed module scaling factors and HRR curves used in each scenario.

Table 14 Results Summary of 5 MWh Battery Room Thermal Scenarios (100% SOC)

Scenario	Bottom	Middle	Top
TR - Start Time of Rack B - s	3050	5150	8200
Melting Start Time (s)	5250	5600	7200
Post-Melt Start Time (s)	5650	6200	7850
Melting Duration (s)	400	600	650
THR Battery Room (GJ)	162,42	171,74	158,53
Melting After water Submerssion	Melting not triggered	Melting not triggered	Melting not triggered
Peak HRR - kW	13737	12769	10046
Combustion Duration (s)	24490	36553	52835
TR - Start Time of Rack B - s	3050	5150	8200

4.5 Estimation of Flame Geometry Based on HRR and Ejected Gas Composition

The estimation of flame geometry during battery thermal runaway is important because flame height and width determine the way heat dissipates in a battery room, how likely it is to ignite surrounding racks, and how much thermal load is imposed on nearby structures. While this method was not directly used in the present analysis, it is introduced here to show where it might be useful in future research or design. Flame geometry prediction is particularly relevant for fire spread assessment between racks, predicting

local heat flux on steel bulkheads and decks, and supporting the design of marine battery room fire barriers or ventilation systems.

The flame height and base diameter of a lithium iron phosphate (LFP) battery module were estimated during thermal runaway. The method is based on jet flame approach, which uses Heskestad's flame correlations to look at battery fire conditions. [58]

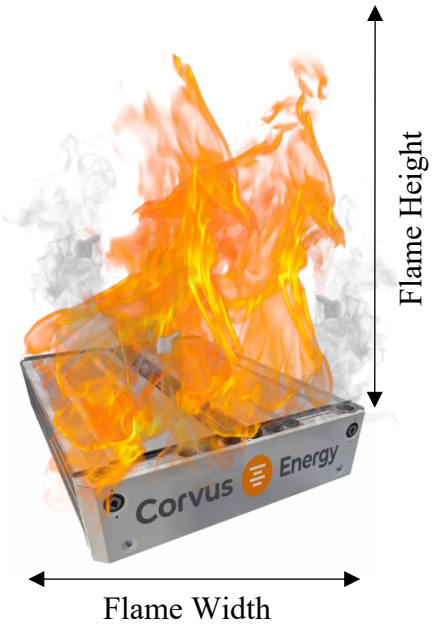

Figure 58 Module, Rack Level Estimation of Flame height and diameter Based on HRR

The gas composition released during thermal runaway is a significant variable in the calculation, as it influences jet density and combust ion heat. A mixture suitable for LFP fires was used. It had 26% CO_2, 43% H_2, 12% C_2H_4, 10% CO, 6% CH_4, and 3% other things. Although CO_2 is inert, it affects the density and thermal properties of the flame jet. Xinwei Yang, Hewu and Li [59]

Using this mixture, we find out the effective heat of combustion and the specific heat ratio. The jet flame temperature was assumed about 1023 K, which is higher than the temperature of the air around it.The spread sheet tool for this can be used in two ways: if the HRR is known, flame geometry can be estimated, and if the flame size is measured, HRR can be calculated backward.

These results should be used to find out how fire spreads between racks and how heat affects steel structures in small marine battery spaces.

Appendix A has detailed calculations that show each step.

4.6 Sensitivity Analysis

The sensitivity analysis was conducted to assess the impact of variations in battery room capacity (5–25 MWh) and rack spacing (0.1–1.7 m) on the thermal response, structural requirements, and fire safety of a marine battery room in a bottom-up thermal runaway (TR) propagation scenario. This case was chosen because it shows the most severe propagation path, where flames and heat go straight up to the roof structure, which causes the roof to melt faster than in cases where the heat and flames come from the top or middle. Appendix C has the results for other initiation cases and changes in state of charge (SOC) (100%, 50%, 0%).

4.6.1 Effect of Rack Spacing and Room Density

As the spacing between racks increases, the total room volume rises significantly (Fig. 59). For instance, at 25 MWh capacity, increasing rack spacing from 0.1 m to 1.7 m results in a room volume growth from ~447 m³ to ~1535 m³. This larger volume lowers the room energy density (kWh/m³), as the same stored energy is distributed over a larger space. Lower density improves heat dissipation and delays roof melting but requires substantially more construction material and space.

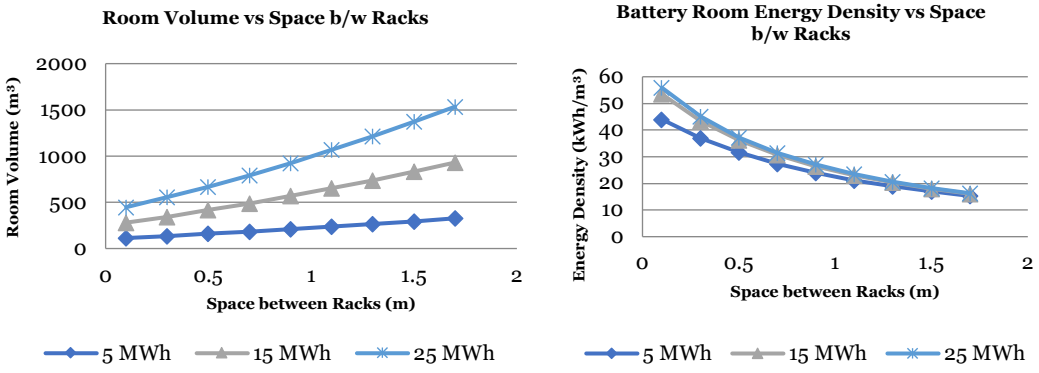

Figure 59 Effect of Rack Spacing on Battery Room Volume and Weight Density for Different System Capacities

Steel Mass Requirement

There is a direct trade-off between the space between racks and the amount of steel needed for structural integrity (Fig. 60). To hold up the roof and walls, bigger rooms need stronger steel structures. For instance, at 25 MWh, the steel needed goes from about 39 t at 0.3 m spacing to more than 115 t at 1.7 m spacing. This increase directly leads to higher installation costs and penalties for heavier vessels, which shows that making things safer by increasing spacing also comes with big costs and design challenges.

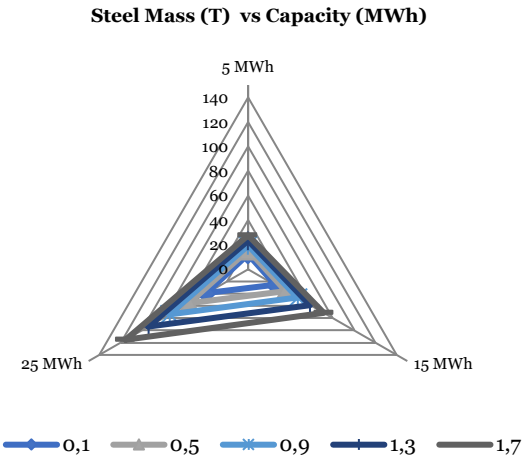

Figure 60 Steel Mass Requirement of Battery Room Capacity and Rack Spacing

4.6.2 Sensitivity Analysis at 100% SOC

Roof Melting Time

Roof melting onset time is highly correlated with rack spacing and battery room capacity (Fig. 61). For high-capacity rooms (20-25 MWh), the roof may fail within 80-90 minutes with such a small spacing (0.1m). Melt times improve significantly as spacing increases, exceeding 3-4 hours in some configurations. Room density (m^3/MWh) is a critical safety parameter. Higher densities (compact layouts) reduce roof survival, while lower densities (spaced layouts) increase survival but require more steel and space.

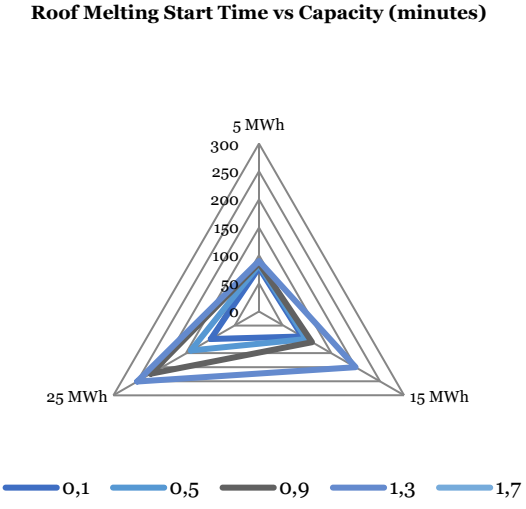

Figure 61 Effect of Rack Spacing on Roof Melting Onset Time (5MWh, 100% SOC)

Trade-Off Between Density, Melting Time, and Steel

The results show a three-way trade-off:

1. Less density (more space) means a longer roof survival time, but it also means more steel is needed and costs more.

2. More compact design and lower construction cost, but less fire resistance in the structure. A bigger room (from 5 MWh to 25 MWh) makes these effects even stronger because both the amount of steel needed and the amount of heat that can be released increase in a non-linear way.
3. For very large capacities (>20 MWh), compact high-density layouts cause the roof to melt too quickly (<2 hours), and layouts that are too big put too much stress on the steel and cost too much.
4. If we go to a room with a lot of space (like 25 MWh+), spacing increases go from compact and efficient (high kWh/m³, low steel, short melt margin) to safe but heavy and expensive (low kWh/m³, high steel, long melt margin).
5. The best region is usually mid-spacing (about 0.9 to 1.1 m), where you get the steep part of the melt-time improvement curve while keeping the space requirement and steel within a manageable range. Pushing spacing past that point usually results in smaller safety gains for each extra tonne of steel and each extra m³/MWh.

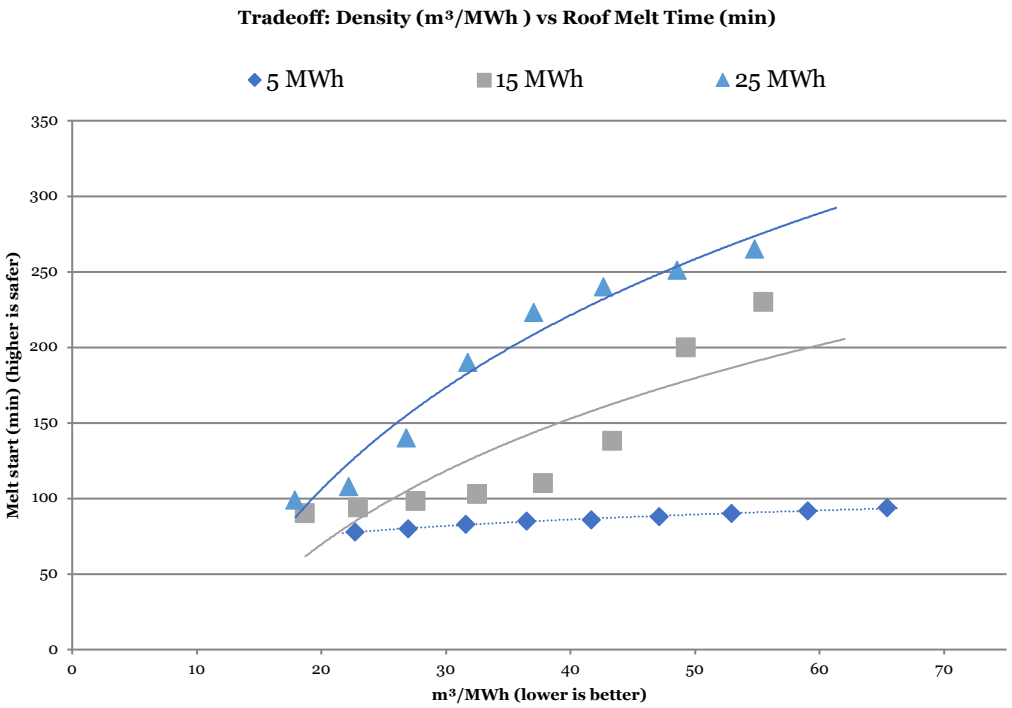

Figure 62 Trade-Off Between Battery Room Density and Roof Melting (100% SOC)

1. Select a target melt-time (regulatory + response time buffer) and determine the smallest spacing that meets it at the design MWh.
2. Look for layout "steps" (additional rack rows/aisles). Stay just before a step that will balloon L×W and steel.

3. As a first pass at 15-25 MWh, use the 0.9-1.1 m band; ensure that it meets melt-time targets based on your detection/suppression assumptions.
4. If melt-time is limited at compact spacing, consider non-spacing mitigation measures first (ceiling insulation/intumescent, overhead water mist/deluge, zoned ventilation/exhaust, early detection) before increasing spacing.
5. If the vessel layout allows, use compartmentalization (two 12.5 MWh rooms instead of one 25 MWh room); it reduces step-jumps in volume and steel while improving survivability.

4.6.3 Sensitivity Analysis at 50% SOC

To assess the impact of state of charge (SOC) on fire response in marine battery rooms, the sensitivity analysis was conducted again with the batteries charged to 50%. The geometric relationships between spacing, room density, and steel mass stay the same, but the thermal response and roof melting times get a lot better than they do in the 100% SOC case. The next few paragraphs talk about each parameter and how it affects ship design.

Roof Melting Time

The most significant effect of lowering SOC is increased roof survival times. Roof melting begins more slowly at 50% SOC than at 100% SOC across all capacities and spacings. For example, at 25 MWh and 0.3 m spacing, survival increases from ~3 h 45 min (at 100% SOC) to nearly 5 hours. At 5 MWh and 0.1 m spacing, survival time increases from ~1 h 30 min to nearly 2 hours. This demonstrates that SOC management is an effective operational safety strategy, allowing designers to extend survival times without physically expanding the battery room or adding too much steel. Maintaining a low SOC during harbor stays or idle periods may serve as a preventive measure against rapid fire escalation.

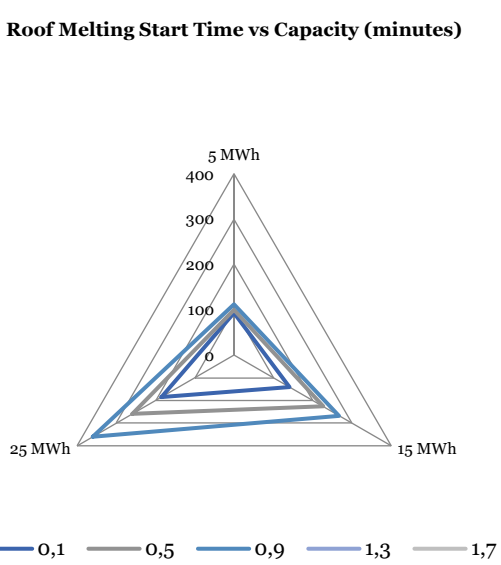

Figure 63 Effect of Rack Spacing on Roof Melting Onset Time (50% SOC)

Trade-Off Between Density, Melting Time, and Steel

Compact layouts reduce steel and footprint but result in shorter survival times, whereas spacious layouts improve safety but require more weight and cost. However, at 50% SOC, the safety curve shifts upwards. This means that configurations that were borderline unsafe at 100% SOC (e.g., 25 MWh at 0.5 m spacing) become viable at 50% SOC, with survival times far exceeding the 3-hour threshold generally considered acceptable for firefighting intervention. Designers benefit from this flexibility: rather than oversizing the battery room, moderate spacing (0.5-0.9 m) combined with SOC management can provide both safety and cost efficiency.

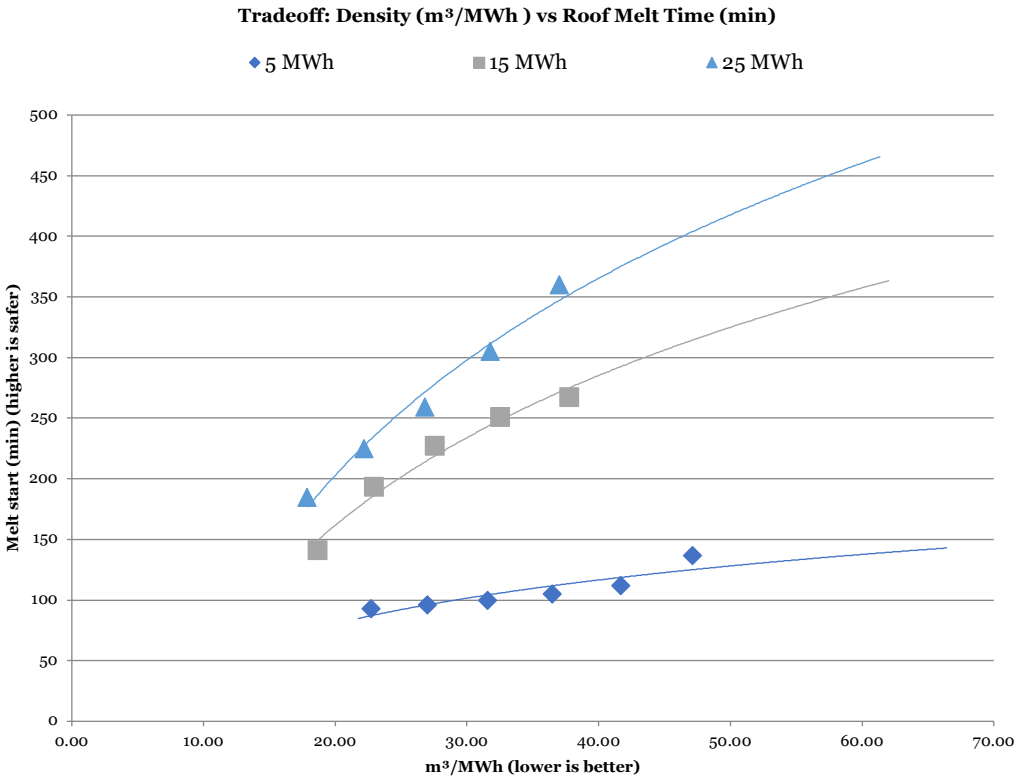

Figure 64 Trade-Off Between Battery Room Density and Roof Melting Time (50% SOC)

1. Operational flexibility: Reducing SOC during port or standby periods can provide similar fire resilience to structural modifications while requiring no additional space or weight.
2. Layout decisions: Designers should avoid extremes neither too compact nor too spacious and instead use balanced layouts with moderate spacing.

4.6.4 Sensitivity analysis at 0% SOC

Roof melting start time

The roof has the least amount of thermal load at 0% SOC compared to all other SOC levels. For all capacities and spacings, the times it takes for melting to start are much longer than for 100% and 50% SOC. For many combinations of capacity and spacing at 0% SOC, the roof never melts. This means that the roof stays below the melting point for the entire event. In practice, once the spacing is wide enough (especially at small to mid-capacities), the combination of lower room density and the gentler fire behaviour at 0% SOC keeps roof temperatures below the critical level.

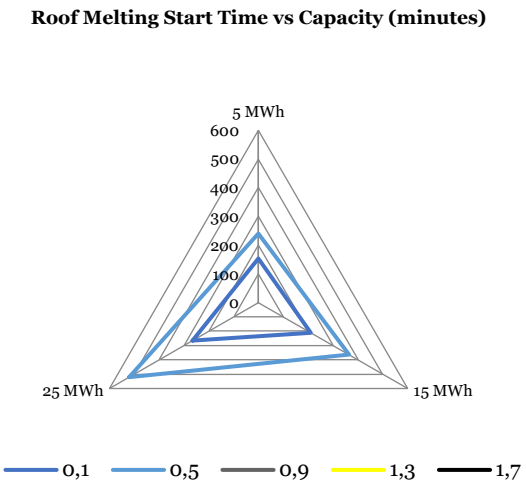

Figure 65 Effect Rack Spacing on Roof Melting Onset Time (0% SOC)

Trade-Off Between Density, Melting Time, and Steel

1. The volume vs capacity lines show how much you "spend" on ship space as you open aisles. Each spacing step improves the melt time curves while moving you up the steel curves and down the density axis.
2. At 0% SOC, the trade-off (density vs melt time) plot is at its highest: for the same density, you get more minutes (or no melting at all). At 50% SOC, the curve decreases but remains favorable, and at 100% SOC, it is lowest.

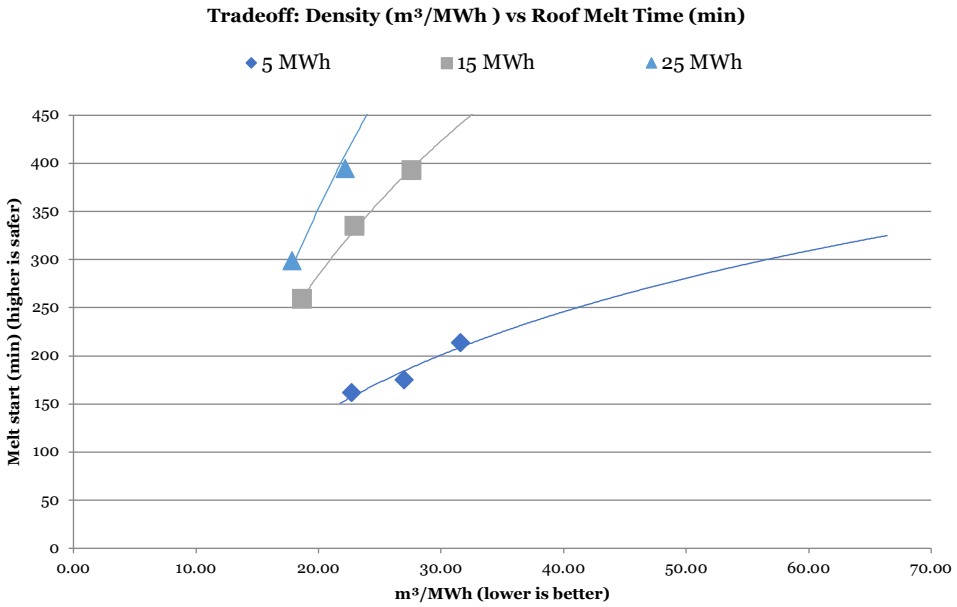

Figure 66 Trade-Off Between Battery Room Density and Roof Melting Time (0% SOC)

1. When the ship is in port, on lay-up, or when demand is low, keep the battery room at ≤50% SOC. When possible, go very low (toward 0%).

This one operational choice often turns "early melt" cases into "late melt" or even no-melting cases, without changing the structure.

2. If you have more than 20-25 MWh, don't use a single hyper-compact, high-density room. You can either: make the spacing wider so that it falls into the moderate band, or divide the space into smaller rooms or racks so that one fire can't heat the whole roof at once. This keeps the times for melting and the steel/space in balance.
3. In the bottom-up scenario, you can further lower the heat flux on the roof by using the geometry/SOC strategy along with detection, water-based cooling/suppression, and exhaust management.
4. If a layout doesn't show any melting at your planned operational SOC (for example, ≤50%) and the spacing is in the moderate range, you are in a strong region. If 100% SOC still melts the roof too quickly, change the geometry (add spacing or divide it into compartments) before adding additional systems.

4.6.5 Seawater Flooding Analysis

In this section we will discuss what happens when the room filled with battery is flooded with seawater when it experiences thermal runaway. In the earlier chapters, we have already shown that in dry conditions the roof of the room begins to melt in about one to a half-hour time frame, based on where the fire starts at the bottom, middle, or at the top racks. In this case, we want to know what happens when flooding the room changes that outcome. From the literature review given in Chapter 2 we also understand that if batteries are submerged in seawater, the water will begin to flood the electrode surfaces and can extinguish subsequent reactions, but that this could take up to 90 minutes before the cells would be completely quenched. This implies that both when the flooding begins and the rate at which water enters the room are important considerations.

At a flow rate of 8 m^3/min, when seawater is forced into the room, it takes approximately 15 minutes for a 5 MWh room to fill. If the flooding is started early on, i.e., around 58 minutes after the fire begins, the room is fully flooded by about 1 hour 13 minutes, just in time to prevent the roof from otherwise melting in the Bottom-Up case. In this scenario, the cooling prevents the failure of the steel. But if it is postponed until about 1 hour 32 minutes, then the room would not be occupied to capacity until 1 hour 47 minutes after initiation, after the roof has already started to melt in the Top-Down scenario. This means that procrastinated action reduces the effectiveness of seawater as a mitigation measure.

The effect of flow rate is important too. At 2 m^3/min reduced rate, the same 5 MWh room would take around 58 minutes to fill fully. In such a case, earlier pump starting becomes vital. If the crew starts flooding at around 58 minutes

(3500 s), the room will still be safe even under reduced flow, as it will be still submerged prior to steel melting process initiation. The same trend has been shown for the intermediate flow rates of 4, 6, and 12 m³/min: the lower the flow, the earlier action needs to be initiated in order to achieve the same protection. This means that pre-initiation is more important than employing very high flow rate, yet increased flow rates add safety margin.

Table 15 Effect of Seawater Submersion on Roof Melting for a 5 MWh Battery Room at 100% SOC (Fill 100%) (8 m³/min)

Water Fill Start (s)	Rack Spacing (m)	Scenario	Dry Melt Start (min)	Melt After Submersion (s)	Melt After Submersion (min)	Safe?
3500	0.1	Bottom	67.5	Not triggered	-	Yes
3500	0.1	Middle	70	Not triggered	-	Yes
3500	0.1	Top	86.7	Not triggered	-	Yes
3500	0.5	Bottom	71.7	Not triggered	-	Yes
3500	0.5	Middle	75	Not triggered	-	Yes
3500	0.5	Top	94.2	Not triggered	-	Yes
3500	1.0	Bottom	75.8	Not triggered	-	Yes
3500	1.0	Middle	80.8	Not triggered	-	Yes
3500	1.0	Top	102.5	Not triggered	-	Yes
4500	0.1	Bottom	67.5	4250	70.8	Borderline
4500	0.1	Middle	70	4400	73.3	Borderline
4500	0.1	Top	86.7	Not triggered	-	Yes
4500	0.5	Bottom	71.7	4500	75	Borderline
4500	0.5	Middle	75	4700	78.3	Borderline
4500	0.5	Top	94.2	Not triggered	-	Yes
4500	1.0	Bottom	75.8	Not triggered	-	Yes
4500	1.0	Middle	80.8	Not triggered	-	Yes
4500	1.0	Top	102.5	Not triggered	-	Yes
5500	0.1	Bottom	67.5	4250	70.8	No
5500	0.1	Middle	70	4400	73.3	No
5500	0.1	Top	86.7	5400	90	No
5500	0.5	Bottom	71.7	4500	75	No
5500	0.5	Middle	75	4700	78.3	No
5500	0.5	Top	94.2	Not triggered	-	Borderline
5500	1.0	Bottom	75.8	4750	79.2	No
5500	1.0	Middle	80.8	5050	84.2	No
5500	1.0	Top	102.5	Not triggered	-	Borderline

Table 16 Safety outcome matrix for seawater flooding in a 5 MWh battery room at 100% SOC (Fill 100%)

Water Fill Start (s)	Rack Spacing (m)	Bottom-Up	Middle-Out	Top-Down	Overall Result
3500	0.1	Safe	Safe	Safe	Safe
3500	0.5	Safe	Safe	Safe	Safe
3500	1.0	Safe	Safe	Safe	Safe
4500	0.1	Borderline	Borderline	Safe	Borderline
4500	0.5	Borderline	Borderline	Safe	Borderline
4500	1.0	Safe	Safe	Safe	Safe
5500	0.1	Unsafe	Unsafe	Unsafe	Unsafe
5500	0.5	Unsafe	Unsafe	Borderline	Unsafe
5500	1.0	Unsafe	Unsafe	Borderline	Unsafe

This table 17 shows the net result of flooding seawater at different initiation times. If flooding initiates early (at 3,500 s), the structure is fully protected and is Safe in all cases. If flooding is begun later, at 4,500 s, the outcome becomes Borderline melting will just start in some ignition scenarios before cooling stops. At very late late flooding (5,500 s), the building is largely Unsafe, because the roof starts melting before water can quench the fire. Rack spacing has minimal effect compared to how soon the flooding begins. Similar trends were observed in larger battery rooms of 15 MWh and 25 MWh capacity, indicating that the timing of seawater activation is more critical than room size.

4.6.6 Analysis Summary

5MWh Battery Room:
This Fig. 67 shows the effect of state of charge (SOC) and rack spacing on fire behaviour in a 5 MWh battery room. The left y-axis gives onset time of roof steel melting, and the right y-axis gives the total released heat (THR) during bottom-up thermal runaway. Higher SOC and lower rack spacing relate to earlier melting and greater heat release.

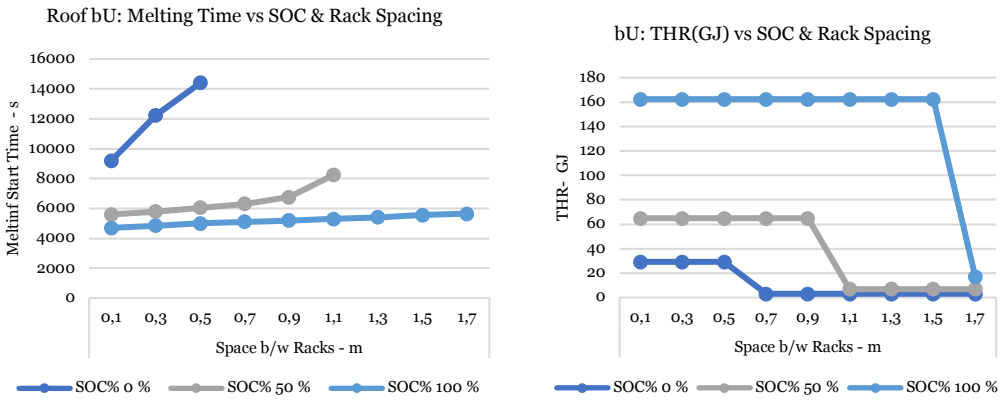

Figure 67 5MWh Battery Room Effect of state of charge (SOC) and rack spacing on (a) roof melting start time and (b) total heat release (THR) during bottom-up (BU) thermal runaway propagation.

15MWh Battery Room:

This Fig. 68 shows how SOC and rack spacing affect fire behavior in a 15 MWh battery room. The left plot is the onset time of roof melting, and the right plot is the total heat release (THR) in bottom-up thermal runaway. Higher SOC and closer rack spacings result in faster steel melting and greater total energy release.

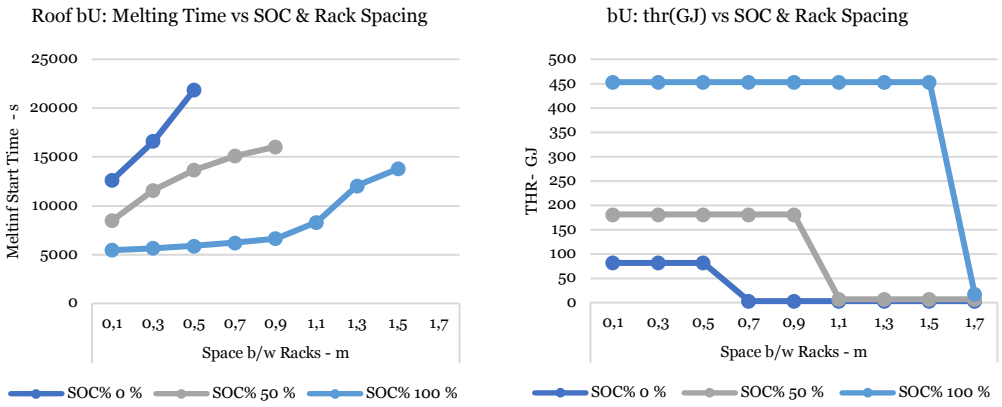

Figure 68 15MWh Battery Room Effect of state of charge (SOC) and rack spacing on (a) roof melting start time and (b) total heat release (THR) during bottom-up (BU) thermal runaway propagation.

25MWh Battery Room:

This Fig. 69 shows how SOC and rack space influence fire behavior in a 25 MWh battery room. The left graph shows the beginning time of roof melting, and the right graph shows total heat release (THR) via bottom-up thermal runaway. Steel melting is earlier and the room releases more total heat with higher SOC and denser rack space.

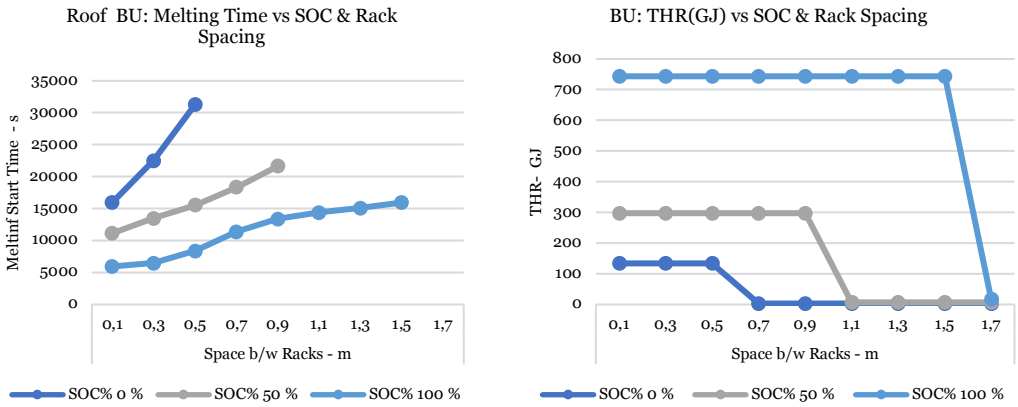

Figure 69 25MWh Battery Room Effect of state of charge (SOC) and rack spacing on (a) roof melting start time and (b) total heat release (THR) during bottom-up (BU) thermal runaway propagation.

Note: This section only shows the main sensitivity results to make it easier to read and understand. The Appendix C has more detailed outputs, such as how the state of charge (SOC) affects things, how thermal runaway propagates from the top down and from the bottom up case, and the HRR curves and THR values for each battery room configuration.

5 Conclusion

This thesis investigated at the thermal runaway behavior of large-scale lithium-iron-phosphate (LFP) battery rooms in fully electric ships. The goal was to understand how various parameters, such as state of charge (SOC), rack spacing, battery room capacity, and exposed surfaces, influence fire growth and structural survival. To accomplish this, a spreadsheet-based tool was created using experimental heat release rate (HRR) and total heat release (THR) data from large-scale fire tests and scaled from cell to module to rack to full battery rooms. As discussed in (Chapter 1), this responds to recent maritime battery incidents (MF Ytterøyningen, MS Brim Explorer) and the regulatory gap created by DNV's 5 MWh limit for single battery rooms [30] which highlighted the need for practical design tools for larger installations.

The first key objective was to model TR initiation and propagation, was achieved by scaling cell and rack fire test data to full-room layouts, showing how SOC and ignition location affect HRR and survival. (see Research Objectives Chapter 1,6). The findings clearly show that SOC is the most powerful driver of thermal runaway severity. Fires were extremely severe at 100% SOC: roof structures melted in 80-120 minutes for 5 MWh rooms with compact layouts, and survival time in large 25 MWh rooms rarely exceeded four hours. Reducing SOC to 50% increased survival time by 30-50%, whereas at 0% SOC, many room layouts did not melt at all. This confirms previous research findings by Wang et al. 2017; FM Global 2020 at the cell and module levels as we reviewed in Chapter 2 Section 2,6. Cells with high SOC released violent flames and had a higher peak HRR, whereas partially discharged cells produced smaller fires. [43]. This thesis provides a quantification of the SOC effect at the full-room scale, demonstrating that lowering SOC from 100% to 50% can buy over an hour of additional survival time, and that at 0% SOC, structural melting may not occur at all, even under worst-case bottom-up flame propagation. (see Chapter Objectives 1,6).

The second key objective was that how rack spacing affects both roof melting behavior and room energy density (m^3/MWh). (see Research Objectives Chapter 1,6). The finding are compact layouts with spacings of 0.1-0.3 m produced high densities and rapid roof melting. In contrast, increasing the spacing decreased energy density, spread the flames, and significantly delayed melting. For example, at 25 MWh and 0.3 m spacing, roof failure occurred at approximately 3 hours and 45 minutes at 100% SOC, but with wider spacing, survival extended beyond five hours at 50% SOC. However, the benefits of spacing peaked at about 1.3-1.5 m, while the costs in terms of steel mass and lost ship space continued to rise. FM Global tests reported similar behavior: racks placed closer together facilitated propagation, and wider aisles reduced flame spread and delayed structural collapse (see Chapter 2). These

quantified spacing effects also reflect DNV's current rules, which restrict single rooms above 5 MWh unless compensatory safety measures such as greater separation or compartmentalization are provided. For ship design, a recommendation is to have a "moderate" spacing range of 0.5-0.9 m as the best balance.

Larger rooms 15 or 25 MWh carry more energy, so the risk potential is greater. However, the additional steel mass in their structure acts as a buffer, causing roof melting to take longer than in smaller 5 MWh rooms. In this thesis, the roof in a 25 MWh room lasted nearly twice as long as in a 5 MWh room with the same SOC and spacing. This dual effect greater hazard and greater resilience has not been highlighted in previous module or rack scale studies. It is important for marine design because it means that large rooms are not necessarily less safe; they can give crews more time to respond.

Modelling only the roof as the exposed area to heat resulted in shorter survival times but including both the roof and the walls of the battery room as heat-absorbing surfaces delayed melting by 30-60 minutes in small and medium-sized rooms. However, at high SOC and large capacities, even roof+wall scenarios failed after two to three hours, demonstrating that passive protection alone cannot prevent structural collapse.

Another aspect is the study of seawater flooding for thermal runaway prevention (see Research Objectives Chapter 1,6) as an emergency suppression method. The model predicted that flooding with 8 m^3/min flow rate will entirely protect a 5 MWh room where roof melting starts at (4,050 s ≈ 67 min) if flooding started in advance (at 3,500 s ≈ 58 min) roof melting was fully eliminated for all cases of ignition. However, the delayed flooding (4,500 s ≈ 75 min) produced borderline results, and very late flooding (5,500 s ≈ 92 min) failed to prevent collapse, making the room unsafe. Rack spacing had only a minor effect on the outcome with respect to initiation time. The same trends were observed for larger 15 MWh and 25 MWh rooms, confirming that timing is critical rather than scale. According to Bertei et al [60], shallow flooding causes only a portion of the battery to come into contact with seawater, resulting in slower gas release and longer time for explosive concentrations to reach the atmosphere. As the water level rises, more cells are submerged, resulting in faster hydrogen and chlorine generation and an earlier reach of critical limits. At very high fill levels, nearly all cells react with seawater, rapidly producing gas and quickly reaching explosive atmospheres, especially if no venting is provided. (see Chapter 2,5)

Future enhancements to this work should include validation using advanced fire simulations like COMSOL or FDS, the incorporation of experimental HRR data for other chemistries like NCA and LTO, and detailed modeling of

gas production and explosion risk. More full scale fire tests on marine battery installations are also required to validate the results and suppression effectiveness.

In conclusion, As discussed in (Chapters 1,4 & 2,7) the absence of complete marine battery room large-scale thermal runaway data has been a critical gap for ship designers, particularly with current maritime incidents and the limitations of conventional suppression systems. DNV's rules now set a 5 MWh limit to a single battery space, but allow larger rooms up to 25 MWh only if compensatory measures such as separation, barriers, enhanced ventilation, and active cooling are demonstrated.[30] This thesis shows why such measures are needed: the analysis given a quantification of how SOC, rack spacing, and room size regulate roof melting and survival times, and demonstrated how flooding time of seawater in the room is essential to the outcome. Through mapping from cell and rack-scale experiments [4, 61] to full-room design rules, the work provides designers with open ways of testing compliance against DNV regulations and safety margins in large installations. The findings therefore strengthen the interplay between state-of-the-art fire research, regulatory requirements, and ship design practice, while also offering a basis for refining class rules as ESS scale beyond 10-25 MWh.

6 References

1. Wikipedia. *Comparison of commercial battery types*. Available from: https://en.wikipedia.org/wiki/Comparison_of_commercial_battery_types.
2. batteryuniversity, *BU-205: Types of Lithium-ion.*
3. Yang Wang , X.L., Yuxin Zhang ,Long Liu, *Hazard comparison of thermal runaway of electric marine battery cabinet under different trigger modes.* 2024.
4. Ditch Benjamin and Z. Dong, *Fire Hazard of Lithium-ion Battery Energy Storage Systems: 1. Module to Rack-scale Fire Tests.* Fire Technology, 2020. **59**(6): p. 3049-3075.
5. greencubes, *Types of Lithium.*
6. Wikipedia. *Sodium-ion battery*. Available from: https://en.wikipedia.org/wiki/Sodium-ion_battery.
7. Wikipedia. *Lithium–sulfur battery*. Available from: https://en.wikipedia.org/wiki/Lithium%E2%80%93sulfur_battery.
8. Wikipedia. *Lithium iron phosphate battery*. Available from: https://en.wikipedia.org/wiki/Lithium_iron_phosphate_battery.
9. electrichybridvehicletechnology, *LFP vs NMC thermal runaway.* 2025.
10. Lang Huang, et al., *Revealing thermal runaway routes in lithium-sulfur batteries.* 2022.
11. Flash Battery, *Sodium batteries: The technology of the future?* 2023.
12. samaterials, *Lithium-Sulfur Batteries vs. Lithium-Ion Batteries: A Comparative Analysis.* 2025.
13. Kevin Clemens. *World's Largest Electric Ferry Carries 275 Tons of Batteries*. 2025; Available from: https://eepower.com/news/worlds-largest-electric-ferry-carries-275-tons-of-batteries/#.
14. Derecktor Shipyards. *Hybrid Electric Ferries Launch: A New Chapter in Sustainable Marine Transit*. 2024; Available from: https://derecktor.com/hybrid-electric-ferries-launch-a-new-chapter-in-sustainable-marine-transit/.
15. EMSA. *EMSA guidance on Safety of Battery Systems onboard*. Available from: https://maritimecyprus.com/2024/01/29/emsa-guidance-on-safety-of-battery-systems-onboard/.
16. EMSA. *Battery Energy Storage Systems (BESS)*. Available from: https://www.emsa.europa.eu/electrification/bess.
17. OffShore Energy, *Freudenberg: Xalt Energy's batteries to power 1st all-electric ferry in New Zealand.* 2021.
18. abc.net.au. *World's largest '100 per cent electric' ship launched by Tasmanian builder Incat*. 2025; Available from: https://www.abc.net.au/news/2025-05-02/incat-launches-worlds-largest-battery-electric-ship-hull096/105243498.
19. McKay. *Wellington Ika Rere Electric Ferry*. 2022; Available from: https://www.mckay.co.nz/work/ika-rere/.
20. Freudenberg, *Cleaner Passage.* 2020.
21. National Fisherman, *Banking on batteries: Price drops and expanded options change the hybrid power model.* 2022.
22. abcnews.go, *Hybrid-powered cruise ship could be key to lessening greenhouse gas emissions from ocean travel.* 2019.

23. CNN travel, *Sustainable ships: The world's most eco-conscious cruises*. 2023.

24. Bresler, A., *On Norway's Coast, This Ultra-Sustainable Cruise Line Has a Northern Lights Guarantee.* 2023.
25. Marinelink. *Energy Storage Systems Continue to Expand in North American Maritime Markets*

. 2021; Available from: https://www.marinelink.com/news/energy-storage-systems-continue-expand-484556#.
26. Corvus Energy, *MF Ytterøyningen on 10th of October in 2019 Investigation Report.* 2020.
27. The Norwegian Safety Investigation Authority, *Fire on board 'MS Brim' in the outer Oslofjord.* 2021.
28. DNV, *DNV GL 3rd Maritime Battery Workshop delivers refreshing transparency.* 2020.
29. Spyros E Hirdaris, *Lecture Notes on Basic Naval Architecture.* 2021.
30. DNV, *Safety philosophies Document code: DNV-CG-0660.* 2023.
31. ZEM Grenland Energy and DNV-GL, *DNV GL Guideline for large maritime battery systems.*
32. DNV.GL, *DNV GL Handbook for Maritime and Offshore Battery Systems.* 2016.
33. Roshan Sebastian, *A review of fire mitigation methods for li-ion battery energy storage system.* 2022.
34. Pongkorn Meelapchotipong, Chinda Charoenphonphanich, Manop Masomtob, and Nattanai Kunanusont, *Seawater submersion for cylindrical lithium-ion batteries thermal runaway prevention.* 2024.
35. Zhizuan Zhou, et al., *Experimental study of thermal runaway propagation along horizontal and vertical directions for LiFePO4 electrical energy storage modules.* 2023.
36. Chen, H., et al., *Experimental Investigation of Thermal Runaway Behavior and Hazards of a 1440 Ah LiFePO4 Battery Pack.* 2023.
37. Norwegian Maritime Authority (NMA), *Draft Regulations on ships using battery systems with lithium-ion cells with a total capacity of 20 kWh or more* 2025.
38. Energy, C., *Corvus blue whale specification sheet.*
39. Marinelink. *Corvus ESS Powers the World's First Fully Electric Offshore Vessel*. 2025; Available from: https://www.marinelink.com/news/corvus-ess-powers-worlds-first-fully-521899.
40. Marinelink. *Corvus Energy Gets DNV's Blessing for Blue Whale Marine Storage System*. 2024; Available from: https://www.marinelink.com/news/corvus-energy-gets-dnvs-blessing-blue-514588.
41. Karlsson Björn, *Enclosure Fire Dynamics.* 2011.
42. Dougal Drysdale, *An Introduction to Fire Dynamics.* 2011.
43. incompliancemag, *Energy Release Quantification for Li-Ion Battery Failures.* 2022.
44. Qinzheng Wang, et al., *Multidimensional fire propagation of lithium-ion phosphate batteries for energy storage.* 2024.
45. FM Global, *Sprinklered Test of a 125 kWh Energy Storage System Comprised of LNO/LMO Batteries.* 2021.

46. EZ STEEL INDUSTRIAL CO., L. *Shipbuilding Steel Weight Formula - Ship Plate Density and Coating Weight*. Available from: https://www.ezindustrialtube.com/Tech_Service/shipbuilding-steel-weight-formula---ship-plate-den.html.
47. Belis Bos & Louter (Eds.) et. al, *Considerations for the Integration of Glass in Superyacht Structures.* 2022.
48. Group, S.P., *What Temperature Does Steel Melt?*
49. Engineeringtoolbox, T. *Metals - Specific Heats*. Available from: https://www.engineeringtoolbox.com/specific-heat-metals-d_152.html.
50. Engineering ToolBox. *Metals and their latent heat of fusion.*; Available from: https://www.engineeringtoolbox.com/fusion-heat-metals-d_1266.html?
51. Energy, C. *Electric and Hybrid Car Ferries*. Available from: https://corvusenergy.com/electric-and-hybrid-car-ferries.
52. Corvus Energy. *Corvus Energy Products*. Available from: https://corvusenergy.com/products.
53. Kim Klokkervold, 2021.
54. Maritime battery forum. *Corvus Energy Blue Whale ESS awarded RINA Type Approval*. 2025; Available from: https://www.maritimebatteryforum.com/news/corvus-energy-blue-whale-ess-awarded-rina-type-approval.
55. Battery Design from chemistry to pack. *Prismatic Cells*. Available from: https://www.batterydesign.net/battery-cell/formats/prismatic-cells/.
56. Akkula.fi. *EVE MB31 LiFePO4 314Ah 3.2V 1kWh prismatic battery cell Grade A*. Available from: https://akkula.fi/tuote/eve-mb31-grade-a-lifepo4-314ah-32v-1kwh-prismaattinen-akkukenno-ruuviliitoksin/?srsltid=AfmBOooxJcxznUB-U6YCHwhz7b8T6hPYIcPxlzizuja7poltoZUuOib8.
57. Zhi Wang et. al, *Fire behavior of lithium-ion battery with different states of charge induced by high incident heat fluxes.* 2018.
58. *An experimental study on thermal runaway characteristics of lithium-ion batteries with high specific energy and prediction of heat release rate.* 2020.
59. Xinwei Yang, W. Hewu, and M. Li, *Experimental Study on Thermal Runaway Behavior of Lithium-Ion Battery and Analysis of Combustible Limit of Gas Production.* 2022.
60. Bertei et al, *Safety Assessment of Scenarios Triggered by Accidental Seawater Immersion of Lithium Batteries in Innovative Naval Applications.* 2018.
61. Wang, Q., et al., *Combustion behavior of lithium iron phosphate battery induced by external heat radiation.* Journal of Loss Prevention in the Process Industries, 2017. **49**: p. 961-969.

7 Appendix A

	Parameter	Value	Units	Description[4]
Cell	Chemistry	LFP	-	Lithium Iron Phosphate
	Capacity	20	Ah	From Table 1
	Voltage	3,3	V	From Table 1
	Energy	0,066	kWh	Capacity × Voltage / 1000
	Format	Prismatic	-	From Table 1
	Nominal Dimensions	227 × 161 × 72.5	mm	Table 1
Module	Cell Count	78	cells	From Table 1
	Capacity	120	Ah	From Table 1
	Voltage	42,9	V	From Table 1
	Energy	5,148	kWh	Capacity × Voltage / 1000
	Mass	49	kg	From Table 1
	Nominal Dimensions	700 × 270 × 180	mm	Table 1
	Electrolyte Mass	2,6	kg	Table 2
	Plastic Mass	4,9	kg	Table 2
	Electrolyte Energy	72,8	MJ	ΔHc = 28 MJ/kg
	Plastic Energy	186,2	MJ	ΔHc = 38 MJ/kg
	Electrical Energy	18,5328	MJ	kWh × 3.6
	Total Combustible Energy	277,5328	MJ	Sum of energies
	Peak Chemical HRR	413	kW	Figure 5
	Convective HRR	214	kW	
	Total HRR (THR) Chemical	143	MJ	HRR integration
	Total HRR (THR) Covective	101	MJ	HRR integration
Rack	Module Count	16	modules	16 per rack
	Voltage	686	V	From Table 1
	Energy	82,32	kWh	Cap × Volt × Module Count
	Mass	784	kg	Module count × module mass
	Nominal Dimensions	660 × 770 × 1760	mm	Table 1
	Total Combustible Energy	4440,5248	MJ	16 × module total energy
	Peak Chemical HRR	2540	kW	Figure 16
	Convective HRR	1680	kW	
	Total HRR (THR) Chemical	3810	MJ	Figure 16
	Total HRR (THR) Covective	2770	MJ	χ_{rad} ~0.27

Appendix A. 1 Summary of Experimental Thermal Runaway Data at Module and Rack Levels (FM Global)

			Parameter	Value	Units	Description
Corvus Energy Blue Whale	Cell	Specifications	Cell Voltage	3,3	V	Nominal voltage per LFP cell
			Cell Capacity	20	Ah	Rated capacity of each prismatic cell
			Cell Energy	0,066	kWh	Cell voltage × capacity / 1000
	Module		Cells in Parallel	31,4	-	To achieve 120 Ah from 20 Ah cells
			Cells in Series	24,24242	-	To achieve 42.9 V from 3.3 V cells
			Total Cells	761,2121	cells	Total number of cells in module
			Nominal Voltage	80	V	From Corvus datasheet
			Capacity	628	Ah	From Corvus datasheet
			Energy	50,24	kWh	Energy = Voltage × Capacity / 1000
			Mass	395	kg	From datasheet

			Cells in Parallel (for current/Ah)	31,4	V	13 series cells × 3.3 V
			Cells in Series (for voltage)	24,24242	Ah	6 parallel cells × 20 Ah
			Total Cells	761,2121		24S31P configuration (24 in series, 31 in parallel)
		Combustible	Combustible Fraction	15,31 %	-	Assumed fraction of module weight
			Combustible Mass	60,45918	kg	Weight × 15%
			Electrolyte Fraction	34,67 %	-	From FMG module
			Plastic Fraction	65,33 %	-	From FMG module
			Electrolyte Mass	20,95918	kg	Combustible mass × electrolyte fraction
			Plastic Mass	39,5	kg	Combustible mass × plastic fraction
			Electrolyte Energy	586,8571	MJ	Mass × ΔH = 28 MJ/kg
			Electrical Energy	180,864	MJ	kWh × 3.6
			Plastic Energy	1501	MJ	Mass × ΔH = 38 MJ/kg
			Total Combustion Energy	2268,721	MJ	Sum of chemical energies
		TR Results	Chemical THR Ratio	52 %	-	From FMG module
			Chemical THR	1168,969	MJ	51% of combustion energy
			Convective THR Ratio	71 %	-	From FMG module
			Convective THR	825,6352	MJ	≈ 70.6% of chemical THR
	Rack		Modules	9		No. of modules in one rack
			Combustible Fraction	15 %	-	Assumed combustible fraction of module weight
			Combustible Mass	544,1327	kg	Total combustible mass = total rack mass × combustible fraction
			Electrolyte Fraction	35 %	-	Electrolyte share of combustible mass (from FM Global)
			Plastic Fraction	65 %	-	Plastic share of combustible mass (from FM Global)
			Electrolyte Mass	188,6327	kg	Electrolyte mass = Combustible mass × Electrolyte fraction
			Plastic Mass	355,5	kg	Plastic mass = Combustible mass × Plastic fraction
			Electrolyte Energy	5281,714	MJ	Electrolyte energy = mass × ΔH (28 MJ/kg)
			Electrical Energy	1627,776	MJ	kWh × 3.6
			Plastic Energy	13509	MJ	Plastic energy = mass × ΔH (38 MJ/kg)
			Total Combustion Energy	20418,49	MJ	Sum of plastic and electrolyte energies
			Chemical THR Ratio	86 %	-	Chemical THR as % of combustion energy (from FM Global)
			Chemical THR	17519,2	MJ	THR = Ratio × Total Combustion Energy
			Convective THR Ratio	73 %	-	Convective THR as % of chemical THR (from FM Global)
			Convective THR	12737,06	MJ	THR = Ratio × Chemical THR

Appendix A. 2 THR Estimates for Corvus Blue Whale Module Based on FM Global Experimental Data - 100 SOC%

		Parameter	Value	Units	Description
FM	Mod	FMG Module THR (Chemical)	143	MJ	Chemical THR from FMG module test

		FMG Module THR (Convective)	101	MJ	Convective THR from FMG module test
		FMG Module Duration	2360	s	Duration from FMG module test
		FMG Module Start Time	3000	s	Start time of combustion from FMG graph
		FMG Module End Time	5360	s	End time of combustion from FMG graph
		FMG Module Peak HRR (Chemical)	413	kW	Peak chemical HRR from FMG
		FMG Module Peak HRR (Convective)	214	kW	Peak convective HRR from FMG
	6 Modules - 32kWh	FMG Intermediate THR (Chemical)	1152	MJ	THR from 6-module cabinet test
		FMG Intermediate THR (Convective)	758	MJ	Convective THR from 6-module test
		FMG Intermediate Duration	8100	s	Combustion duration for 6-module test
		FMG Intermediate Start Time	2940	s	Start time of intermediate test combustion
		FMG Intermediate End Time	12600	s	End time of intermediate test combustion
		FMG Intermediate Peak HRR (Chemical)	500	kW	Peak HRR in 6-module test
		FMG Intermediate Peak HRR (Convective)	312	kW	Convective peak HRR in 6-module test
	Rack 16 Modules - 83kWh	FMG Rack THR (Chemical)	3810	MJ	Chemical THR from 16-module test
		FMG Rack THR (Convective)	2770	MJ	Convective THR from rack test
		FMG Rack Duration	6000	s	Combustion duration for full rack test
		FMG Rack Start Time	2220	s	Start time from rack test
		FMG Rack End Time	8100	s	End time from rack test
		FMG Rack Peak HRR (Chemical)	2540	kW	Peak chemical HRR (rack)
		FMG Rack Peak HRR (Convective)	1680	kW	Peak convective HRR (rack)
Corvus	Module - 50kWh	Corvus Module THR (Chemical)	1169	MJ	Input chemical THR for Corvus module
		Corvus Module THR (Convective)	826	MJ	Input convective THR for Corvus module
		Est. Corvus Peak HRR (mod-based)	779	kW	Scaled from FMG single module
		Est. Corvus Combustion Duration	6748	s	Scaled from FMG Module
	Rack - 450kWh	Corvus Rack THR (Chemical)	17519	MJ	Input chemical THR for Corvus Rack
		Corvus Rack THR (Convective)	12737	MJ	Input convective THR for Corvus Rack
		Est. Corvus Peak HRR (mod-based)	11679	kW	Scaled from FMG Rack
		Est. Corvus Combustion Duration	12866	s	Scaled from FMG Rack

Appendix A. 3 Scaled Combustion Duration Estimates for Corvus Blue Whale Module Based on FM Global Fire Test Results

Estimation of Flame Geometry Based on HRR and Ejected Gas Composition

Equation 1: Flame Height Ratio

$$\frac{L_b}{D} = \begin{cases} 1.2 \; if \; Rm < 0.1 \\ 0.405 \; Rm^{-\frac{1}{2}} \; if \; Rm \geq 0.1 \end{cases}$$

Equation 2: Buoyancy-Controlled Flame Height

$$\frac{L_b}{D} = -1.02 + 15.6 \cdot N^{1/5}$$

Equation 3: Gas Release Momentum Ratio (RM)

$$RM = 1.36 \cdot \left(\frac{T_\infty}{T_j}\right)\left(\frac{c_p \cdot \Delta T_f}{H_c/r}\right)^{4/5}\left(\frac{\rho_\infty/\rho_s}{r^2}\right)^2 \cdot N^{2/5}$$

Equation 4: Non-Dimensional Parameter (N)

$$N = \frac{c_p \cdot T_j}{g \cdot D \cdot \rho_j^2 \cdot \left(\frac{H_c}{r}\right)} \cdot \frac{\dot{Q}^2}{D^5}$$

Equation 5: Jet Gas Density

$$\rho_j = \left(1 + \frac{\kappa - 1}{2} M^2\right)^{-\frac{1}{\kappa - 1}} \cdot \frac{P_j}{R \cdot T_j}$$

κ (Kappa) of a Gas Mixture

$$\kappa = \left(\sum_i \frac{x_i}{\gamma_i - 1}\right)^{-1} + 1$$

Step 1: Buoyancy-Controlled Flame Height

$$L_b = \frac{L_f}{\frac{L_f}{L_b}} = \frac{1.8029}{1.2} = 1.5024\ m$$

Step 2: Flame Height Ratio

$$\frac{L_b}{D} = \frac{1.5024}{0.9} = 1.6694$$

Step 3: Dimensionless Parameter N

$$N = \left(\frac{1.6694 + 1.02}{15.6}\right)^5 = 0.0001523$$

Step 4: RM Calculation

$$RM = 1.36 \cdot \left(\frac{T_\infty}{T_j}\right)\left(\frac{c_p \cdot \Delta T_f}{H_c/r}\right)^{4/5}\left(\frac{\rho_\infty/\rho_s}{r^2}\right)^2 \cdot N^{2/5}$$

$$T_{ratio} = \frac{T_\infty}{T_s} = \frac{293}{1023} = 0.286$$

$$H_{ratio} = \frac{c_p \cdot \Delta T_f}{H_c/r} = \frac{1000 \cdot 500}{43049221.88/10.8} = 0.1254$$

$$\left(\frac{\rho_\infty}{\rho_s}\right)^2 = \left(\frac{1.2}{4.361}\right)^2 = 0.0757$$

$$RM = 1.36 \cdot 0.286 \cdot (0.1254)^{\frac{4}{5}} \cdot (0.0757 \cdot 0.0001523)^{\frac{2}{5}} = 0.006582$$

Step 5: Apply Equation for Q

$$\dot{Q} = \sqrt{\frac{N \cdot D^5 \cdot g \cdot D \cdot \rho_s^2 \cdot \left(\frac{H_c}{r}\right)}{c_p \cdot T_s}}$$

$$\dot{Q} = \sqrt{\frac{0.0001523 \cdot 0.9^6 \cdot 9.81 \cdot 0.9 \cdot (4.361)^2 \cdot \left(\frac{43049221.88}{10.8}\right)}{1000 \cdot 1023}}$$

$$\dot{Q} = 524.0\, kW$$

Parameter	Value	Units	Description
Lf	1,80296193	m	Observed flame height
D	0,9	m	Flame base diameter
cp	1000	J/kg·K	Specific heat
Delta_Tf	500	K	Temperature rise in flame
Hc	43049221,88	J/kg	Heat of combustion
r	10,8	-	Stoichiometric air/fuel ratio
rho_s	4,361	kg/m³	Ejected gas density
g	9,81	m/s²	Gravity
T_ratio	0,286412512	-	T_inf / T_s
H_ratio	0,125438	-	cp * ΔTf / (Hc / r)
H_ratio^0.8	0,189995	-	(H_ratio)^0.8
density_term	0,002359	-	rho_inf / (rho_s * r^2)
density_term^0.4	0,002359	-	(density_term)
RM	0,000175	-	Full RM from simplified Eq. 3
Lf/Lb	1,2	-	From Eq. 1
Lb	1,502468275	m	Buoyancy-controlled flame height
Lb/D	1,669409194	-	Lb / D
N	0,000152287	-	From Eq. 2
H_ratio^3	6,33E+19		(Hc/r)^3
kappa	1,515530023	-	Specific heat ratio
rho_inf	1,2	kg/m³	Ambient air density
P_inf	101000	Pa	Atmospheric pressure
T_inf	293	K	Ambient temp
T_s	1023	K	Flame gas temp
M	1,2	-	Mach number (assumed)
P_s	2364000	Pa	Internal gas pressure

Appendix A. 4 Module, Rack Level Estimation of Flame height and diameter Based on HRR

Thermal runaway results for 5MWh Battery room

5MWh Battery Room (Bottom-UP)

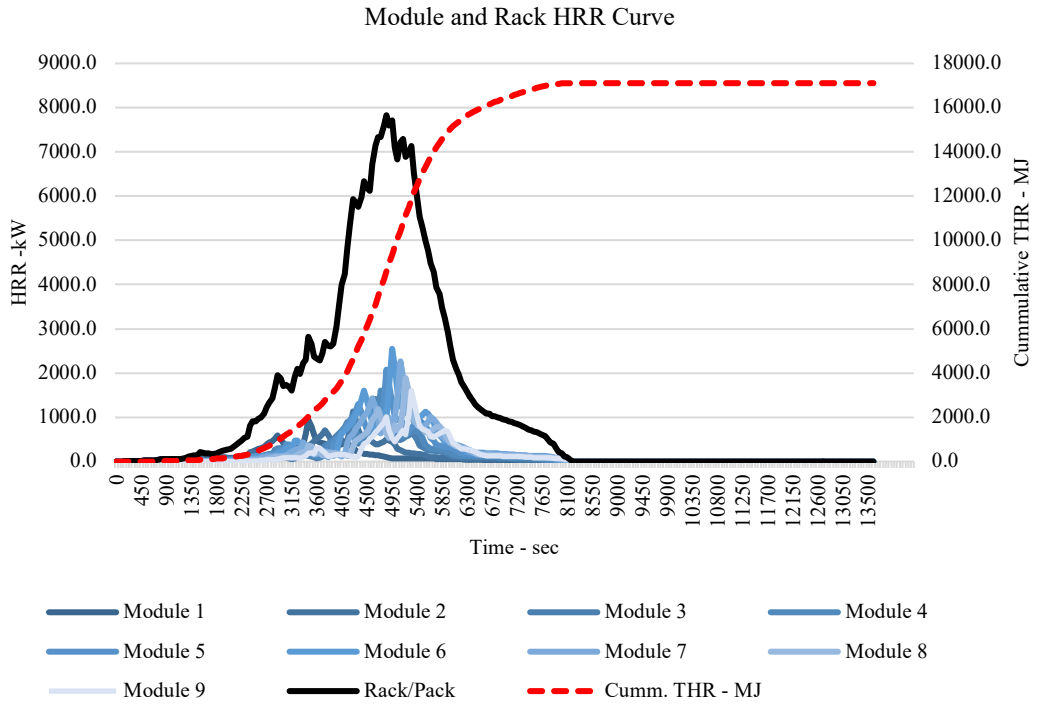

Rack Spacing 0,1m

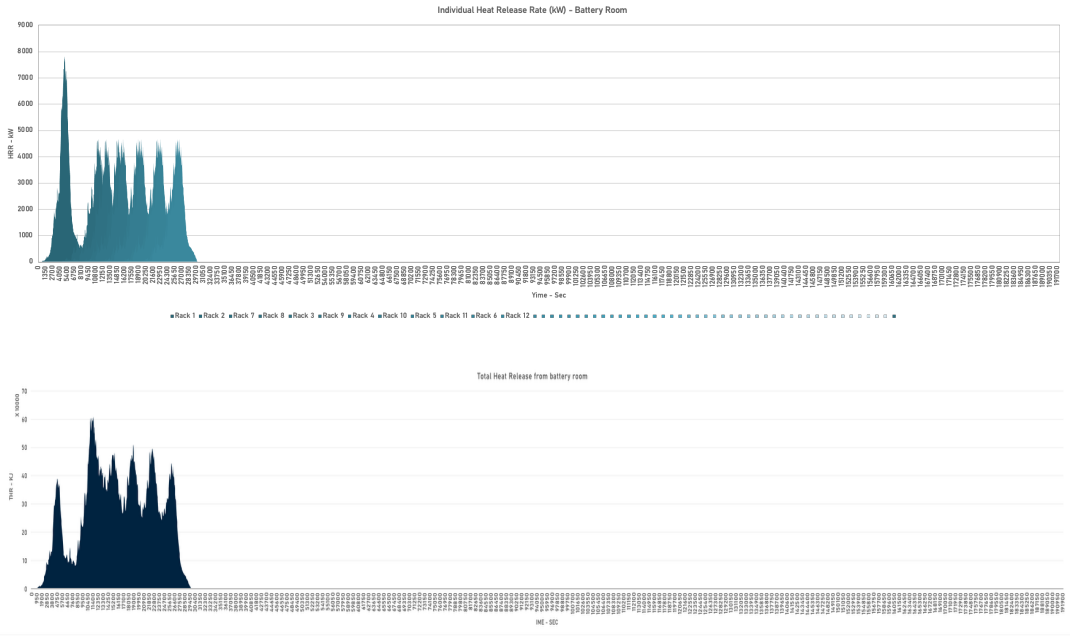

Rack Spacing 1m

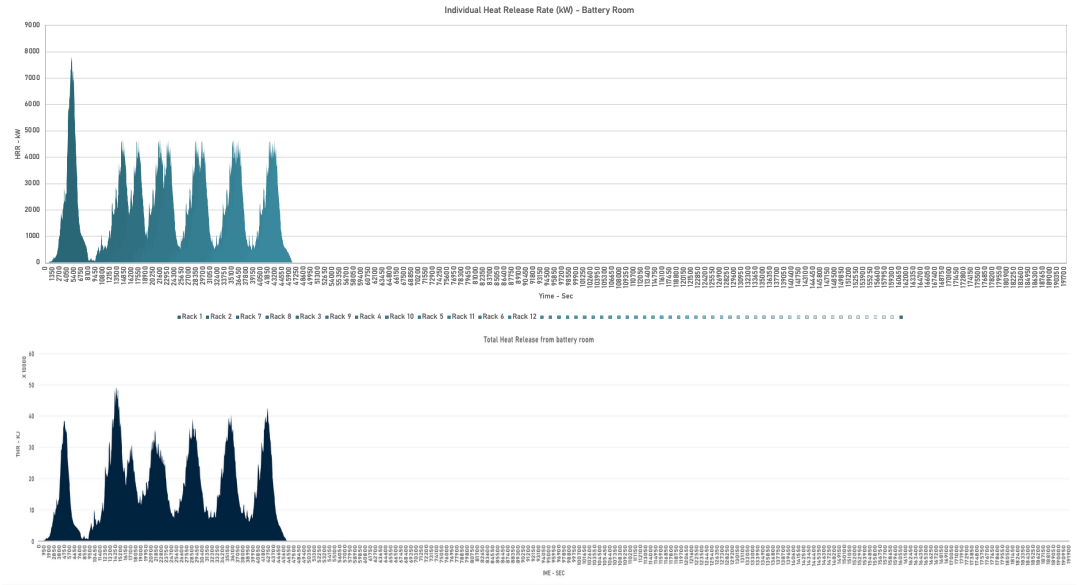

5MWH Battery Room (Middle OUT)

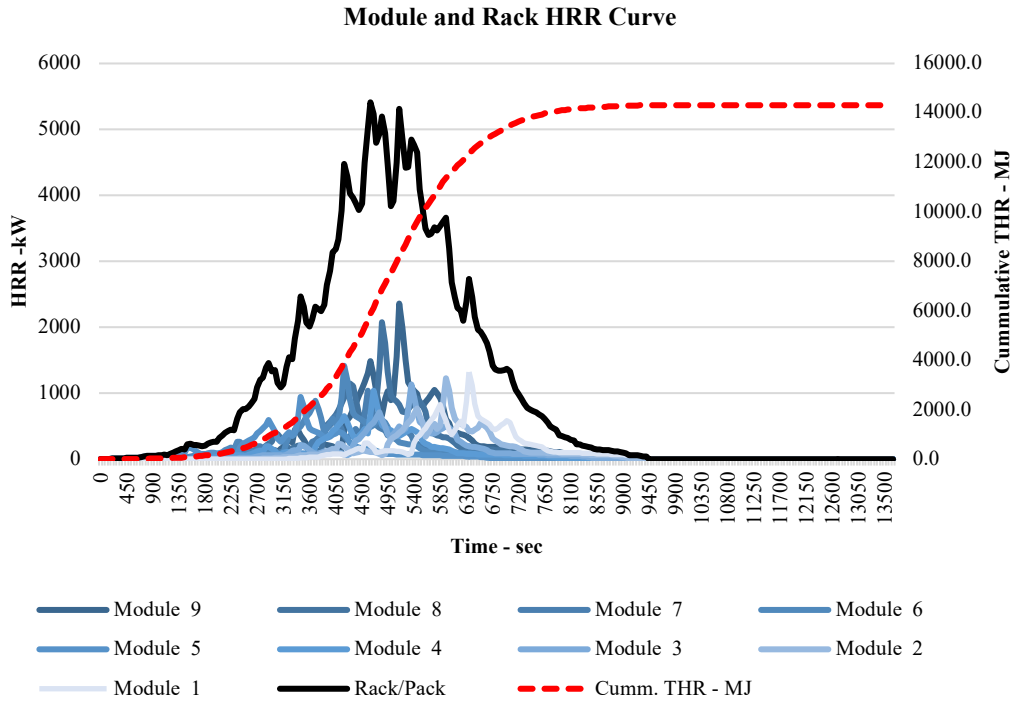

<u>Rack Spacing 0,1m</u>

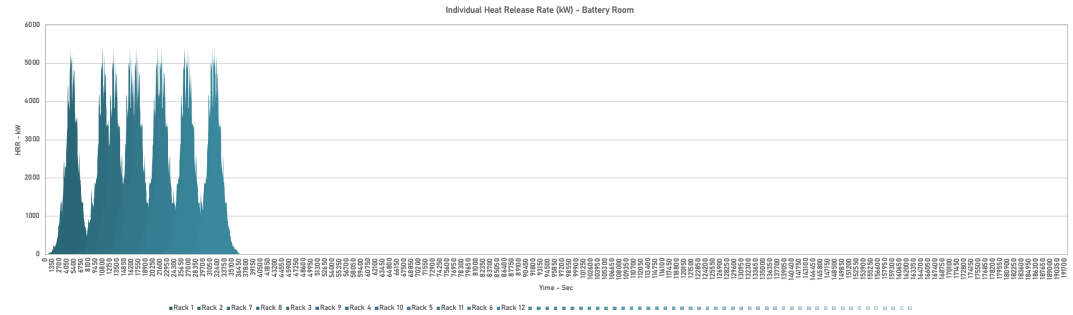

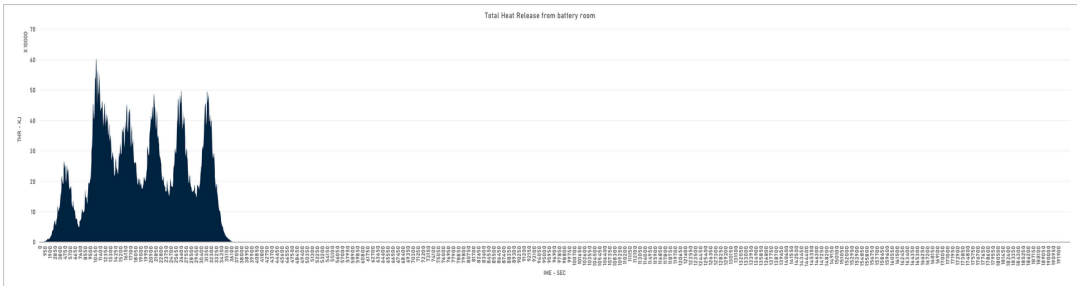

Rack Spacing 1m

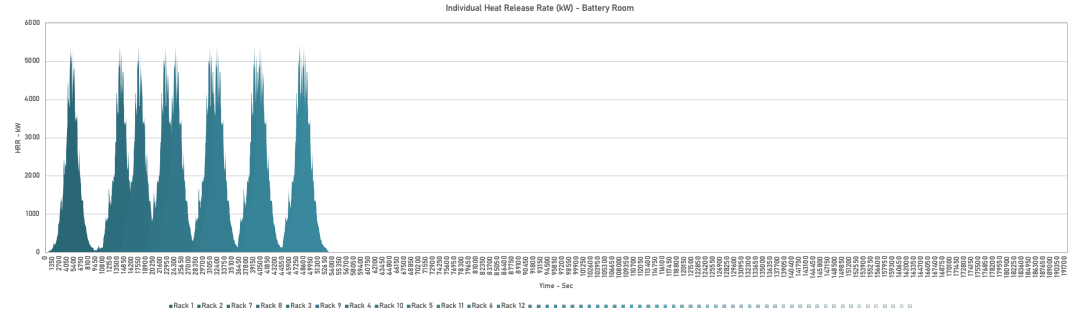

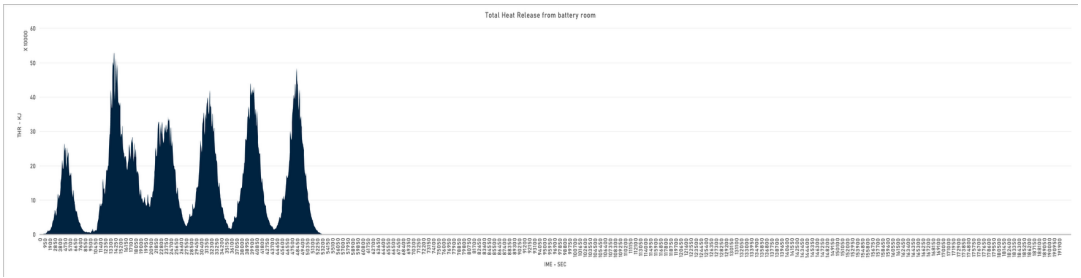

5MWh Battery Room (Top-DOWN)

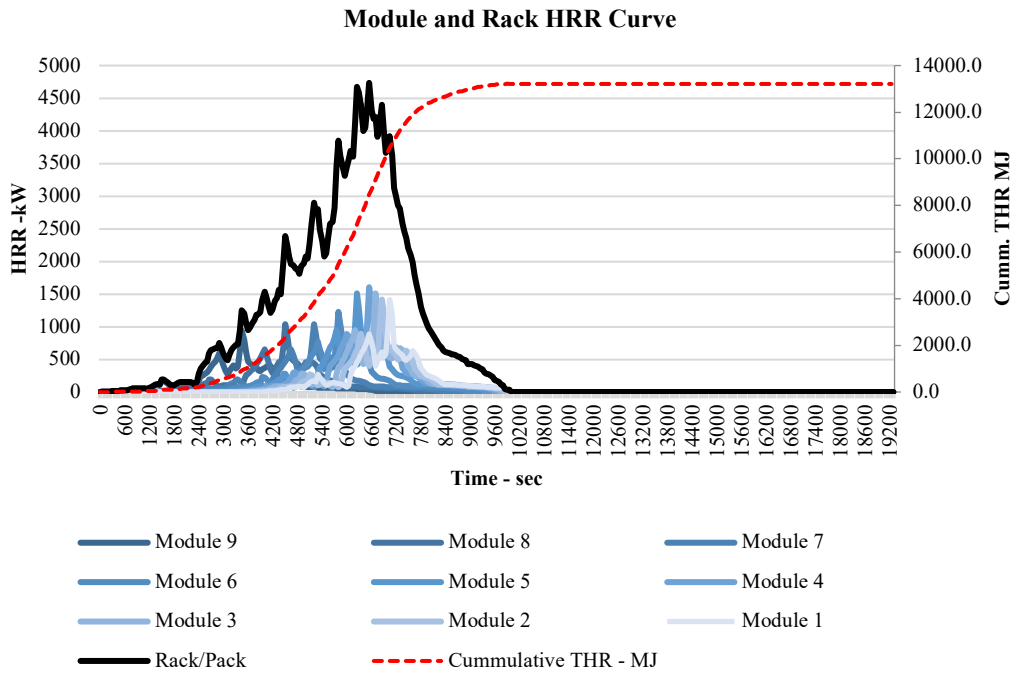

Rack Spacing 0,1m

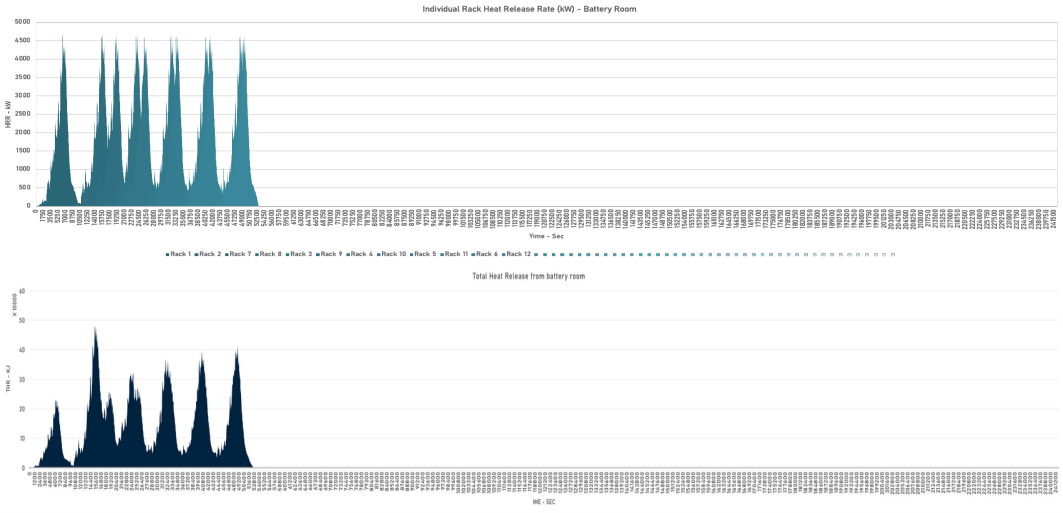

Rack Spacing 1m

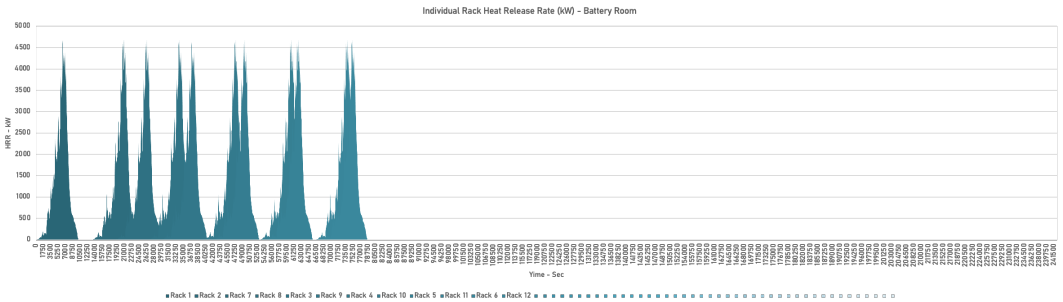

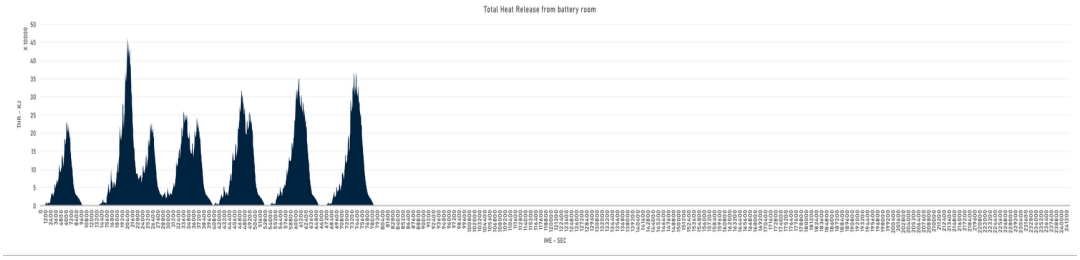
Total Heat Release from battery room
TIME - SEC

8 Appendix B

Appendix B. 5 User Input Interface for Battery Room Capacity, SOC, Propagation Scenario, Structural Exposure, and Mitigation Parameters

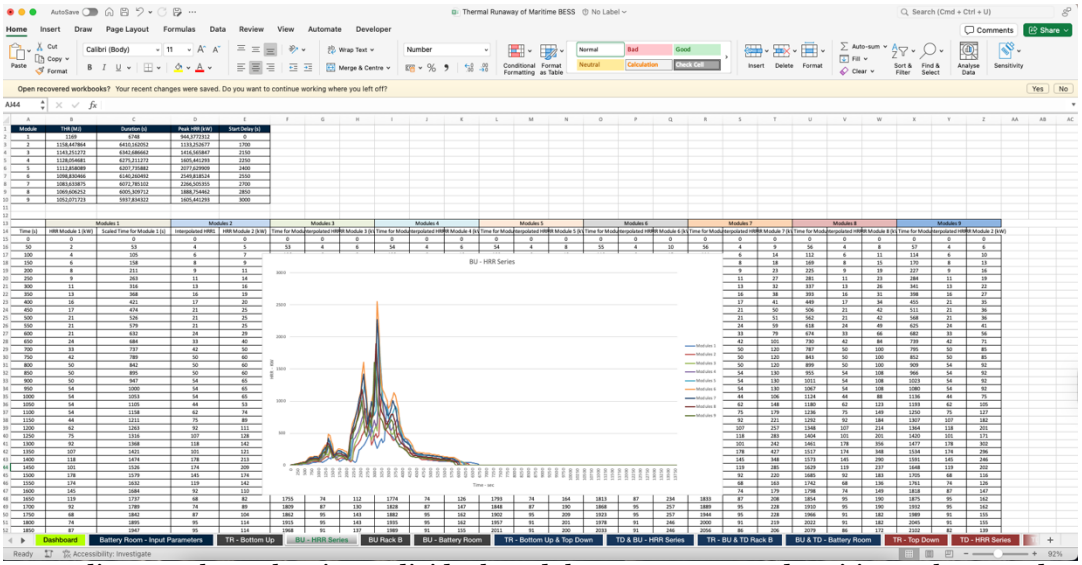

Appendix B. 6 Sheet Showing Individual Module HRR Curves and Ignition Delays Used to Generate the Total Rack HRR Curve

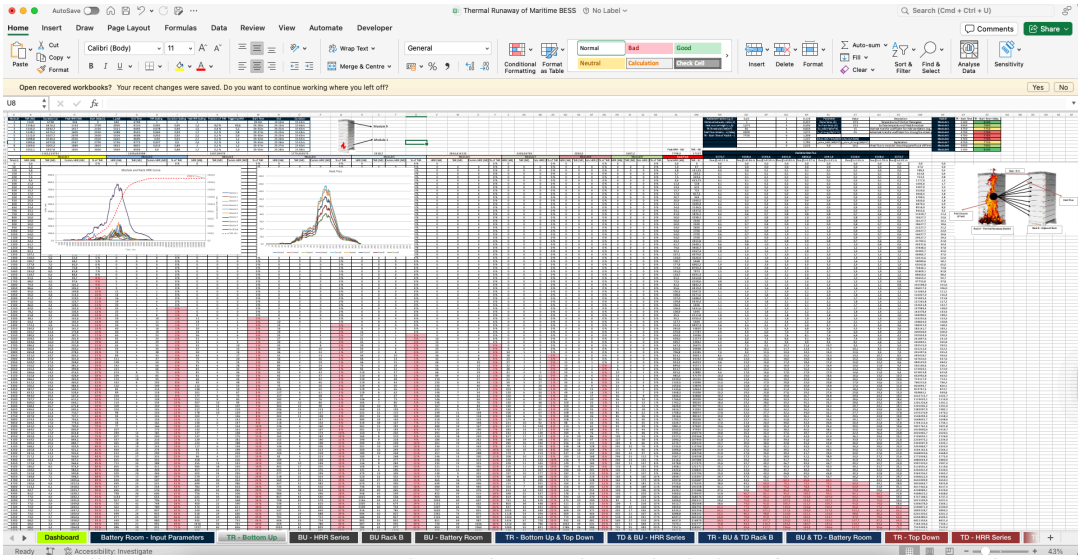

Appendix B. 7 HRR Curve Generation and Heat Flux Calculations for Bottom-Up Rack Propagation Case HRR Curve Scaling for 9-Module Rack and Heat Flux Calculations

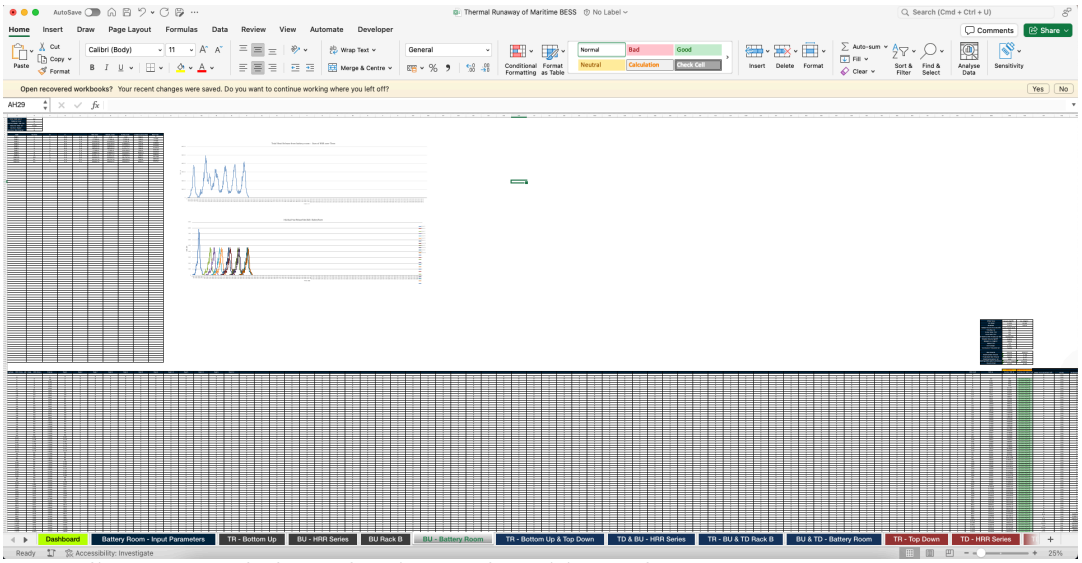

Appendix B. 8 Excel Sheet Showing Rack Ignition Delays, Battery Room HRR Curve Over Full Combustion Duration, and Predicted Onset of Steel Melting

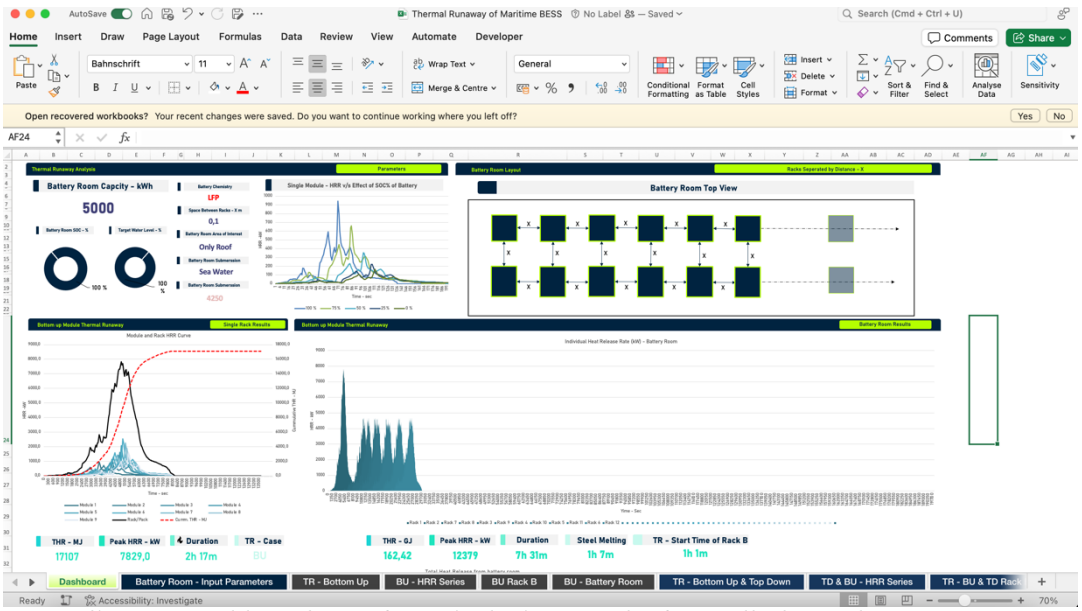

Appendix B. 9 Dashboard Interface Displaying Results from All Thermal Runaway Scenarios and Overall Summary of Battery Room Response

9 Appendix C

5MWh Battery Room (Area of Interest - Battery Room Roof)

SOC	0 %	BU	TD & BU	TD	BU	TD & BU	TD	BU	TD & BU	TD	BU	TD & BU	TD
		Melting Start - s			THR - GJ			Duration - s			Peak HRR - kW		
Rack Spacing	0,1	9750	11250	14300	46	49	45	41816	51400	68175	2471	2237	1888
	0,3	10550	14050	21800	46	49	45	57368	67207	100299	1951	2063	2427
	0,5	12850	18700	25150	46	49	45	69096	82504	115341	1884	1958	2744
	0,7	#N/A	#N/A	#N/A	5	4	4	14282	16471	17695	1360	955	834
	0,9	#N/A	#N/A	#N/A	5	4	4	14282	16471	17695	1360	955	834
	1,1	#N/A	#N/A	#N/A	5	4	4	14282	16471	17695	1360	955	834
	1,3	#N/A	#N/A	#N/A	5	4	4	14282	16471	17695	1360	955	834
	1,5	#N/A	#N/A	#N/A	5	4	4	14282	16471	17695	1360	955	834
	1,7	#N/A	#N/A	#N/A	5	4	4	14282	16471	17695	1360	955	834

SOC	50 %	BU	TD & BU	TD	BU	TD & BU	TD	BU	TD & BU	TD	BU	TD & BU	TD
		Melting Start - s			THR - GJ			Duration - s			Peak HRR - kW		
Rack Spacing	0,1	7350	7850	10150	91	96	89	36988	46399	63023	5402	4944	4092
	0,3	7650	8150	10450	91	96	89	47951	57362	78320	4796	4722	3913
	0,5	7850	8500	10800	91	96	89	56110	68579	93362	4141	4543	4425
	0,7	8050	8850	11200	91	96	89	62228	72659	103050	4026	4439	5544
	0,9	8250	9300	11650	91	8	7	64268	14530	15602	3953	2197	1845
	1,1	8500	9950	12400	10	8	7	12513	14530	15602	3059	2197	1845
	1,3	8850	10950	#N/A	10	8	7	12513	14530	15602	3059	2197	1845
	1,5	9300	#N/A	#N/A	10	8	7	12513	14530	15602	3059	2197	1845
	1,7	10450	#N/A	#N/A	10	8	7	12513	14530	15602	3059	2197	1845

SOC	100 %	BU	TD & BU	TD	BU	TD & BU	TD	BU	TD & BU	TD	BU	TD & BU	TD
		Melting Start - s			THR - GJ			Duration - s			Peak HRR - kW		
Rack Spacing	0,1	4700	4900	6150	162	172	159	27804	36553	52835	12379	12552	10046
	0,3	4850	5000	6350	162	172	159	36727	45221	62268	11013	11488	10126
	0,5	5000	5200	6650	162	172	159	38767	47516	66857	10796	11271	9776
	0,7	5100	5350	6850	162	172	159	41827	50575	77055	10430	10961	9476
	0,9	5200	5450	7050	162	172	159	46926	56694	80624	9974	10926	9493
	1,1	5300	5600	7250	162	172	159	48455	57969	83939	9960	10937	9517
	1,3	5400	5750	7400	162	172	13	49475	61283	11023	10004	10941	4699
	1,5	5550	5950	7600	162	14	13	51515	10293	11023	10033	5420	4699
	1,7	5650	6100	7750	17	14	13	8938	10293	11023	7798	5420	4699

15MWh Battery Room (Area of Interest - Battery Room Roof)

SOC	0 %	BU	TD & BU	TD	BU	TD & BU	TD	BU	TD & BU	TD	BU	TD & BU	TD
		Melting Start - s			THR - GJ			Duration - s			Peak HRR - kW		
Rack Spacing	0,1	15550	18500	21300	129	139	128	41816	51400	68175	2471	2237	1888
	0,3	20150	19600	27100	129	139	128	57368	67207	100299	1951	2063	2427
	0,5	23600	23900	30900	129	139	128	69096	82504	115341	1884	1958	2744
	0,7	#N/A	#N/A	#N/A	5	4	4	14282	16471	17695	1360	955	834
	0,9	#N/A	#N/A	#N/A	5	4	4	14282	16471	17695	1360	955	834
	1,1	#N/A	#N/A	#N/A	5	4	4	14282	16471	17695	1360	955	834
	1,3	#N/A	#N/A	#N/A	5	4	4	14282	16471	17695	1360	955	834
	1,5	#N/A	#N/A	#N/A	5	4	4	14282	16471	17695	1360	955	834
	1,7	#N/A	#N/A	#N/A	5	4	4	14282	16471	17695	1360	955	834

SOC	50 %	BU	TD & BU	TD	BU	TD & BU	TD	BU	TD & BU	TD	BU	TD & BU	TD
		Melting Start - s			THR - GJ			Duration - s			Peak HRR - kW		
Rack Spacing	0,1	8800	10400	13700	255	273	252	36988	46399	63023	5402	4944	4092
	0,3	10550	13450	19350	255	273	252	47951	57362	78320	4796	4722	3913
	0,5	14800	17000	23450	255	273	252	56110	68579	93362	4141	4543	4425
	0,7	17900	18550	25500	255	273	252	62228	72659	103050	4026	4439	5544
	0,9	19300	#N/A	#N/A	255	8	7	64268	14530	15602	3953	2197	1845
	1,1	#N/A	#N/A	#N/A	10	8	7	12513	14530	15602	3059	2197	1845
	1,3	#N/A	#N/A	#N/A	10	8	7	12513	14530	15602	3059	2197	1845
	1,5	#N/A	#N/A	#N/A	10	8	7	12513	14530	15602	3059	2197	1845
	1,7	#N/A	#N/A	#N/A	10	8	7	12513	14530	15602	3059	2197	1845

SOC	100 %	BU	TD & BU	TD	BU	TD & BU	TD	BU	TD & BU	TD	BU	TD & BU	TD
		Melting Start - s			THR - GJ			Duration - s			Peak HRR - kW		
Rack Spacing	0,1	5450	5800	7450	453	487	449	27804	36553	52835	12379	12552	10046
	0,3	5650	6200	7850	453	487	449	36727	45221	62268	11013	11488	10126
	0,5	5900	6650	8300	453	487	449	38767	47516	66857	10796	11271	9776
	0,7	6200	7400	9800	453	487	449	41827	50575	77055	10430	10961	9476
	0,9	6650	11750	17350	453	487	449	46926	56694	80624	9974	10926	9493
	1,1	8300	13050	19450	453	487	449	48455	57969	83939	9960	10937	9517
	1,3	12050	14400	#N/A	453	487	13	49475	61283	11023	10004	10941	4699
	1,5	13800	#N/A	#N/A	453	14	13	51515	10293	11023	10033	5420	4699
	1,7	#N/A	#N/A	#N/A	17	14	13	8938	10293	11023	7798	5420	4699

25MWh Battery Room (Area of Interest - Battery Room Roof)													
SOC	0 %	BU	TD & BU	TD	BU	TD & BU	TD	BU	TD & BU	TD	BU	TD & BU	TD
		Melting Start - s			THR - GJ			Duration - s			Peak HRR - kW		
Rack Spacing	0,1	17950	17650	24000	212	223	180	41816	51400	68175	2471	2237	1888
	0,3	23700	23550	34450	212	223	180	57368	67207	100299	1951	2063	2427
	0,5	31150	33350	47000	212	223	180	69096	82504	115341	1884	1958	2744
	0,7	#N/A	#N/A	#N/A	5	4	4	14282	16471	17695	1360	955	834
	0,9	#N/A	#N/A	#N/A	5	4	4	14282	16471	17695	1360	955	834
	1,1	#N/A	#N/A	#N/A	5	4	4	14282	16471	17695	1360	955	834
	1,3	#N/A	#N/A	#N/A	5	4	4	14282	16471	17695	1360	955	834
	1,5	#N/A	#N/A	#N/A	5	4	4	14282	16471	17695	1360	955	834
	1,7	#N/A	#N/A	#N/A	5	4	4	14282	16471	17695	1360	955	834

SOC	50 %	BU	TD & BU	TD	BU	TD & BU	TD	BU	TD & BU	TD	BU	TD & BU	TD
		Melting Start - s			THR - GJ			Duration - s			Peak HRR - kW		
Rack Spacing	0,1	11800	12950	18000	418	450	377	36988	46399	63023	5402	4944	4092
	0,3	15800	15950	22250	418	450	377	47951	57362	78320	4796	4722	3913
	0,5	18600	18950	25650	418	450	377	56110	68579	93362	4141	4543	4425
	0,7	20700	20650	27550	418	450	377	62228	72659	103050	4026	4439	5544
	0,9	22150	#N/A	#N/A	418	8	7	64268	14530	15602	3953	2197	1845
	1,1	#N/A	#N/A	#N/A	10	8	7	12513	14530	15602	3059	2197	1845
	1,3	#N/A	#N/A	#N/A	10	8	7	12513	14530	15602	3059	2197	1845
	1,5	#N/A	#N/A	#N/A	10	8	7	12513	14530	15602	3059	2197	1845
	1,7	#N/A	#N/A	#N/A	10	8	7	12513	14530	15602	3059	2197	1845

SOC	100 %	BU	TD & BU	TD	BU	TD & BU	TD	BU	TD & BU	TD	BU	TD & BU	TD
		Melting Start - s			THR - GJ			Duration - s			Peak HRR - kW		
Rack Spacing	0,1	5950	6850	8600	744	801	740	27804	36553	52835	12379	12552	10046
	0,3	6500	9000	13500	744	801	740	36727	45221	62268	11013	11488	10126
	0,5	8400	11150	16300	744	801	740	38767	47516	66857	10796	11271	9776
	0,7	11400	12600	19100	744	801	740	41827	50575	77055	10430	10961	9476
	0,9	13400	14250	20450	744	801	740	46926	56694	80624	9974	10926	9493
	1,1	14400	14850	21550	744	801	740	48455	57969	83939	9960	10937	9517
	1,3	15100	15900	#N/A	744	801	13	49475	61283	11023	10004	10941	4699
	1,5	15950	#N/A	#N/A	744	14	13	51515	10293	11023	10033	5420	4699
	1,7	#N/A	#N/A	#N/A	17	14	13	8938	10293	11023	7798	5420	4699

Appendix C 1 Comparative sensitivity analysis for 5 MWh, 15 MWh, and 25 MWh battery rooms, showing the influence of SOC (0%, 50%, 100%) and rack spacing (0.1–1.7 m) on roof melting start time, total heat release.

DEPARTMENT OF INDUSTRIAL AND MATERIALS SCIENCE
CHALMERS UNIVERSITY OF TECHNOLOGY
Gothenburg, Sweden 2025
www.chalmers.se

CHALMERS
UNIVERSITY OF TECHNOLOGY